PEOPLE'S DEMOCRATIC REPUBLIC OF ALGERIA
MINISTRY OF HIGHER EDUCATION AND SCIENTIFIC RESEARCH

University of Mohamed Boudiaf - M'sila
Faculty of Technology
Department of Electronic

THESIS

A dissertation submitted for the degree of
DOCTORAT

Field**:** Electronic

Option**:** Micro-waves and Telecommunication

By: MAACHE Mouhssin

THEME

Design and Optical Studies of Photonic Components Using Slow Light Properties

« Conception et Etudes Optiques de Composants Photoniques en Utilisant Les Propriétés de Lumière Lente »

Presented and publicly defended the …/…/2019

JURY MEMBERS:

SAIGAA Djamel	**Professor**	**Univ. of M'sila**	**Chairman**
HOCINI Abdesselam	**Professor**	**Univ. of M'sila**	**Supervisor**
KHEDROUCHE Djamel	**Professor**	**Univ. of M'sila**	**Co-supervisor**
HOBAR Farida	**Professor**	**Univ. of Oum EL Bouaghi**	**Examiner**
BOUCHEMAT Thouraya	**Professor**	**Univ. of Constantine1**	**Examiner**
BOUCHEMAT Mohamed	**Professor**	**Univ. of Constantine1**	**Examiner**

2018/2019

To my parents

Acknowledgements

This thesis work was carried out in Signal and Systems Analysis Laboratory (LASS), Electronics Department of the University of M'sila, under the scientific direction of Professor ***Abdesselam HOCINI****.*

I would like to express my deep gratitude to my thesis supervisor, Professor ***Abdesselam HOCINI****, for having entrusted me with this work and ensuring the supervision of this thesis, and I am very grateful for the confidence that he has given me, his wise advice, his availability and the constant support that he has given me during the elaboration of this work.*

*I would like to thank my Co-supervisors, prof****. Djamel KHEDROUCHE*** *for his time, patience, consideration, and support by thoughts and motivation.*

I would like to express my deepest sense of gratitude to Dr. ***Khaled MNAYMNEH*** *from National Research Council Canada for his deep understanding, encouragements, supports, and invaluable assistance. he has always supported me and never let me down.*

Thanks to ***Saber BENAMRA****,* ***Ibrahim BERA****,* ***Souleymane DJAAFAR****, Dr.* ***Safia ARAFA****,* ***Khadija BELABBES****, for their encouragements, supports, and invaluable assistance.*

I express my deep gratitude to Mr. ***Djamel SAIGAA****, professor at the University of M'sila, for his interest in my work by doing the honour of chairing the jury of my defense.*

I would like to extend my sincere thanks to all members of the jury:

I would like to thank Mrs. ***Farida HOBAR****, professor and rector of larbi Ben m'hidi university Oum El Bouaghi, for her interest in this work and for having agreed to examine my work by taking part in the thesis jury.*

I would like to thank Mrs. ***Thouraya BOUCHEMAT****, professor at Constantine University 1, for her interest in this work and for having agreed to examine my work by taking part in the thesis jury.*

My thanks also go to Mr. ***Mohamed BOUCHEMAT****, professor at Constantine University 1, for his interest in this work and for having agreed to examine my work by taking part in the thesis jury.*

Table of contents

Chapter II: Slow Light In Photonic Crystals

Chapter III: Simulation Methods and Tools

Chapter IV: Results and discussions

List of figures

Chapter I

Chapter II

Chapter III

Chapter IV

List of tables

List of Abbreviations

λ_0	Free-space wavelength
λ	wavelength
a	Lattice constant of a photonic crystal
r	Radius of a photonic crystal hole or rod
n	Refractive index
n_{eff}	Effective refractive index
ω	Angular frequency
c	Speed of light in vacuum
k	Wave vector
BZ	Brillouin zone
IBZ	Irreducible Brillouin Zone
PhC	Photonic Crystal
PCW1	Photonic Crystal waveguide 1
PCW2	Photonic Crystal waveguide 2
PWE	Plane wave expansion
FDTD	The Finite Difference Time Domain Method
TE	Transverse Electric.
TM	Transverse Magnetic.
v_p	Phase velocity
v_g	Group velocity
n_g	Group index
GVD	group velocity dispersion
NDBP	The normalized delay bandwidth product

General Introduction

General introduction

Think about it, how has technology changed over the past years? We live in the era of technological world where the latest advancements keep surprising us all. For the past 70 years, semiconductor physics has played a vital role in almost every aspect of modern technology. Advances in this field have allowed scientists to tailor the conducting properties of certain materials and have initiated the transistor revolution in electronics. New research suggests that we may now be able to tailor the properties of light [1]. The key in achieving this goal lies in the use of a new class of materials called photonic crystals. What is photonics? the particle of light is called the photon, that's why the technology is called photonics which is a combination of the word photon and electronics. Photonics can be considered to be the science and applications of light; These applications use the photon in the same way that electronic applications use the electron. one of the reasons why photonics is the future? Is that light travels faster than electricity. Light can make devices like computers mobile phones and medical instruments faster and more energy efficient. There's a big need to make things faster less energy smaller and more cheaply. The solution is replacing electrons with photons.

Today, the world is witnessing a technological revolution especially data, information and communications technology. Photonic crystals, which prohibit the propagation of light for frequencies within a band gap, have enabled exciting new ways to control light and construct integrated optical devices. Hence, the use of photonic crystals in modern optical telecommunication systems has become necessary in order to achieve miniature tunable and functional devices which can be exploited for a broad range of applications [2] [3] [4]. The extreme speed at which light moves, and the fact that photons do not tend to interact with transparent matter, is of enormous benefit to mankind. But faster is not always better, as the well-known fable of the hare and the tortoise. Using light smartly rather than simply relying on its speed offers many opportunities [5]. Since the notion of slow light first became a reality more than a 19 years ago, scientists have been exploring its use in fundamental studies of light-atom systems as well as for long-term applications in all-optical data processing, quantum communication and sensors [6]. Slow light promotes a stronger light–matter interaction; It offers additional control over the spectral bandwidth of the interaction, and it allows us to delay and temporarily store light in all-optical memories. It is also anticipated that it can enhance linear and nonlinear effects and so miniaturize functional photonic devices, because slow light compresses optical energy in space, as a light pulse enters a photonic-crystal waveguide operating in the slow-light regime the pulse length is compressed, resulting in an increased intensity [7] [8]. Slow light can be achieved by

using material induced dispersion as electromagnetically induced transparency (EIT) and coherent population oscillations (CPO), or structurally induced dispersion such as photonic crystals (PhC's) [9]. Photonic crystal (PhC) line defect waveguide (W1) is one of the most suitable and attractive structures for realizing the slow light effect. This is because such a line defect structure operates at room temperature and has a high potential for on-chip integration by modifying the initial PhC structure. The photonic crystal line defect waveguide W1 allows ultra-small components and low group velocity vg due to its strong optical confinement by the photonic bandgap (PBG).
In this work, we study the properties of photonic crystal waveguides and how we can slow down the light and make this low speed useful. This thesis is organized as follow:

In Chapter 1 of this thesis, we review the fundamental properties of Photonic crystals (PhC's). We give a general idea of what are photonic crystals, which are a special class of optical media with periodic modulation of permittivity classified mainly into three categories: one-dimensional (1D), two-dimensional (2D), and three-dimensional (3D) crystals according to the periodicity of dielectric material along one or more axes. The main attention is paid to the most important feature of the photonic crystals which is the photonic band gaps: certain frequencies do not pass through the structure and why does the photonic band gap appear. Then describe different kinds of photonic crystal lattices and introduce and discuss the basic terminology in PhC such as cavity and waveguide. We review the photonic crystal slab that promises easier fabrication using existing techniques. Finally, we cite some applications of photonic crystals.

In chapter 2, we concentrate on the Basic concepts of slow light, what is slow light and how do we slow down the light, we discuss the background information about photonic crystal waveguide and their simulation. Line-defect waveguide parameters and dispersion relations are presented. Then we explain the slow light away from the band-edge, and many approaches is discussed to achieve small group velocity. Slow light has limitations such as, group velocity dispersion and loss propagation, these limitations are discussed. We have mentioned various ways to achieve flat band slow light and how compensate the dispersion. We compare between the cavities and slow light waveguide and how the slow light waveguide behaves like a single mode cavity of arbitrary length. In the last of this chapter we cite some applications of slow light and we give two examples "buffer and sensor" for further clarification of the subject.

In chapter 3, we present the numerical methods that we used to simulate our work such as Plane wave expansion (PWE) and The Finite Difference Time Domain Method (FDTD). Then, we present Rsoft software, in particular two modules "BandSOLVE" and "FullWAVE". We proved

the strength and accuracy of these modules by re-simulate some important and famous papers published in this domain.

Chapter 4, is devoted to a discussion of our results and gives some conclusions. The structures proposed are essentially based on line-defect waveguide W1. We discuss and present the W1 parameters and dispersion relations. In the issue of slow light, we design and study two photonic crystal waveguides PCW1 and PCW2, the first proposed method lies on inserting reduced air holes with a half period in the middle of the waveguide and shifting only the second rows of air holes adjacent to the center waveguide, and keep the position of the first rows unchanged which lead to a high group index and wide bandwidth. The second design obtained by enlarging the entire holes of the PhC and shifting the first and second rows adjacent to the line defect in the propagation direction of light, and by engineering the dispersion curve we reducing the unwanted dispersion and achieve constant group index over a broad wavelength range. Finally, we proposed an application of our PCW2 as a buffer.

Chapter I

Photonic Crystals

Chapter I Photonic Crystals

What are photonic crystals?

I. Introduction:

Photonic crystals (PhCs) are materials patterned with a periodicity in dielectric constant, which prohibit the propagation of light for frequencies within a band gap. Preventing light from propagating in certain directions with specified frequencies, have enabled exciting new ways to control light and construct integrated optical devices. Hence, the use of photonic crystals in modern optical telecommunication systems has become necessary in order to achieve miniature tunable and functional devices which can be exploited for a broad range of applications [2] [3] [4] .

I.1 Photonic crystals (PhCs) 1D, 2D and 3D

A photonic crystals (PhCs) are an engineered optical material represented by natural or artificial structures with periodic modulation of the refractive index. Photonic crystals are classified mainly into three categories, that is, one-dimensional (1D), two-dimensional (2D), and three-dimensional (3D) crystals according to the periodicity of dielectric material along one or more axes [10] as shown in figure 1.

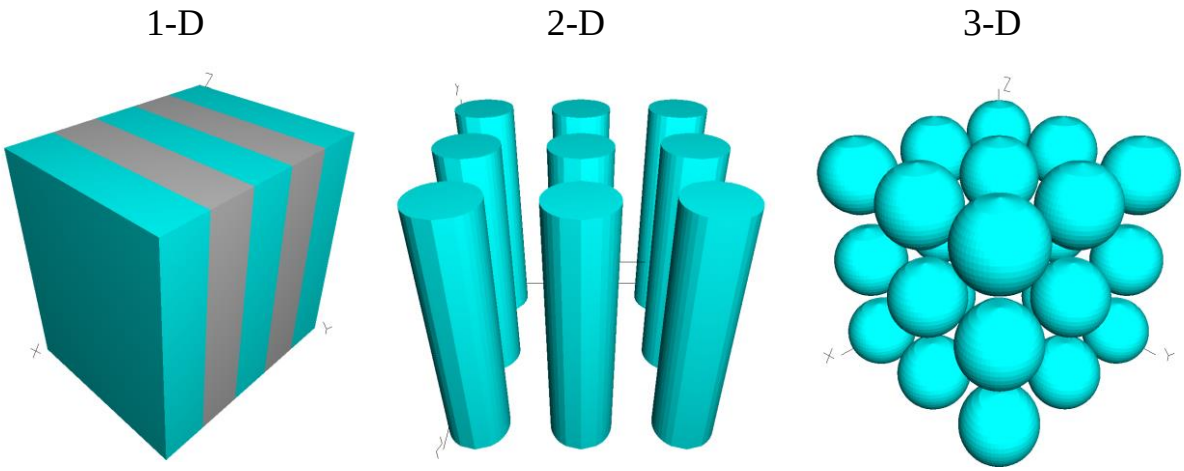

Figure 1: Representation of one, two and three-dimensional photonic crystals.

I.1.1 One-dimensional photonic crystals

In order to gain an intuitive understanding of the photonic bands and bandgaps, we examine the simplest possible case, a one-dimensional system (1D) shown in figure 2. The periodic modulation of the permittivity occurs in one direction only (multilayer film), while in two other directions structure is uniform. Lord Rayleigh (1887) published one of the first analyses of the optical properties of multilayer films. This type of photonic crystal can act as a mirror (a Bragg mirror) for light with a frequency within a specified range, and it can localize light modes if there are any defects in its structure [11]. Such structures are widely used as antireflecting coatings which allow to decrease dramatically the reflectance from the surface and are used to improve the quality of lenses, prisms and other optical components [12].

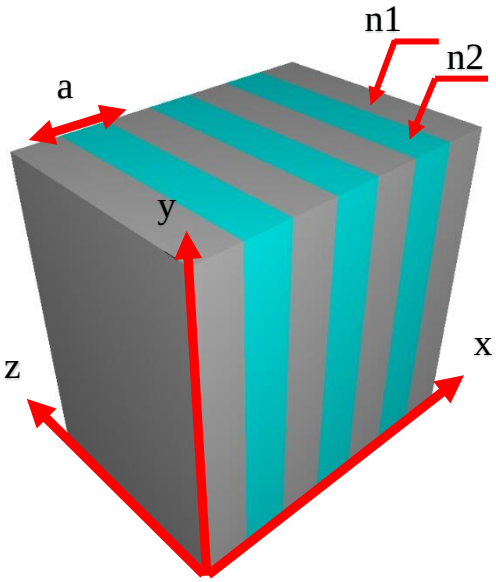

Figure 2: One-dimensional photonic crystals, the dielectric periodicity in one direction along the axis X.

I.1.2 The photonic band gap of 1D PhC

The multilayer presented in figure 3 consists of alternating layers of material with different refractive index n1=3.48 (Si), n2=1 (air) and the lattice vector (period) a=1 um, the primitive lattice vector is $a\hat{x}$ then the primitive reciprocal lattice vector is $(2\pi/a)\ \hat{x}$ and the Brillouin zone is $-\pi/a < k_x \leq \pi/a$.

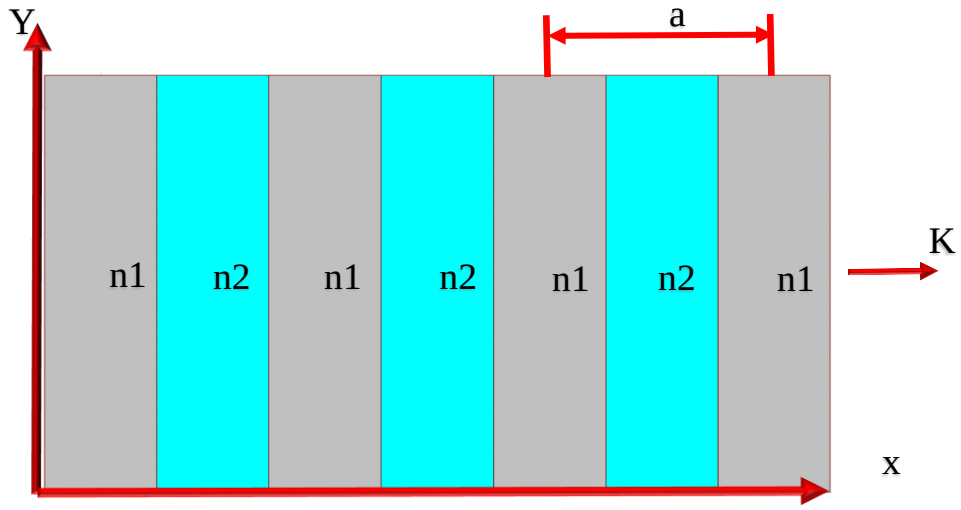

Figure 3: 1D Photonic crystal of multilayer with alternating dielectric layers in the x direction.

We consider electromagnetic waves that propagate in the X direction, crossing the sheets of dielectric at normal incidence.

At first, we selected a homogeneous dielectric medium a silicon bulk, we know that the speed of light is reduced by the refraction index. The modes lie along the light line given by $\omega(k) = ck/n$.

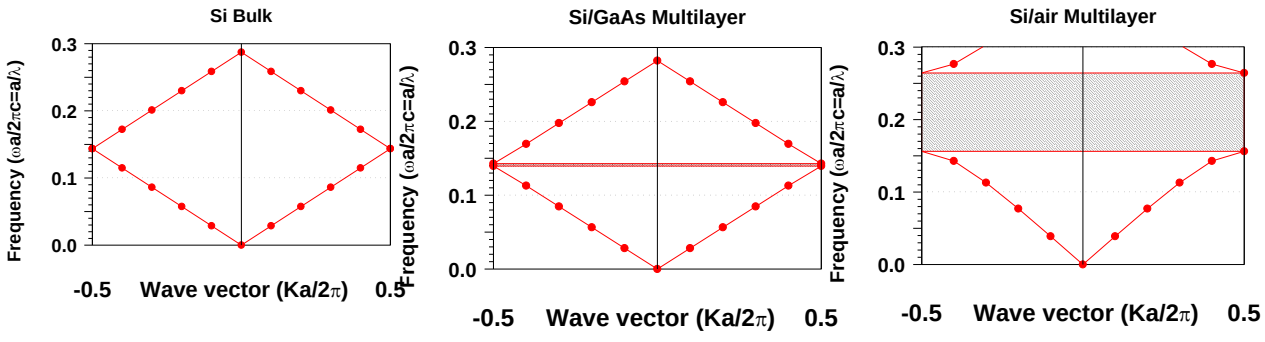

Figure 4 The photonic band structures, computed for three different multilayer films. In all three cases, each layer has a width 0.5a. (a) Every layer has the same refractive index n=3.48. (b) layers alternate between n_{si}=3.48 and n_{GaAs}=3.6. (c) layers alternate between n_{si}=3.48 and n_{air}=1.

We calculate the photonic band structure as shown in figure 4 (a), we notice that there is no band gap. Figure 4(b) which is for a nearly-homogenous medium, we see a gap between the upper and lower branches of the lines. There is no frequencies allowed within this gap, this is what we call a photonic band gap. When the dielectric contrast increased (n_{si}/n_{air}) the band gap become wider as shown in figure 4(c).

I.2 Why does the photonic band gap appear?

We can understand the gap's physical origin by considering the electric field mode profiles for the states immediately above and below the gap. The gap between bands 1 and band 2 occurs at the edge of the Brillouin zone, at k = π/a.

We found that the low frequency modes concentrate their energy in the high-ε regions (n2), and the high frequency modes have a larger fraction of their energy in the low-ε regions (n1). With this in mind, it is understandable why there is a frequency difference between the two cases. The mode just under the gap has more of its energy concentrated in the ε=13 (nGaAs =3.6) regions as shown in figure 5(b), the mode upper the gap has more of its energy concentrated in the ε=12 regions (n_{si}=3.48) as shown in figure 5 (a).

The bands above and below the gap can be distinguished by where the energy of their modes is concentrated: in the high-ε regions, or in the low-ε regions. Often, especially in the two- and three-dimensional crystals, the low-ε regions are air regions. For this reason, it is convenient to refer to the band above a photonic band gap as the air band, and the band below a gap as the dielectric band [11].

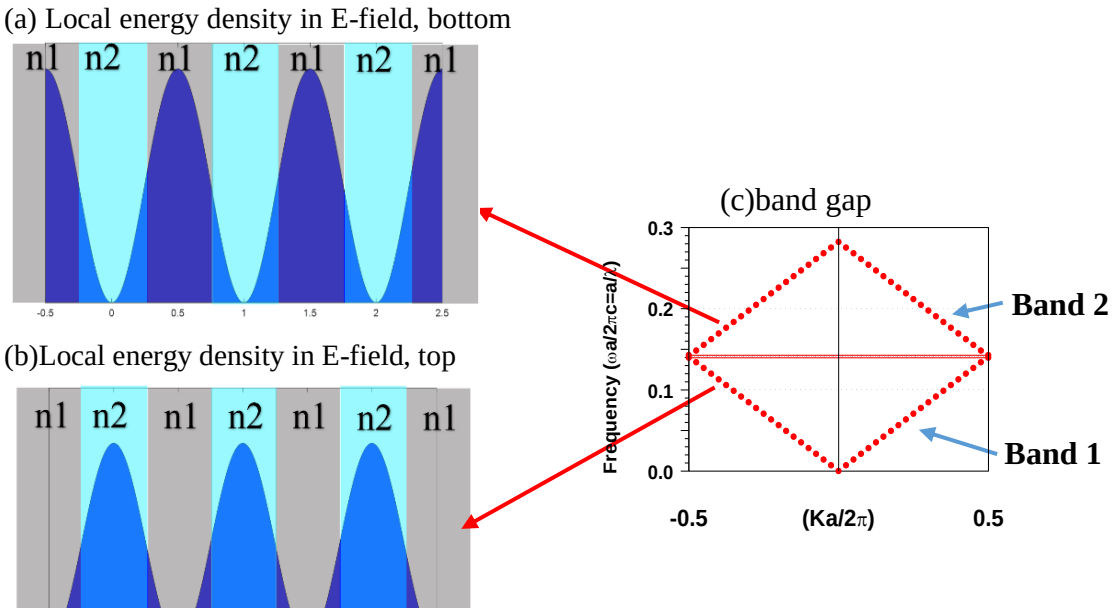

Figure 5 Schematic diagram showing the physical origin of the band gaps (a) electric-field energy density of band 2 (b) electric-field energy density of band 1 (c) dispersion diagram of Si/GaAs multilayer.

I.3 Three-Dimensional Photonic Crystals

Three-Dimensional PhC's are dielectric structure that is periodic along all three directions. At that, the number of possible PhC configurations is much larger than in case of 1D or 2D PhC. Many works are dedicated to the design of new geometric configuration of 3D PhC, which discover new possibilities of their application. PhC's exist throughout the natural world, from opal gemstones and beetles to bird feathers, and butterfly wings, and the common characteristic between all is their iridescent color. This directional-dependent color (color that changes depending on angle of observation), does not arise from any absorption or pigmentation alone but is instead caused by the interaction of light with the periodic or random architecture of these materials' natural design, as shown in figure 6 [13] [14].

However, now we know that all these peculiarities are caused by the microstructure of opal. It consists of a number of microspheres placed at nodes of face-centered cubic (FCC) lattice. Reflectance of such a structure strongly depends on the radiation incident angle. So, when one turns it around, it starts to reflect the radiation with different wavelengths. Thus, optical properties of PhC's are determined by the existence of the periodic modulation of the permittivity or the refractive index of the medium. However, we mention here those geometries that promote the existence of photonic band gaps. As an example, Ho et al. (1990), they determined that dielectric spheres arranged in the diamond structure possess a full photonic band gap. Figure 7 (a) show the unit cell used to calculate the band structure shown in figure 7 (b) the sphere radius r is chosen to be 0.325a, where a is the lattice constant, and the diamond lattice of air spheres have a high dielectric (ε=13) material [15].

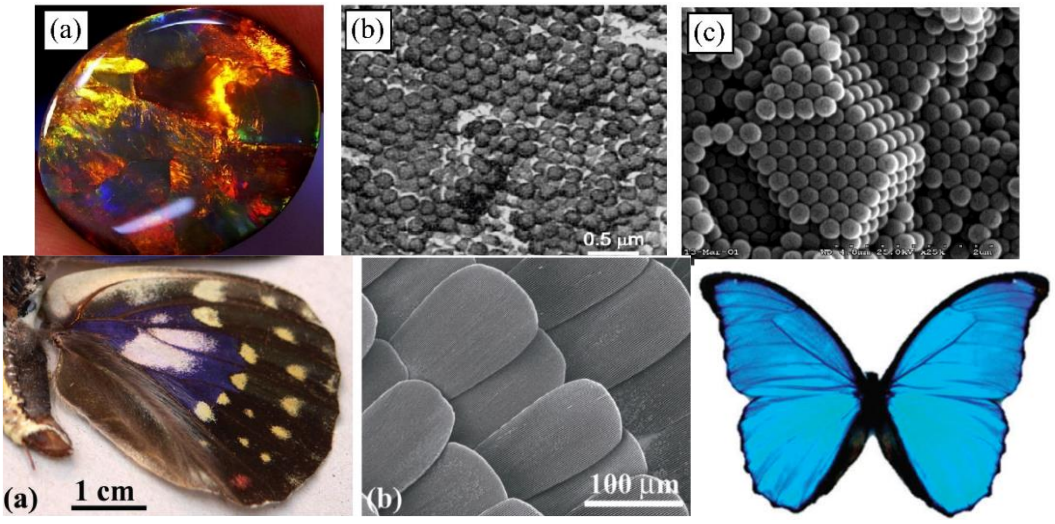

Figure 6 :(a) An example of natural opal, SEM images of (b) natural and (c) artificial opals [13] (e) Wing of the male Sasakia Charonda butterfly (f) the Morpho butterfly [14].

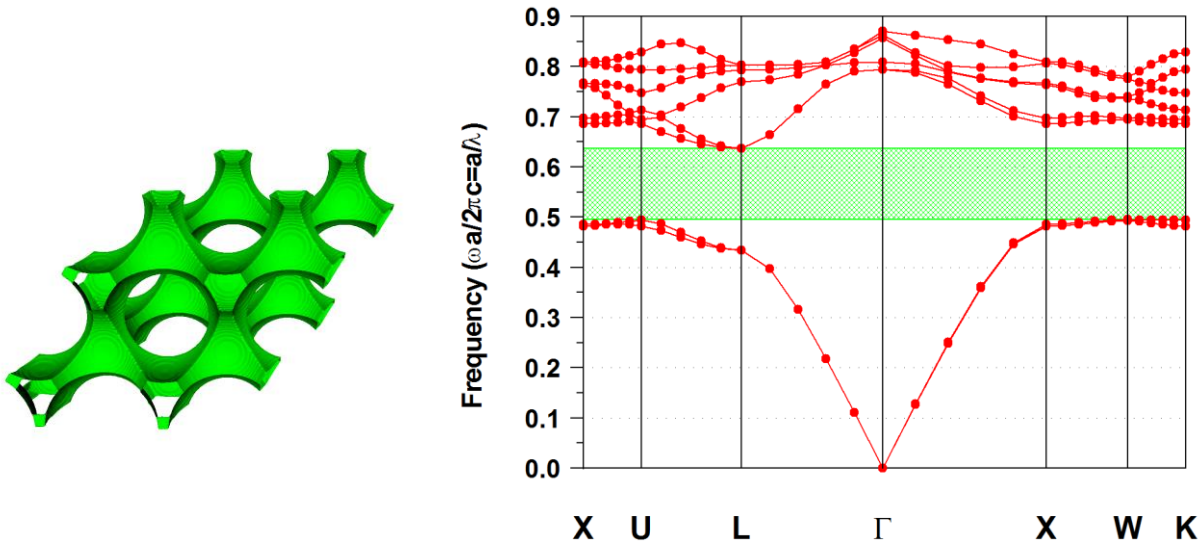

(a) (b)

Figure 7 (a) Unit cell for a diamond lattice (b)calculated photonic band structure for a diamond lattice of air spheres in a high dielectric (ε=13) material. A complete photonic band gap is shown in green.

I.3.1 Yablonovite

Yablonovite are structures that proved to be simpler to manufacture. A slab of material is covered by a mask consisting of triangular array of holes. Each hole is drilled through 3 times, at an angle 35.26° away from normal, and spread out 120° on the azimuth. The crisscross of holes below the surface of the slab, produces a fully three-dimensionally periodic FCC structure as shown in figure 8 (a). Yablonovite was first fabricated on centimeter scales for measurements of microwave propagation. Drilling holes with a radius of 0.234a results in a structure with a complete photonic band gap of 19%, as shown in figure 8 (b). Like the diamond lattice of air spheres, we can think of Yablonovite as two interpenetrating "diamond-like" lattices, one of which is a connected region of dielectric, and the other being a connected air region [16].

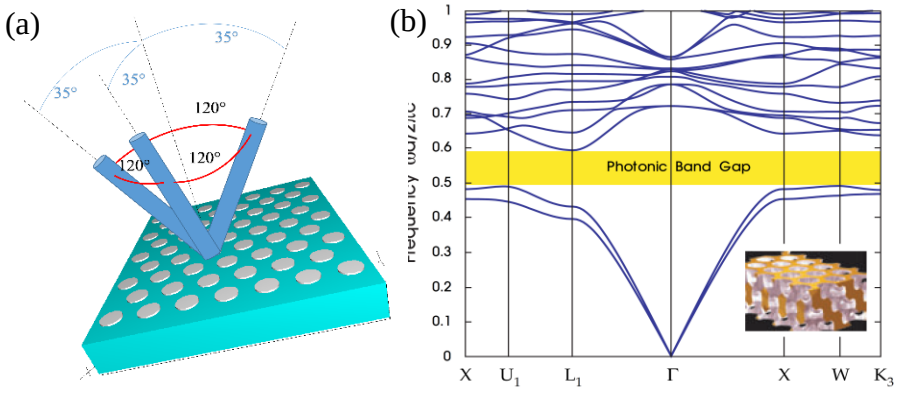

Figure 8 (a) The method for constructing Yablonovite (b) The photonic band structure for Yablonovite [11].

I.3.2 The woodpile crystal

The first three-dimensional photonic crystal with a complete gap to be fabricated on micron scales, for light at infrared wavelengths, was the crystal shown in figure 9 (a) (b). structure is made of layers of dielectric rods with a stacking sequence that repeats itself every four layers. Within each layer, the rods are arranged with their axes parallel and separated by a distance, a. The orientations of the axes are rotated by 90 degrees between adjacent layers. To obtain a periodicity of four layers in the direction of stacking, the rods of second neighbor layers are shifted by a distance of 0.5a in the direction perpendicular to the rod axes. This structure was proposed independently by Ho et al. (1994) and Sözüer and Dowling (1994), The main advantage of the woodpile, as compared to crystals that had been proposed earlier, is that the woodpile can be fabricated as a sequence of layers deposited and patterned by lithographic techniques developed for the semiconductor electronics industry [17] [18] [19] the band gap of this structure, for a dielectric constant of 13/1, is shown in figure 10.

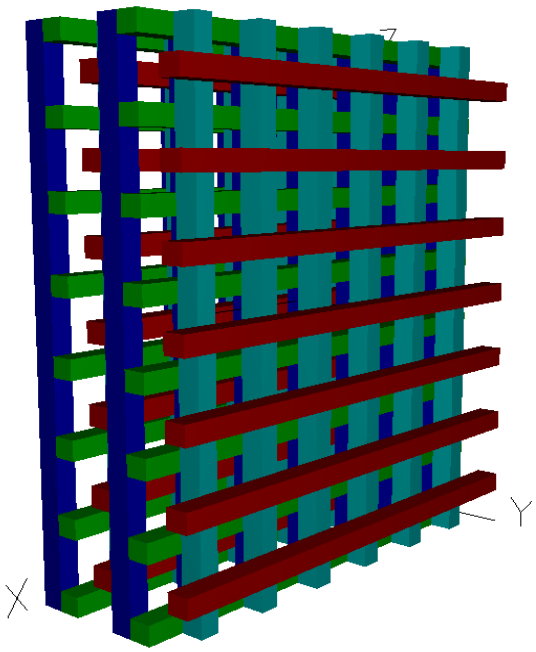

Figure 9 This figure schematically created by Rsoft illustrates the design of the new 3D photonic band gap crystal based on dielectric rods. The structure is built by an orderly stacking of dielectric rods (rectangular in the case shown).

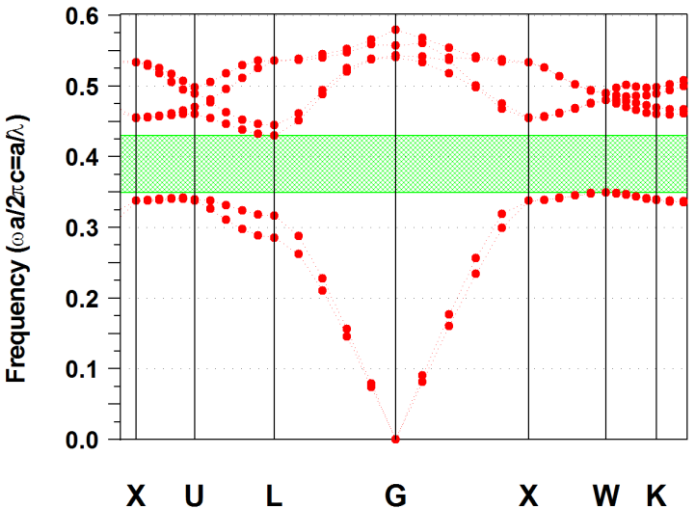

Figure 10 The photonic band structure for the lowest bands of the woodpile structure.

I.4 Two-dimensional photonic crystals

Two-dimensional photonic crystals are periodic along two axes, and extends infinity along the third axis, two-dimensional lattices can inhibit propagation in the lattice plane but not along the axis perpendicular to that plane. It is clear to accept that variation of the elements shape and their placement gives an infinite number of lattice types. However, for technological reasons, there are two commonly used types of the tow-dimensional photonic crystal lattice, square and hexagonal lattice [20] [21] ,these two types can be a 2D hole-type consisting of low refractive index cylinders in a high-index slab or a 2D rod-type consisting of high refractive index cylinders in a low-index background. The unit cell of the PhC with square lattice has the shape of square. The unit cell of hexagonal lattice has the form of regular hexagon as shown in figure 11. Two-dimensional square and hexagonal lattices generate photonic band gaps common to both polarizations. A dielectric structure with a hexagonal lattice of air holes requires a lower index contrast to generate a band gap and gives rise to larger gaps than a square lattice, also it is difficult to obtain a complete band gap using the square lattice. [22]

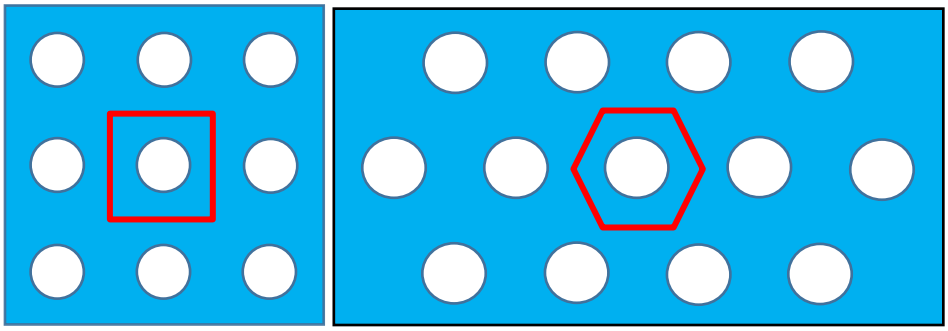

Figure 11 2D PhC lattice types (a) square lattice (b) hexagonal lattice. The red square and the hexagon represent the unit cell of square and hexagonal lattice respectively.

I.4.1 Bravais lattice.

We are interested in 2D dielectric periodic structure. First important concept in periodic structure is a Bravais lattice. Bravais lattice is an infinite array of discrete point with an arrangement and orientation that appears exactly the same from whichever of the points the array is viewed.

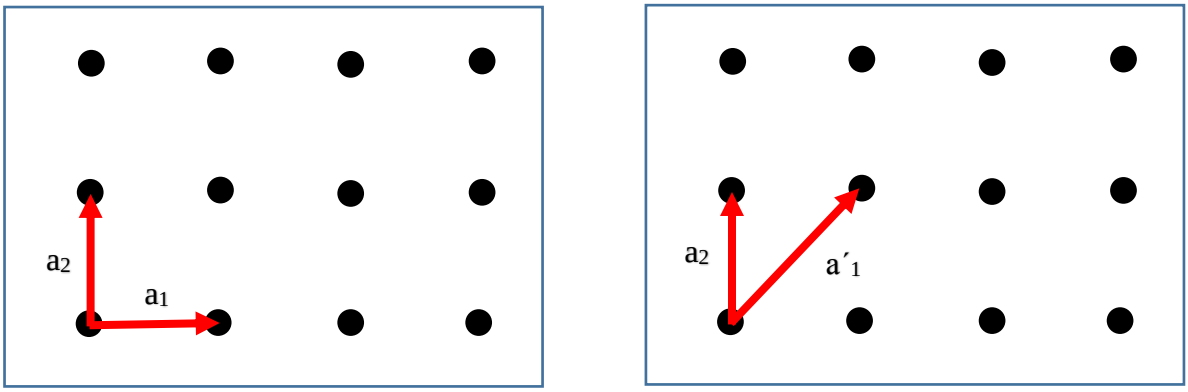

Figure 12 Bravais lattice for a square array of points.

The basis vectors a_1, a_2 are called primitive lattice vectors. They are not unique as shown in figure 12 We could choose basis vectors (a_1, a_2) or (a'_1, a_2).

A primitive unit cell is a region of space which, when translated by the primitive lattice vectors a_i, fills the space. Without overlapping and without leaving any gaps. These primitive unit cells are not unique as shown in figure 13, Each of the three possibilities shown below is a good unit cell.

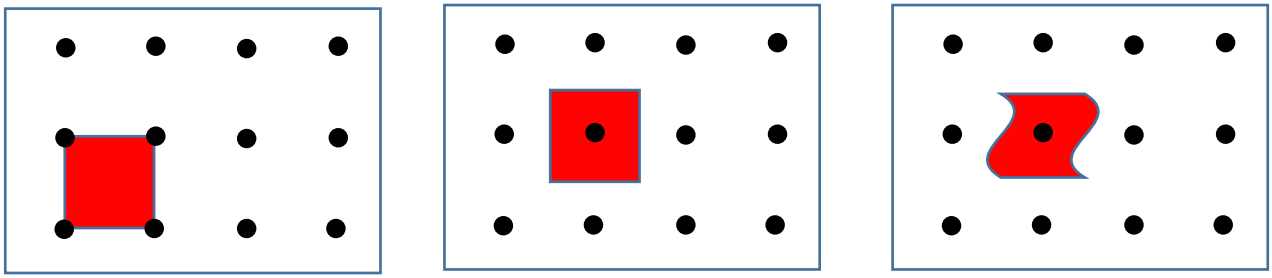

Figure 13 Primitive unit cell in different places.

A two-dimensional lattice is defined by two primitive vectors, non-parallel vectors a1, a2, so that each lattice point is given by [23] :

$$\vec{R} = m\vec{a}_1 + n\vec{a}_2 \qquad \text{I.1}$$

$\vec{R}$ is the lattice vector where m and n are integers.

Figure 14 represent the lattice vector of a square lattice with m=3, n=1.

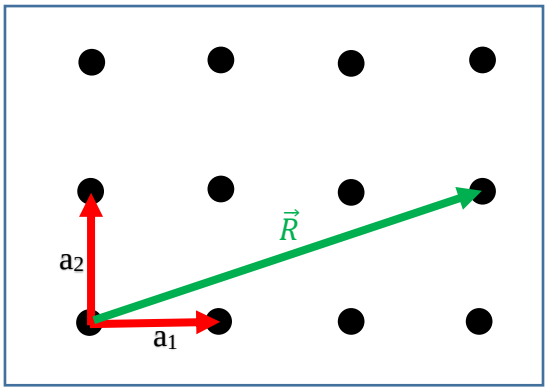

Figure 14 Lattice vector of a square lattice.

I.4.2 The Reciprocal Lattice

If we have the information about primitive lattice vectors of the PhC, we can obtain the primitive reciprocal lattice vectors. Reciprocal lattice just like lattice in coordinate space possesses the periodicity, that is, the translation symmetry. It means that if we take one of the cells and translate it over all possible reciprocal lattice vectors, we will fill whole wave vector space. Let consider the dielectric function in a photonic crystal lattice, the periodic dielectric distribution function [24] can be written as $\varepsilon(\vec{r})$, and $\varepsilon(\vec{r})= \varepsilon(\vec{r}+\vec{R})$ for all lattice vectors $\vec{R}$ as shown in figure 15.

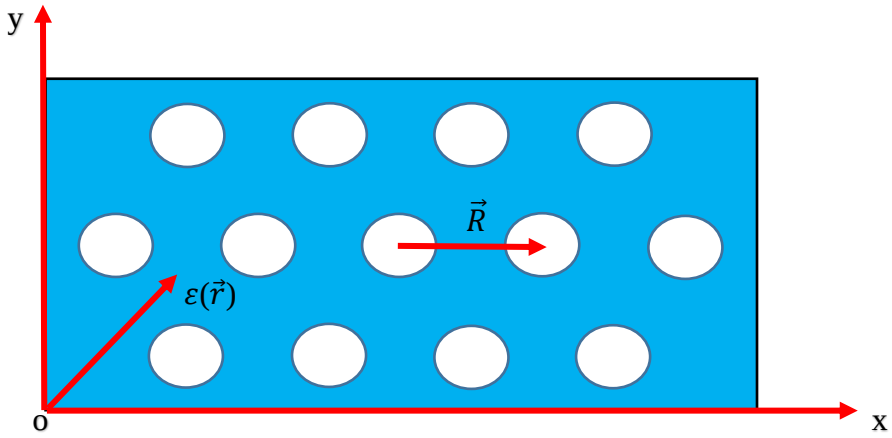

Figure 15 Schematic of hexagonal lattice shows the vector of dielectric distribution function.

For a periodic function, $f\ (\vec{r})$, we can write it's Fourier transform by:

$$f\ (\vec{r})=\int f(\vec{G})e^{i\vec{G}\cdot\vec{r}}\,d\vec{G} \qquad \text{I.2}$$

Also, we have

$f(\vec{r}) = f(\vec{r}+\vec{R})$ I.3

$f(\vec{r}+\vec{R}) = \int f(\vec{G}) e^{i\vec{G}\cdot(\vec{r}+\vec{R})}\, d\vec{G} = f(\vec{r}) = \int f(\vec{G}) e^{i\vec{G}\cdot\vec{r}}\, d\vec{G}$

the above equation is only valid for $f(\vec{G}) = 0$ or $e^{i\vec{G}\cdot\vec{R}} = 1$ for all $\vec{R}$.

We have $f(\vec{r}) = \sum_{\vec{G}} f_G\, e^{i\vec{G}\cdot\vec{r}}$

where the sum is over all $\vec{G}$ vectors such that $e^{i\vec{G}\cdot\vec{R}} = 1$ or $\vec{G}\cdot\vec{R} = 2\pi\cdot N$ for integer N.

the $\vec{G}$ vector form a lattice, the set of $\vec{G}$ vectors are called the reciprocal lattice, and the individual vector $\vec{G}$ are reciprocal lattice vectors.

Let's consider a triangular lattice with lattice vectors $\vec{a}_i$ in real space as shown in figure 16, we can construct the primitive reciprocal lattices with the lattice vectors $\vec{b}_j$ from the condition below

$\vec{a}_i \cdot \vec{b}_j = 2\pi \cdot \gamma_{ij}$ I.4

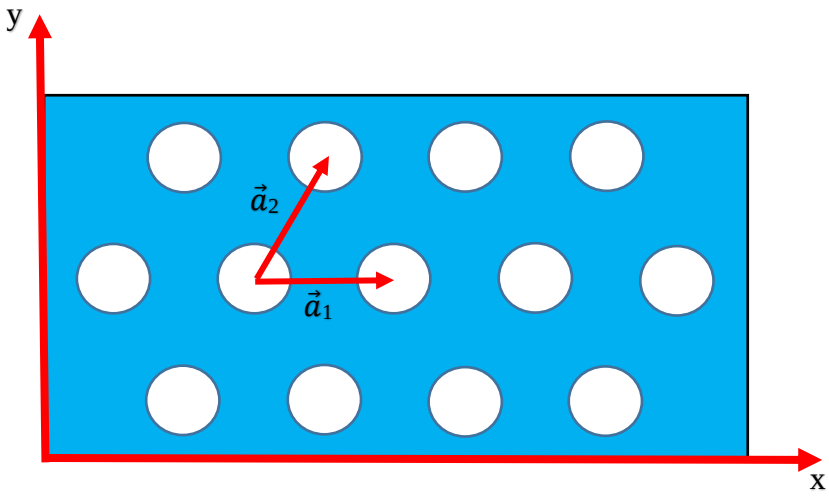

Figure 16 Triangular lattice with two basis vectors in the real space.

$$\vec{a}_i \begin{cases} \vec{a}_1 = a\hat{x} \\ \vec{a}_2 = \frac{a}{2}\hat{x} + \frac{\sqrt{3}}{2}a\hat{y} \end{cases} \quad , \quad |\vec{a}_1| = |\vec{a}_2|.$$

$$\vec{b}_i \begin{cases} \vec{b}_1 = \vec{b}_{1x}\hat{x} + \vec{b}_{1y}\hat{y} \\ \vec{b}_2 = \vec{b}_{2x}\hat{x} + \vec{b}_{2y}\hat{y} \end{cases}$$

For $\vec{a}_i \cdot \vec{b}_j = 2\pi \cdot \gamma_{ij}$

$$\vec{a}_1 \cdot \vec{b}_1 = 2\pi = a b_{1x} \qquad \Rightarrow b_{1x} = \frac{2\pi}{a}$$

$$\vec{a}_2 \cdot \vec{b}_1 = 0 = \frac{a}{2} b_{1x} + \frac{\sqrt{3}}{2} a b_{1y} \qquad \Rightarrow b_{1y} = -\frac{1}{\sqrt{3}} b_{1x} = -\frac{2\pi}{\sqrt{3}a}$$

$$\vec{a}_1 \cdot \vec{b}_2 = 0 = a b_{2x} \qquad \Rightarrow b_{2x} = 0$$

$$\vec{a}_2 \cdot \vec{b}_2 = 2\pi = \frac{a}{2} b_{2x} + \frac{\sqrt{3}}{2} a b_{2y} \qquad \Rightarrow b_{2y} = \frac{4\pi}{\sqrt{3}a}$$

So, we have $\vec{b}_i \begin{cases} \vec{b}_1 = \frac{2\pi}{a}\,\hat{x} - \frac{2\pi}{\sqrt{3}a}\hat{y} \\ \vec{b}_2 = 0\hat{x} + \frac{4\pi}{\sqrt{3}a}\hat{y} \end{cases}$ I.5

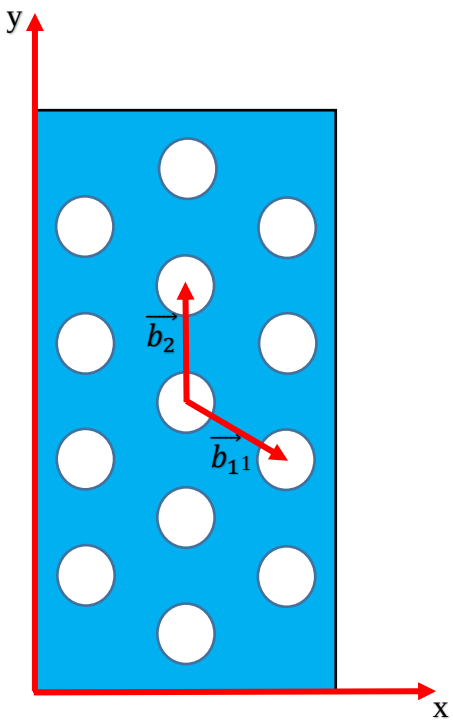

Figure 17 The reciprocal lattice for the triangular lattice.

The reciprocal lattice of triangular lattice is also a triangular lattice rotated by 90° as shown in figure 17.

For a square lattice with basis vectors $\vec{a}_i \begin{cases} \vec{a}_1 = a\hat{x} \\ \vec{a}_2 = a\hat{y} \end{cases}$

Its reciprocal lattice basis vectors are $\vec{b}_i$ $\begin{cases} \vec{b}_1 = \frac{2\pi}{a}\,\hat{x} \\ \vec{b}_2 = \frac{2\pi}{a}\,\hat{y} \end{cases}$ I.6

I.4.3 Brillouin Zone

The region of all allowed wave vectors is called a Brillouin zone, let consider a square lattice, to determine the Brillouin zone geometrically, we draw perpendicular bisectors of every lattice vector that starts at the origin. Each bisector divides the lattice into two half-planes, one of which contains our lattice point. The intersection of all the half-planes that contain our lattice point is the Brillouin zone [11]. The square lattice vectors, its reciprocal lattice vectors, and its Brillouin zone are shown in figure 18.

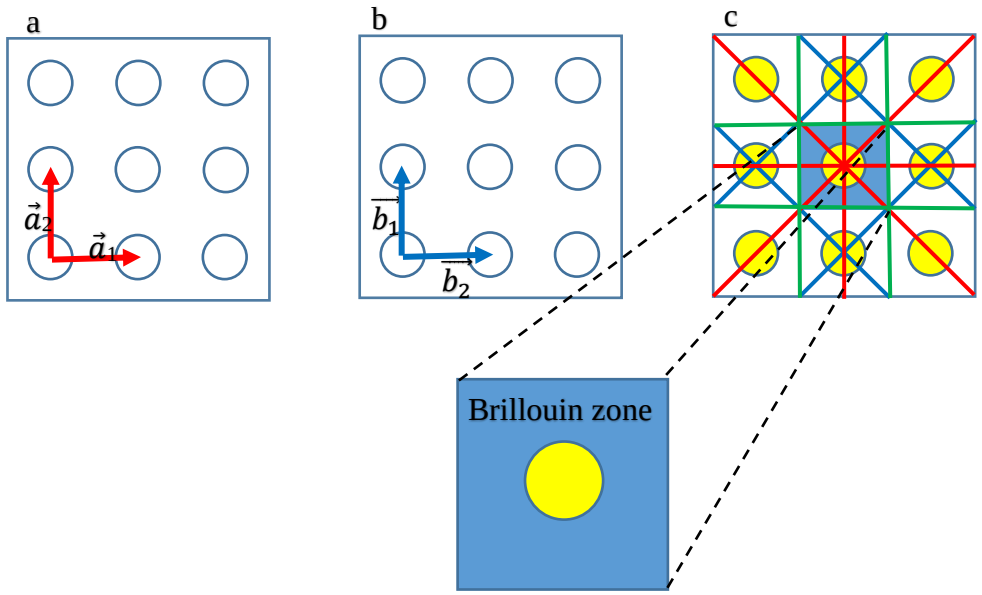

Figure 18 The square lattice. (a) the lattice in real space. (b) the corresponding reciprocal lattice. (c) the construction of the first Brillouin zone.

The same way we obtain the Brillouin zone of triangular lattice as shown in figure 19.

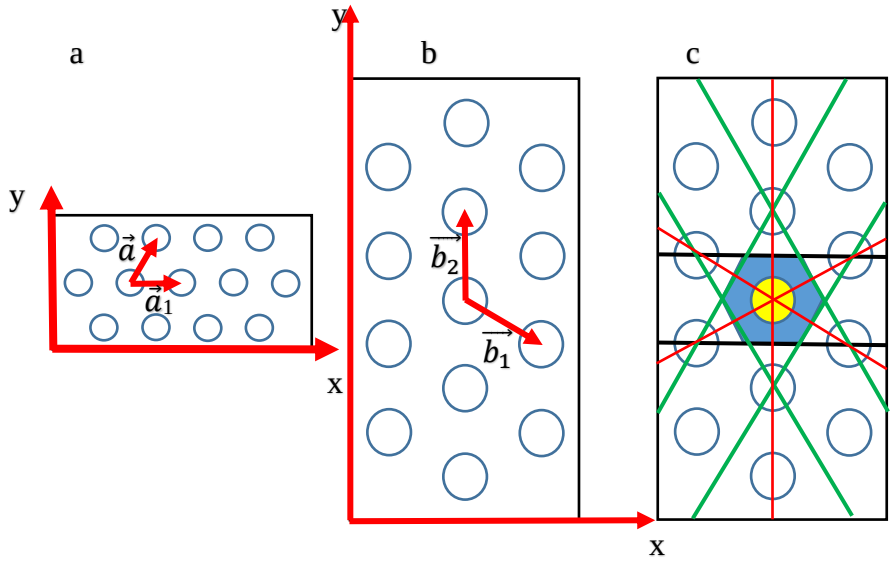

Figure 19 The triangular lattice. (a) the lattice points in real space. (b) the corresponding reciprocal lattice, (c) the Brillouin zone construction. In this case, the first Brillouin zone is a hexagon centered around the origin.

I.4.4 The Irreducible Brillouin Zone

If the field is known at every point inside a single unit cell, then it is also known at any point in an infinite lattice because the field takes on the same symmetry as the lattice so it just repeats itself. Since the reciprocal lattice uniquely defines a direct lattice, knowing the solutions to the wave equation at each point inside the reciprocal lattice unit cell also defines the field everywhere in the infinite reciprocal lattice. Many times, there is still additional symmetry to exploit so the smallest volume of space that completely describes the electromagnetic wave can be smaller than the unit cell itself. The smallest volume of space within the Brillouin zone that completely characterizes the field inside a periodic structure is called the irreducible Brillouin zone. It is smaller than the Brillouin zone when there is additional symmetry to exploit [25]. The irreducible Brillouin zone is the triangular wedge in the upper-right corner; the rest of the Brillouin zone can be related to this wedge by rotational symmetry. The wavenumber k moves along the triangular edge of the irreducible Brillouin zone, from Γ to X to M, as shown in the figure 20 The red triangle represent the irreducible Brillouin zone and the black lines present the edges of the IBZ.

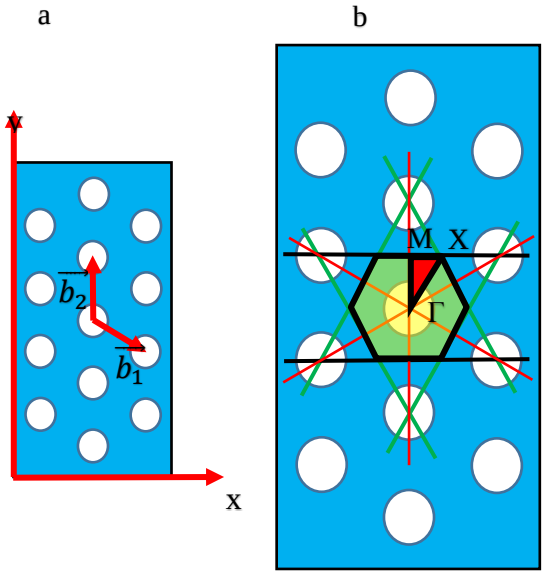

Figure 20 (a) Reciprocal lattice of triangular lattice, (b) the irreducible Brillouin zone (red triangle)

I.4.5 The origin of the photonic band gap in 2D photonic crystals

The existence of a photonic band gap gives rise to a number of interesting and useful properties, the band gap in the photonic crystals is one of the most important parameters, by controlling the band gap characteristics we can manipulate a photon in much the same way that a semiconductor manipulates electrons [26]. 2D photonic crystal band gap can be obtained by the lattice geometry and the parameters (n, a, r) where "n" is the refractive index "a" the lattice constant and "r" the radius, respectively.

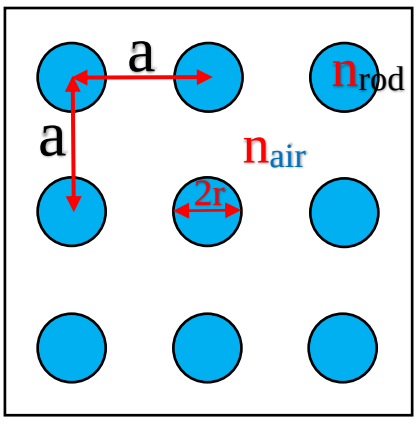

Figure 21 Rectangular dielectric rod array

To clarify the nature of photonic band gaps, let's consider the 2-D photonic crystal with rectangular dielectric rod array, a cross section of this crystal is shown in figure 21.

The rectangular structure has a lattice constant a=1 nm, the refractive index of rod n=3 and the radius of rod r=0.2a nm, the background refractive index is air n=1.

With plan-wave expansion method (PWM), we calculated the band structure ω(k) for TE polarization with fields along (H_z, E_x, E_y), and TM polarization, with fields along (E_z, H_x, H_y), as shown in figure 22. The band structures for TE and TM modes can be completely different. It is possible, for example, that there are photonic band gaps for one polarization but not for the other polarization. For simplicity we consider only the gap between the first (band 0) and the second bands (band 1), which we call the dielectric and the air bands.

Clearly for the TM modes (blue curves), this photonic crystal has a complete band gap between the first and second bands in the normalized frequency range of 0.3207 (ωa/2πc) and 0.4416 (ωa/2πc). In contrast, for the TE modes (red curves) there is no complete band gap. We should be able to explain such a significant fact, and we can, by examining the field patterns in figures 22. The field associated with the lowest TM mode (the dielectric band m=0 where m is the number of band) is strongly concentrated in the dielectric regions. This is quite the opposite with field pattern of the air band.

There, a nodal plane cuts through the dielectric columns, expelling some of the displacement field amplitude from the high-ε region [27] [28].

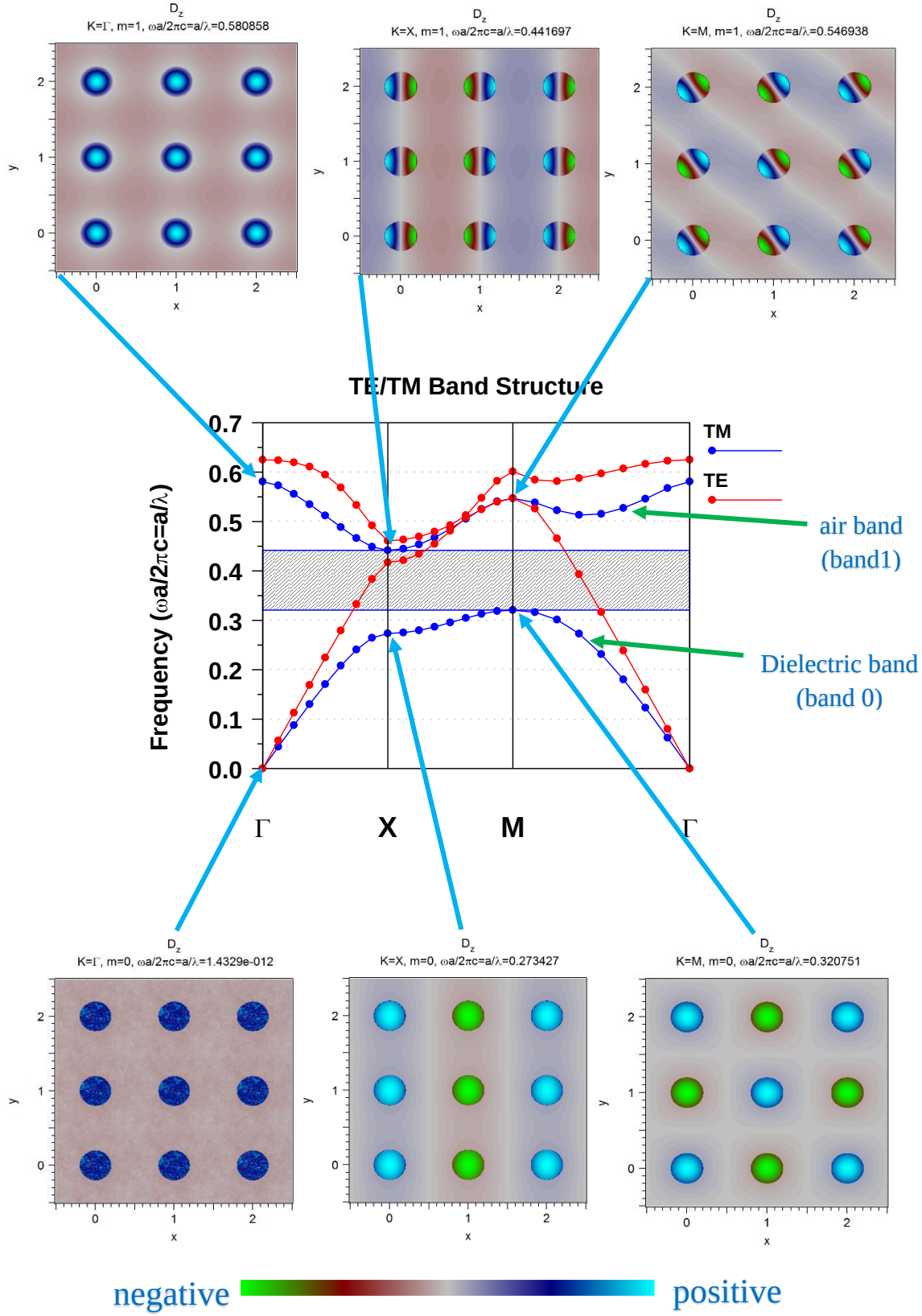

Figure 22 The photonic band structure and the Displacement fields of TM for a square array of dielectric rod with r=0.2a. The blue bands represent TM modes and the red bands represent TE modes.

We see in figure 22. The field patterns of the TM modes of the first band (*dielectric band m=0*) and second band (*air band m=1*), we have noticed that:

1. For modes at the Γ point, the field pattern is exactly the same in each unit cell.
2. For modes at the X point (the zone edge), the fields alternate in sign in each unit cell along the direction of the wave vector Kx, forming wave fronts parallel to the *y* direction.
3. For modes at the M point, the signs of the fields alternate in neighboring cells, forming a checkerboard pattern.

Although the X and M patterns may look like wave fronts of a propagating wave, in fact the modes at these particular **k** points do not propagate at all, they are standing waves with zero group velocity.

The field patterns of the TE modes at the X point for the first and second bands are shown in figure 23. The concentration factors for the TE modes do not contrast as strongly. This is reflected in the field configurations for the lowest two bands, this is the origin of the low concentration factors, and the explanation for the absence of a band gap for TE modes [27].

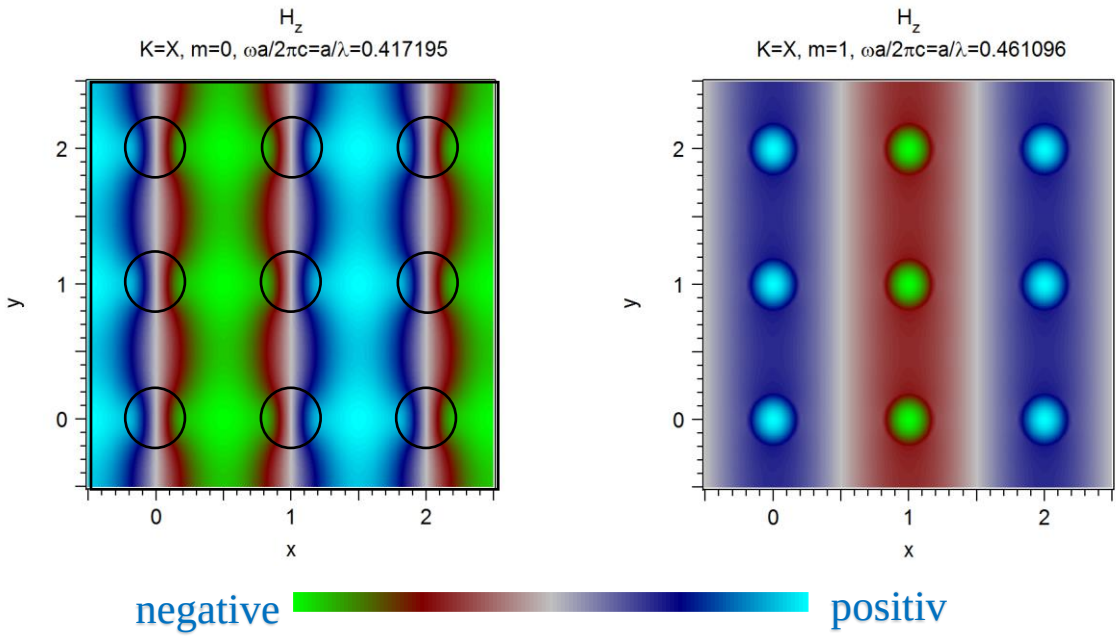

Figure 23 Magnetic fields of the symmetry X point TE states inside a square array of rod dielectric (ε=9).

I.4.6 Complete bad gap for both TE and TM:

In previous section, dielectric structures which had band gaps for individual polarizations were found. In this letter, we present a 2D structure in which these band gaps overlap to form a complete gap which prevents the in-plane propagation of light of any polarization. At the dielectric contrast of GaAs (ε=13), the combination which was found to have a photonic band gap in both polarizations was the triangular lattice of air columns in dielectric which occurs when the radius of the air columns was r=0.48a, where a is the lattice constant. The gap appears in this structure for dielectric contrast for both polarization TE and TM which called complete photonic band gap as shown in figure 24 [29].

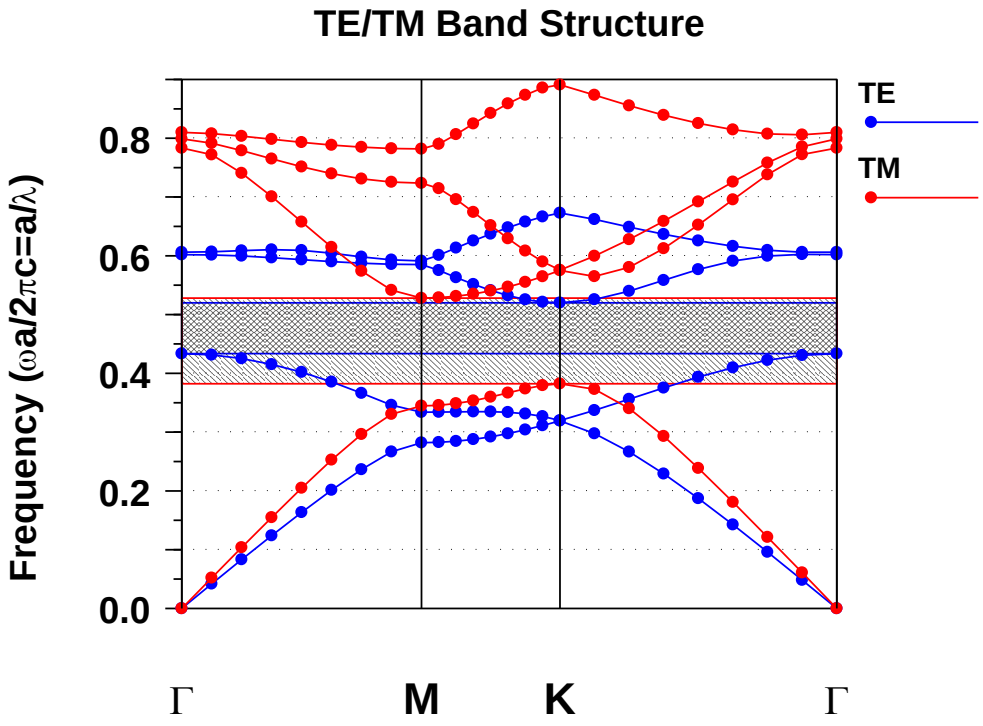

Figure 24 The photonic band structure for the modes of a triangular array of air holes drilled in a dielectric substrate (ε=13). The blue lines represent TE bands and the red lines represent TM bands.

I.5 Defect in two-dimensional photonic crystals

the most interesting applications of photonic crystals are associated with imperfections or defects in a periodic structure. If a small defect is introduced in the photonic crystal, a mode (or group of modes) can be created within the structure at a frequency which lies inside the gap. The defect behaves like a microcavity surrounded by reflecting walls. If the defect has the proper size to support a state in the band gap, and if the radiative transition frequency of the atom matches that

of the defect state, the rate of spontaneous emission will be enhanced [30]. For more illustration we consider a rectangular array of dielectric rods in air that we have seen it before in figure 21 and the corresponding band gap in figure 22. The square lattice exhibits a broad TM gap. We create a defect point (cavity) and line defect (waveguide) in the square lattice as we see below [31] [32]:

I.5.1 The cavity

We can create imperfections that may trap light at a point within the crystal. One class of imperfections of this type involves changing the dielectric medium in some local region of the crystal. Therefore, by simply removing the central rod from the lattice as shown in figure 25 we create a cavity inside the structure, which is effectively surrounded by reflecting walls. If the cavity has the proper size to support a mode in the band gap, then light cannot escape, and we can pin the mode to the defect.

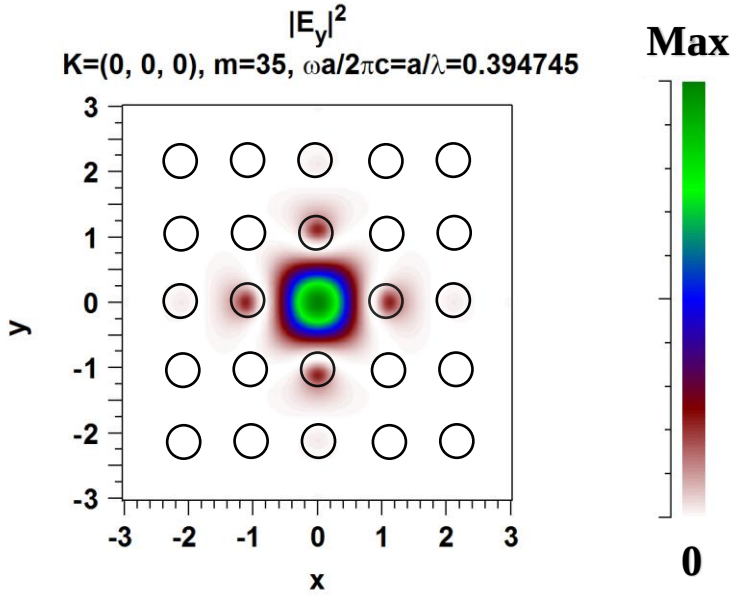

Figure 25 Localized mode profiles of Electric-field of the cavity inside a square lattice rods in air.

I.5.2 Main important parameters of a photonic crystal cavity:

The electric field of the microcavity mode will be enhanced by a scale of Q/V in a photonic crystal microcavity, where Q and V are the quality factor and the mode volume of the photonic crystal microcavity, respectively

I.5.2.1 The quality factor Q:

according to the photon localization theory, the microcavity photon lifetime t can be calculated by $\tau = Q/\omega_0$, where Q and ω_0 are the quality factor and the resonant frequency of the photonic crystal

microcavity, respectively. Therefore, the higher the quality factor Q gets, the longer the microcavity photon lifetime τ is. Quality factor Q is an important parameter for a cavity it mainly describes the photon life time inside the cavity, A common, very general definition for Q is 2π times the 'stored energy' divided by the 'energy lost per oscillation' as follow [33]:

$$Q = 2\pi \frac{\text{stored energy}}{\text{energy lost per oscillation}} = \frac{2\pi}{T} \times \frac{W}{-dW/dt} = \omega_0 \times \frac{W}{-dW/dt} \quad \text{I.6}$$

Where W is the stored energy, T time of cycle and ω_0 resonance frequency.

Also, we can obtain the quality factor Q value from the spectrum and is defined as:

$$Q = \frac{\omega_0}{\text{FWHM}} = \frac{\omega_0}{\Delta\omega} \quad \text{I.7}$$

where ω_0 is the resonant frequency and FWHM is the full width half max of the resonance intensity spectrum figure 26 illustrate how to calculate the quality factor Q from the spectrum.

High quality factor implies a strong photon localization effect of photonic crystal microcavity, which will result in an intense interaction of light and matter in the microcavity.

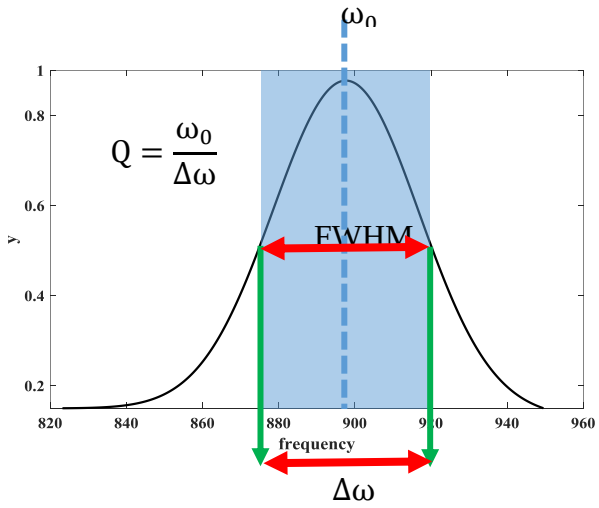

Figure 26 Schematic illustrate how to calculate the quality factor from the spectrum.

I.5.2.2 The modal volume V

This parameter describes the spatial confinement of light within the cavity and corresponds to the actual volume occupied by the field. The modal volume is defined as [34]:

$$V = \frac{\int \varepsilon(r)|E(r)|^2 d^3r}{(\varepsilon(r)|E(r)|^2)_{max}} \quad \text{I.8}$$

Where E(r) is the electric field distribution of the mode.

There are two disadvantages when the modal volume V value increase: the first the large V limits the degree of miniaturization of components. The second is that a large modal volume often translates into a large power requirement.

I.5.3 Examples of photonic crystal cavities

Photonic crystal cavities can be used for various purposes. Which photonic crystal cavity is the best choice strongly depends on the application itself. They can be classified into three categories [11]: point defect cavity, line defect cavity, double heterostructure.

I.5.3.1 Point defect cavity

The simplest kind of photonic crystal cavity can be formed by introducing a point defect into the perfectly periodic photonic crystal structure. A point defect involves a modification of a single hole inside the crystal. The hole can be changed in size and dielectric properties as shown in figure 27.

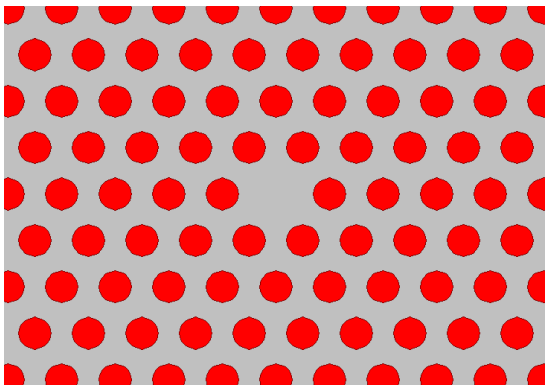

Figure 27 Photonic crystal structure with a point defect cavity.

I.5.3.2 Line defect cavity

A line defect cavity is an extension of a point defect cavity. In this case the defect is extended over several lattice constants in a row as shown in figure 28.

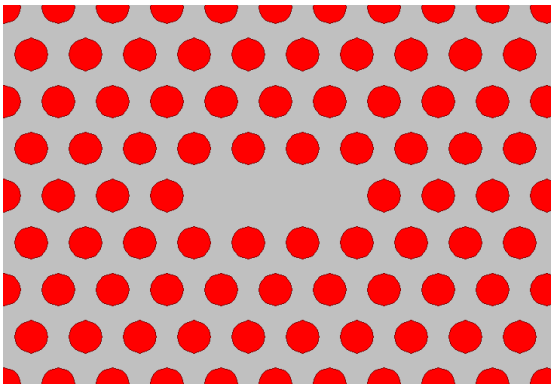

Figure 28 Line defect cavity L3 in 2D PhC structure.

I.5.3.3 Double heterostructure

A photonic crystal heterostructure consists of two photonic crystal line defect waveguides with different lattice constants. A double heterostructure consists of three-line defect waveguides as shown in figure 29.

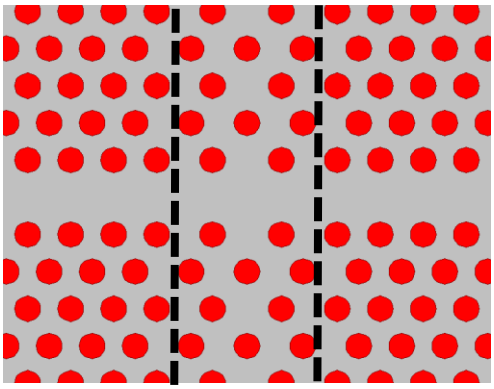

Figure 29 Photonic crystal double heterostructure cavity.

I.5.4 The waveguide

Another type of defect is line defect, we can guide light from one location to another, the light that propagates in the waveguide with a frequency within the band gap of the crystal is confined to it, and can be directed along the waveguide, as shown in figure 30 light that propagates in the waveguide with a frequency within the band gap of the crystal is confined to the defect, and directed along the defect, we use a square array of parallel, infinitely long high dielectric rods in air. The removal of a row of rods breaks the periodicity in one spatial direction. As an example, we assume GaAs rods of circular cross section, with an index of refraction of 3.4, appropriate at optical wavelengths, the largest TM band gaps occurs when the rods have a radius r=0.18a [35] as we see below:

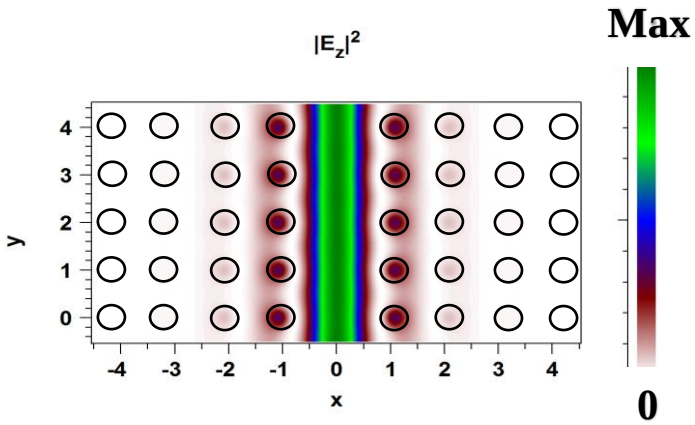

Figure 30 Electric field pattern for the linear defect mode

In figure 31 (a) we show the band structure for the guide created by removing a row of rods in the propagation direction of the waveguide. We find a single guided mode inside the band gap. In Figure 31(b) the waveguide is made by removing three rows of rods in the propagation direction of the crystal. There are now three guided modes inside the gap. It is generally true that the number of bands inside the band gap equals the number of rows of rods removed when creating the guide.

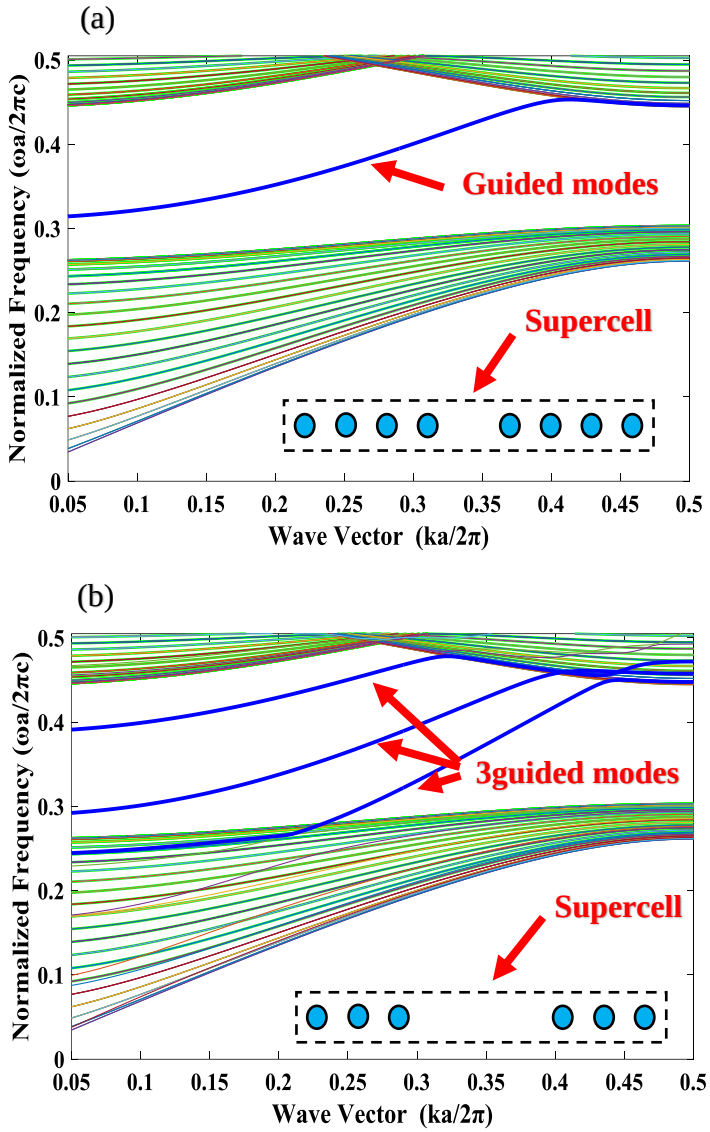

Figure 31 Projected band structure for the line defect (a) formed by removing a row of rods (b) formed by removing 3 rows of rods.

In all the previous sections we considered that the rods or holes of air are infinitely tall in the third direction, now we investigate the case of structure with two-dimensional periodicity but finite extent in the third direction, such structures are known as photonic crystal slabs.

I.6 Photonic crystal slabs:

The discovery of photonic crystals, periodic dielectric materials with a photonic band gap, has opened up new methods for controlling light, leading to proposals for many novel devices. Straightforward application of these results to three dimensions requires a structure with a three-dimensional band gap. Fabricating such structures, however, has been a challenge because they tend to have complex three-dimensional connectivity and strict alignment requirements. Such designs have been the subject of many recent developments. An alternative system, the photonic-crystal slab, has been proposed that promises easier fabrication using existing techniques. This is a dielectric structure that has only two-dimensional periodicity and uses index guiding to confine light in the third dimension. Photonic crystal slabs retain or approximate many of the desirable properties of true photonic crystals, but at the same time are much more easily realized at submicron length scales [36].

We are now going to consider the photonic crystals with a finite thickness as shown in figure 32. A square lattice of rods in air with lattice constant a, radius r=0.2a um and height of 2a. also a triangular lattice of air holes in dielectric, with lattice constant a and radius 0.45a with thickness 0.6a, the dielectric constant of the high index material is ε=12. As we see in figure below the band diagram for both square and triangular slabs, the slab of rods has a gap in its odd modes and the slab of holes has a gap on its even modes, respectively.

A ‘‘band gap’’ It is not a true band gap because there are still radiation modes at those frequencies over the light line (purple line). If we restrict the photonic lattice to a finite thickness then we expect that there will be modes guided by the dielectric slab and radiation modes. Thus, the modes below the light line are guided by the dielectric slab and above the light line the modes are leaky.

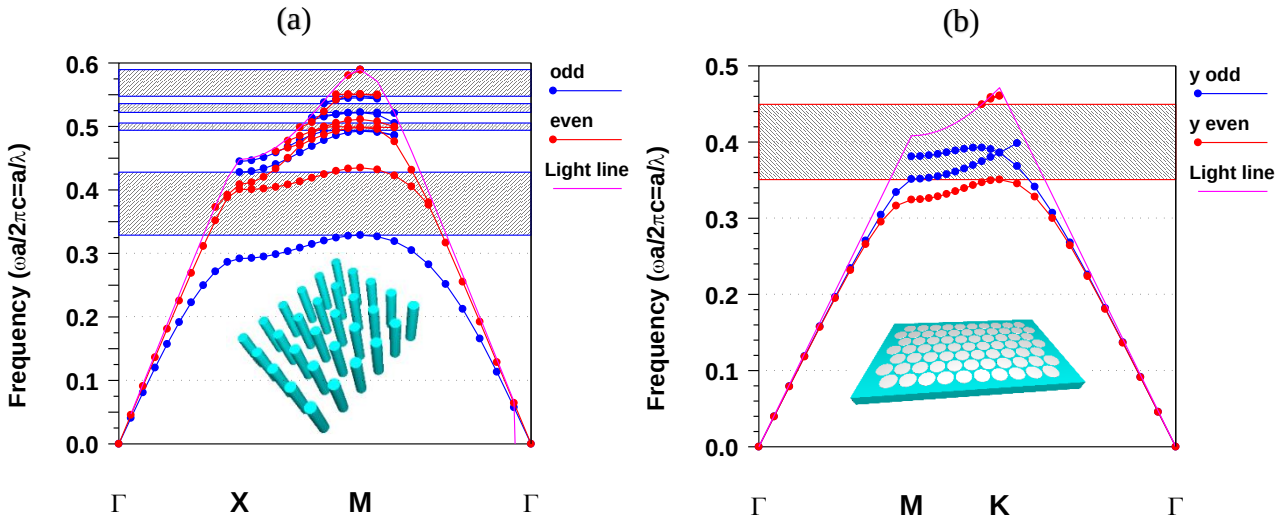

Figure 32 Band diagrams corresponding to the two slabs (a) square lattice of rods in air (b) a triangular lattice of air holes in dielectric.

I.7 Photonic Crystal applications

The majority of applications of photonic crystals utilize the phenomenon of photonic bandgap (PBG) which construct and realize micro/nano-scale integrated photonic devices. In recent years, Many of the promising applications of two and three dimensional photonic crystals obtained in the fabrication of high-quality photonic crystal samples, various integrated photonic devices have been realized as shown in figure 33 [37], such as sensors [38] filters [39] All-optical switching and logic device are essential components of optical computing and ultrahigh-speed information processing systems. The concept of photonic crystal all-optical switching was proposed by Scalora et al. In 1994 and has been reported lately in by Xiaoyong hu et al in 2008. [40] [41]. Photonic crystal filter has great potential applications in the wavelength division multiplex (WDM) systems. Optical channel of the filter can be formed by the photonic crystal microcavity mode. Moreover, multichannel and narrow-band filter can also be realized based on the coupling of several identical photonic crystal microcavities [42] [43] . We have mentioned some examples of applications of photonic crystals but not all applications. Because they are countless. The evolution of photonic crystal applications will certainly lead to a new technological revolution and photonic crystals will be the technology of the near future.

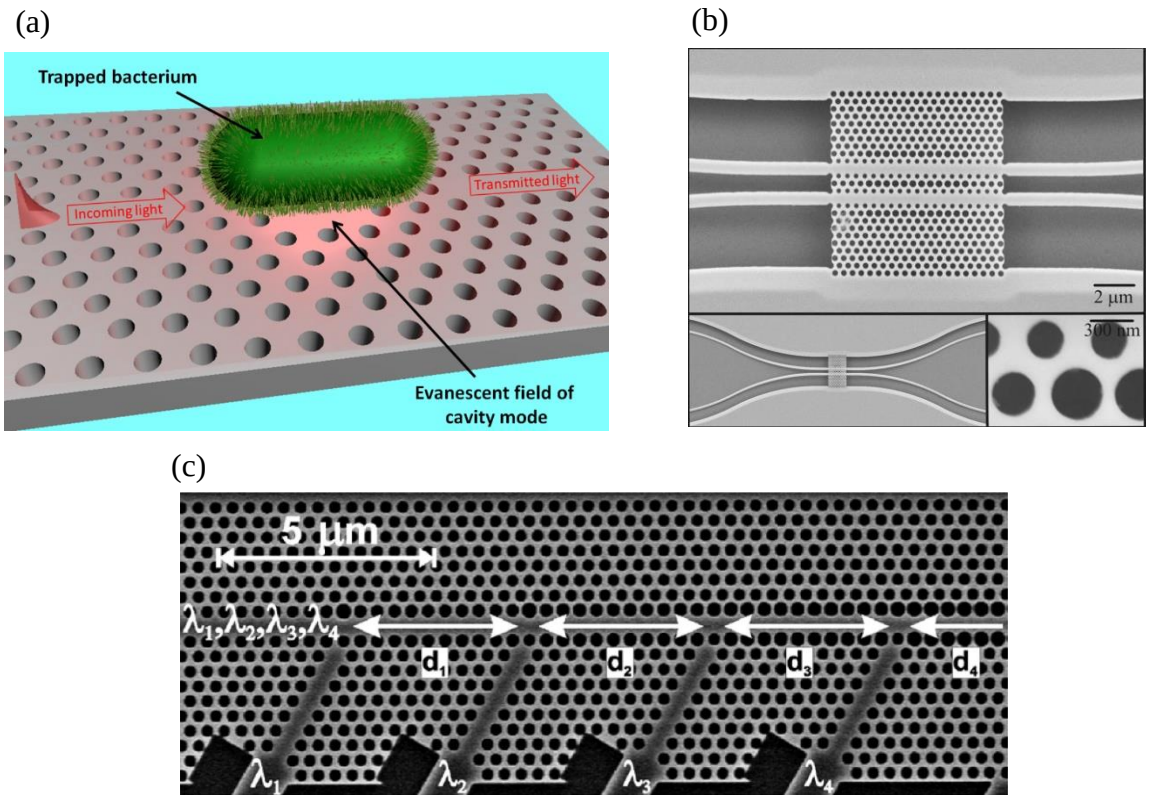

Figure 33 (a) A bacterium in streaming water is attracted to the cavity by the optical trapping force exerted by the resonant evanescent field [38] (b) Scanning electron micrographs of the directional coupler switch [47] (c) SEM of fabricated four-channel demultiplexer [151]

I.8 Conclusion

In this chapter we presented the fundamental concepts of photonic crystals, among these concepts the most important property of the photonic crystals is the photonic band gap (PBG): certain frequencies do not pass through the PhC structure. We also showed the origin and the existence of the photonic band gap. We have introduced the physical, geometrical properties and the different optical properties of photonic crystals as cavities and waveguides that may result from these materials. Preventing light from propagating in certain directions with specified frequencies and controlling the pathways of light is very promising for producing and construct integrated optical devices.

Chapter II

Slow light in Photonic Crystals

Chapter II Slow light in Photonic Crystals

II. **Introduction**

The speed of light in vacuum is extremely fast (c ≅ 3 ×108 m/sec). Light can travel 30 cm in just 1ns. Recently, investigations into reducing the speed of light have been receiving considerable attention from many researchers, with the keyword being slow light [44]. Since the slow light effect was first time demonstrated in line-defect waveguides in 2001 by Notomi et al [45]. Many publications appeared concerning different possible applications. Such as optical delay line [46] optical switching [47]. The novel generation information networks, path switching of optical packets at network nodes have a great important and it is a solution that can perform the task with high data rate, low power consumption, the optical processing based on photonic routers are being developed in order to avoid the conversion from optical to electronic and vice versa. For stores and a adjust the timing of optical packets we need a buffer, an optical buffer instead of mechanical variable delay lines with an optical switch because the old solutions are not ideal due

to their slow response. By controlling the velocity of light with a response speed much faster that the mechanical method we could use it not only for buffering but also for various types of time-domain processing such as re-timing and multiplexing [7] also, the Linear effects, such as phase sensitivity to refractive index changes, scale with the group index of light [48], allowing to reduce the size, and consequently the operating power, of devices such as modulators [49] [50], switches [47] and wavelength converters [51]. Nonlinear effects are also enhanced due to slow light [52] [53] [54] [55] [56], In addition, slow light offers the opportunity to compresses optical signals and optical energy in space as shown in figure 34. When an optical pulse travels in a slow-light waveguide, will be spatially compressed when entering the slow light regime. The front of the pulse, entering the slow light regime first, will travel slower than the back of the pulse which therefore catches up. The resulting pulse will occupy less space, it will be 'spatially compressed' without changing its properties in terms of time and spectrum. If we further assume that no energy is lost at the interface, the same amount of energy is concentrated in a smaller volume, so the intensity of the pulse increases, which reduces device footprint and enhances light-matter interactions [57]. The term 'slow light' refers to a reduction in the group velocity of light. Photonic crystal (PhC) line defect waveguide (W1) is one of the most suitable and attractive structures for realizing the slow light effect. This is because such a line defect structure operates at room temperature and has a high potential for on-chip integration by modifying the initial PhC structure. The photonic crystal line defect waveguide W1 allows ultra-small components and low group velocity vg due to its strong optical confinement by the photonic bandgap (PBG). The line defect waveguide formed by removing dielectric material along one of the directions of the photonic crystal lattice, the defect into the PhC creating a localized band that falls within, and is guided by the photonic band gap [58]. In this chapter we deal with slow light in photonic crystal waveguides based on line defects.

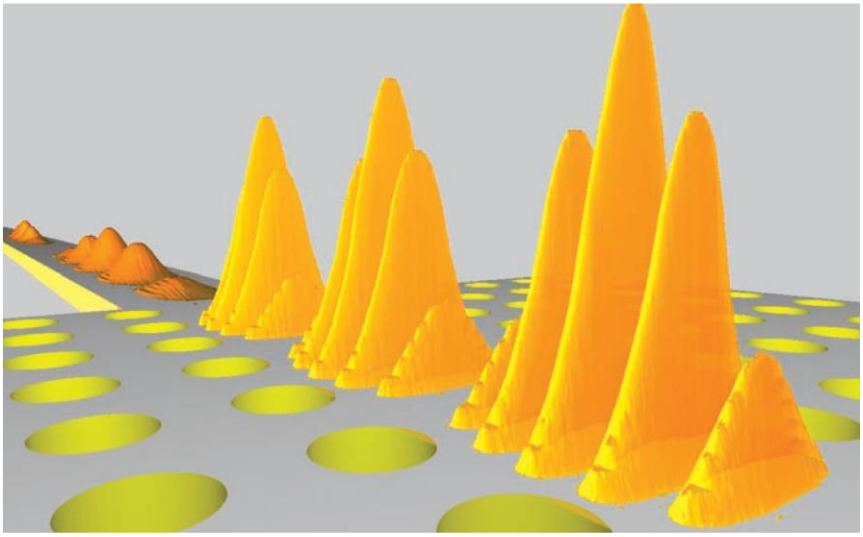

Figure 34 Illustration of the slow-light intensity enhancement. As a light pulse (left) enters a photonic-crystal waveguide operating in the slow-light regime, the pulse length is compressed resulting in increased intensity [5] .

II.1 Basic concepts of slow light

II.1.1 What is slow light?

It is common knowledge that, in vacuum, light propagates with constant velocity $c \cong 3 \times 10\text{^}8$ m/sec. But the velocity of light in a medium is related to the refractive index of the medium, where could be divided into the phase velocity and group velocity. The phase velocity and the group velocity are given by [44]:

$$v_p = \frac{c}{n} = \frac{w}{k} \qquad \text{II.1}$$

When *n* is the refractive index of the medium in which light travels, the speed of light propagation in the medium will be *c*/*n*. Thus, *n* is the index indicating the deceleration of light. The group refractive index *n*g is used in the place of *n*, and the velocity of optical pulses is usually expressed in terms of the group velocity

$$v_g = \frac{c}{n_g} \qquad \text{II.2}$$

Here, v_g is given by dw/dk for the angular frequency of light ω and its wavenumber *k*. In a vacuum, v_g =c since $k = w/c$. In a material and/or structure which have a large first order dispersion coefficient, v_g can be greatly reduced.

II.1.2 How do we slow a wave?

For controlling the velocity of light and slow it down, there are two standard methods. One using material induced dispersion and the other using structural induced dispersion. One of the materials that induced dispersion we mention the electromagnetically induced transparency (EIT) process was used as the slow light mechanism in the celebrated demonstration of Lene Hau. Which reduced the speed of light to 17 m/s in an ultra-cold gas of atoms [6]. By structural slow light, one means that the propagation of light pulses is significantly modified by the (typically periodic on distances scales of the order an optical wavelength) spatial modulation of the optical properties of a material system. A well-known example of such behavior is that of photonic crystals. PhCs are formed by a periodic modulation of the local dielectric constant in either one, two, or three dimensions. By inducing defects in the periodic structure, devices such as resonators and waveguides can be formed [9]. As we have stated before, that the line defect waveguide is one of the most suitable and attractive structures for realizing the slow light effect. We will focus on the two-dimensional triangular lattice photonic crystals with rod-shaped air holes in silicon where the line defect waveguide is obtained by removing out a row of holes from the middle of the photonic crystal along the propagation direction as shown in figure 35. The waveguide can guide light from one location to another, Light propagates through the defect, confined by total internal reflection in the vertical direction and Bragg reflection, due to the PBG, in the lateral direction [59] [60]. Our objective in this chapter is to provide a better understanding of the slow light in photonic crystal waveguide, for this purpose, we will discuss the results and do a re-simulation of the paper that reported by Li et al in ref [61] as follow:

The photonic crystal structure, sequentially, from top to bottom an air layer / silicon (Si) / silica (SiO2) The SOI (silicon on insulator) substrate consisting of silicon (Si) layer with thickness of 220 nm and silica layer with thickness of 2000 nm. The PhC formed by a triangular lattice structure with a lattice constant a=414 nm, the radius is r=0.286a, the waveguide is formed by removing the row of holes as shown in figure 35.

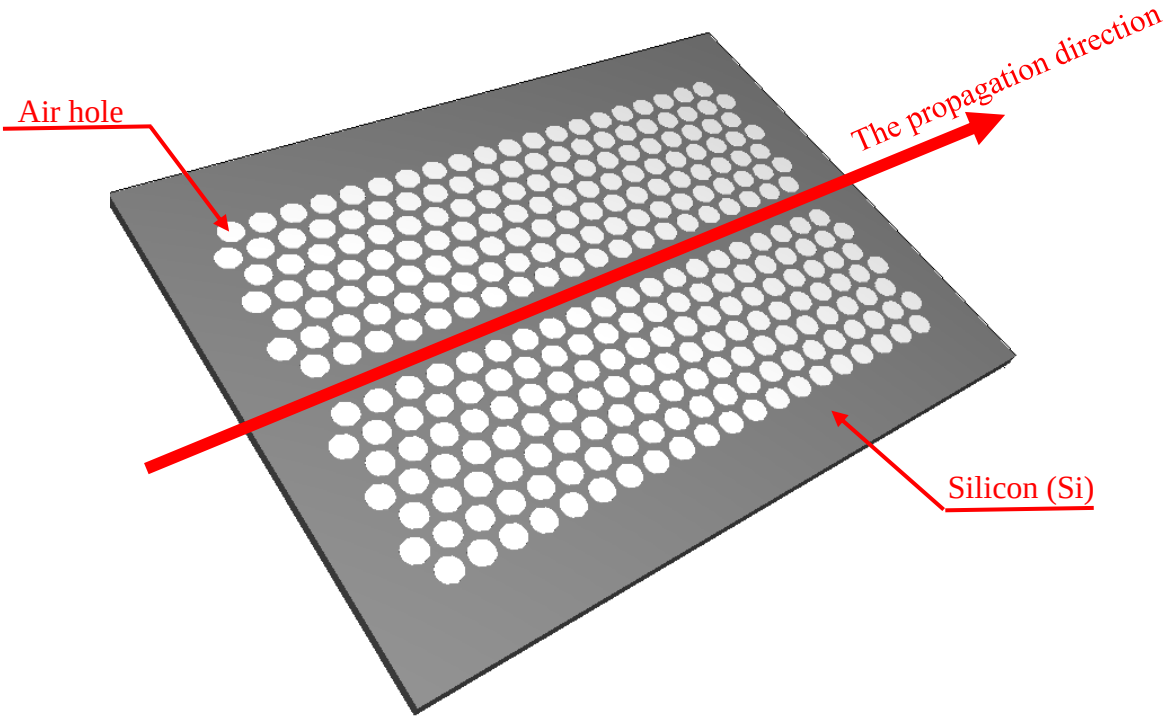

Figure 35 line defect waveguide W1

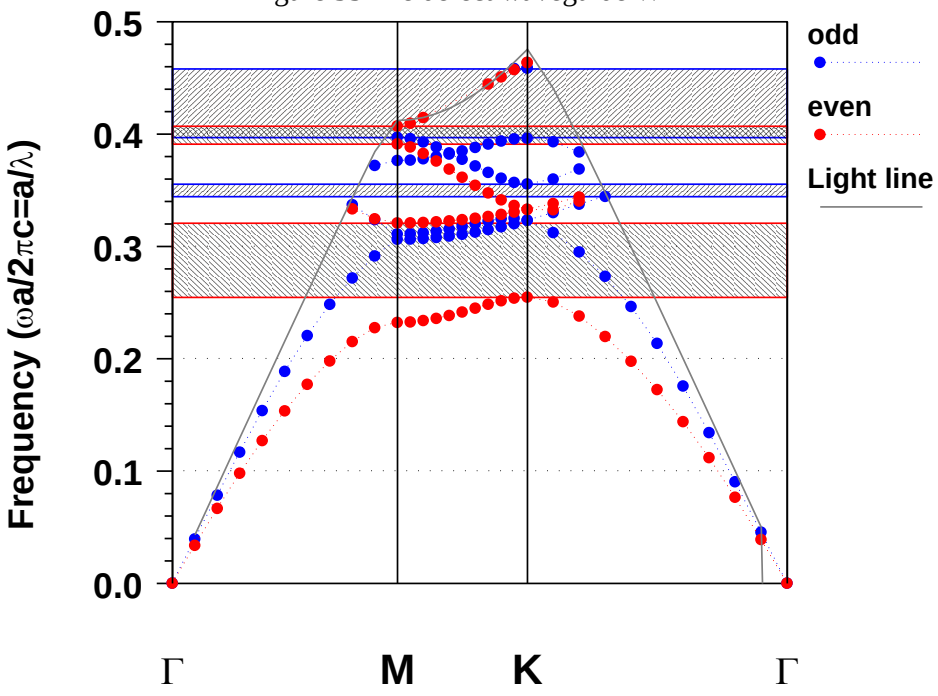

Figure 36 The computed band diagram for a Photonic crystal slab

As we see in figure 36, we notice that for the even mode, there is a large gap in the normalized frequency range of 0.2546 (ωa/2πc) and 0.3206 (ωa/2πc).

II.2 The waveguide band diagram

The dispersion diagram for the line defect waveguide gives us information about the propagation properties of electromagnetic radiation within the photonic crystal. It is a representation in which the available energy states are plotted as a function of propagation direction. The dispersion diagram for the W1 shown in figure 37 have two guided modes, the odd and even modes by solid blue and red curves, respectively. The light confined in the vertical direction of the slab by the index guiding (total internal reflection). In the diagram only, the frequencies below the light cone (the area dotted by green points) are guided, whereas modes above the light cone become leaky.

the band diagram computed for a three-dimensional photonic crystal slab. Light can be localized in all three directions through use the confinement in the directions of the two-dimensional plane by the photonic band-gap and the total internal reflection in the third direction. This type of structures is widely used and easy to fabricate Instead of the complicated three-dimensional photonic crystals [36]

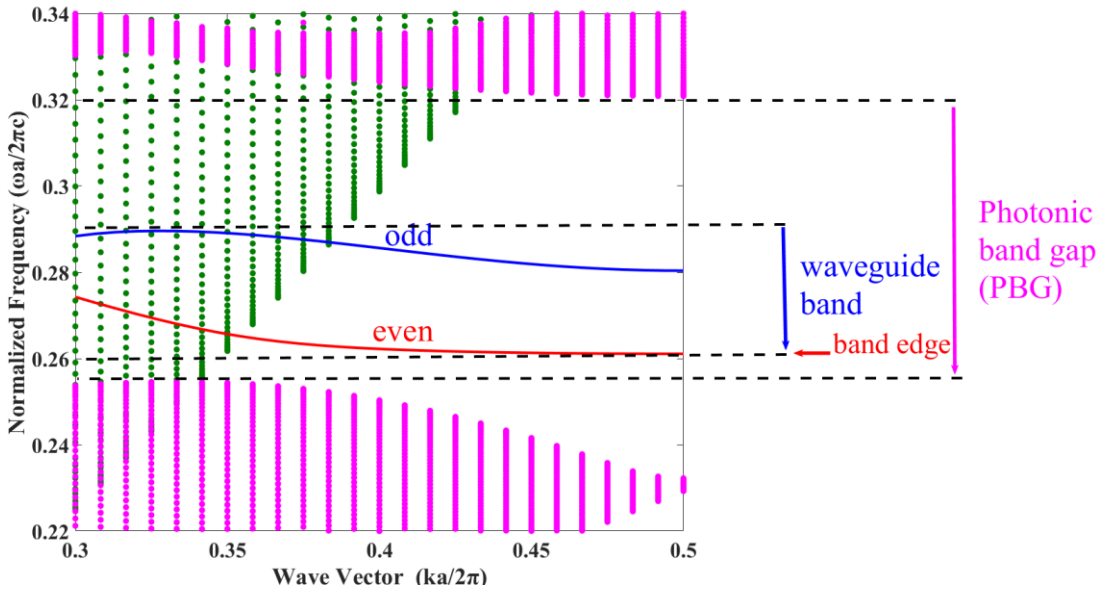

Figure 37 Dispersion diagram of line defect waveguide.

II.3 The group velocity and the group index

The relationship between the group v_g velocity and frequency is given as

$$v_g = \frac{dw}{dk} = \frac{c}{n_g} \quad \text{II.3}$$

Where k is the wavevector and n_g is the group index.

The group velocity vg gives a reasonable measure of the speed at which a pulse travel.

Light can be made to go:

Slow: $v_g \ll$ c

Fast: $v_g > c$

Backwards: v_g negative

To understand the consequences of dispersion of the refractive index, we first consider the propagation of a monochromatic beam of light through a material. The phase velocity (v_p) describes the speed at which the wave-fronts move through the material and is given by $v_p = c/n$. Here, n is the refractive index of the material, which describes effects such as refraction at an interface between two dissimilar materials. A pulse of light is a wave-packet that is composed of an infinite number of monochromatic component waves, where constructive and destructive interference among the waves defines the shape and location of the pulse envelope in space and time. When the pulse propagates through a material system, each monochromatic component wave travels at a different speed because of the frequency dependence of n, resulting in a shift (relative to vacuum propagation) of the regions of constructive and destructive interference. Pulse distortion can also occur. For sufficiently short propagation distances, pulse distortion is not too severe, and the motion of the pulse can be described by v_g given by [62] $v_g = c/n_g$. where

$$n_g = n + w\frac{dn}{dw} \quad \text{II.4}$$

n_g is known as the group index, where w is the light's frequency.

As can be seen from Eq II.4, n_g can be adjusted either by modifying n or by modifying $\frac{dn}{dw}$ (the dispersive contribution to n_g). Most demonstrations of extreme values of ng rely on the dominance of the dispersive contribution to n_g.

II.4 Slow light away from the band edge

The band-edge is the most obvious place for the slow light phenomenon to occur, and it is there where most of the observations of slow light have been made. Despite this convenience, the

band-edge is not the best operating point. First, the dispersion curve near the band-edge is typically parabolic, which means that the group velocity changes rapidly with frequency as shown in figure 38, so an optical pulse with finite bandwidth will disperse over a short distance. Second, the band-edge presents a cut-off point, where the mode turns from propagation to evanescence. Any fabrication tolerance then manifests itself as a local variation of this cut off point, so modes that may propagate as slow modes in one part of the structure may turn evanescent in another. As a result, the slow mode near the band-edge appears to be very lossy [63].

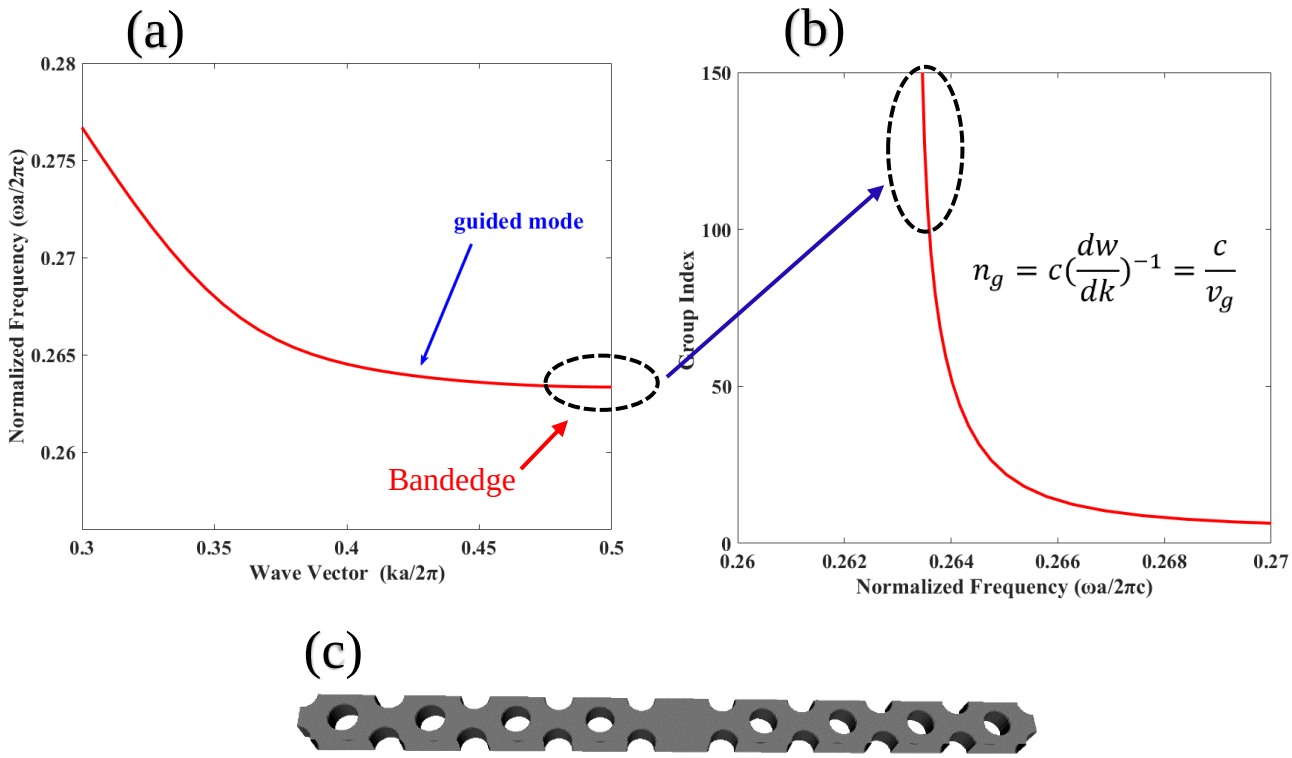

Figure 38 (a) Dispersion relation of the guided mode in the photonic crystal waveguide, as highlighted in red (b) the corresponding group index (c) the supercell used for calculating the dispersion diagram.

The group velocity is usually strongly dependent on the frequency. This effect is quantified by the group velocity dispersion (GVD). Since every optical pulse has a certain spectral content, an optical pulse will experience a broadening due to the GVD, which removes most of the advantages of operating in the slow light regime and severely limits the bandwidth that can be utilized. However, this behavior is not an intrinsic property of the structure, but is subject to design. Designs that are based on a better understanding of slow light operation can overcome this limitation; this so-called dispersion control of pulses in PhCWs is one of the promising applications of photonic crystals [64].

There is several examples of dispersion engineering are known, for example chirping the waveguide properties [65], ellipse-shaped holes [66], changing the waveguide width [67] and changing the position of the first two rows of holes adjacent to the line defect [68]. Most of these dispersion engineering techniques except chirping waveguide rely on the fact that the photonic crystal waveguide supports a gap-guided modes by the band gap and an index-guided mode by total internal reflection, [11].

The modes in the photonic crystal waveguides at frequencies inside the PBG can be categorized with respect to their field distribution as "index guided" or "gap guided". An index guided mode has its energy concentrated inside the defect and interacts only with the first row of holes adjacent to the defect. Its behavior can be simply represented by a dielectric waveguide with periodical corrugation. A gap guided mode interacts with several rows of holes, thus it is dependent on the symmetry of the PC and its PBG. The terms index guided and gap guided do not exactly specify the guidance mechanisms (in the PBG region, all modes are gap guided) but mainly describe the modal field distribution [69]. As an example of slow light waveguide, let's see how changing the position of tows rows of holes adjacent to the center of the waveguide can engineered the dispersion curve for produce slow light regime, as shown in figure 39.

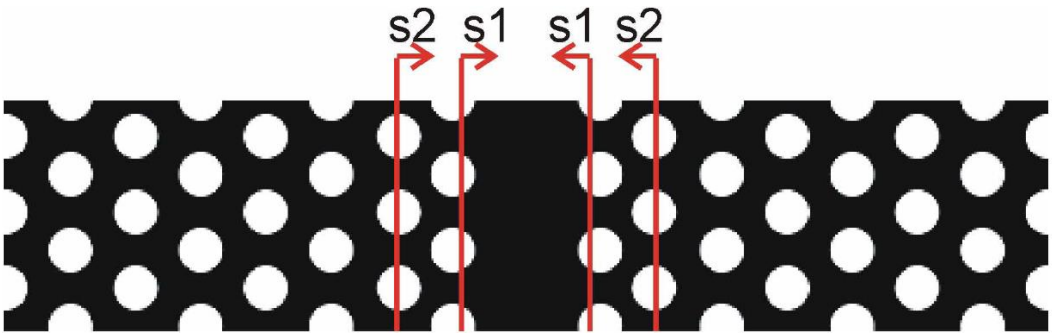

Figure 39 Geometry of the modified W1 PhC waveguides: the first and second rows of holes are displaced symmetrically about the waveguide axis [61]

By using Rsoft software a three-dimensional (3D) calculation was used in certain values of s1 and s2 which is shown in figure 40 (a) and (b) illustrates three operating points taken to highlight the evolution of the dispersion curves and group indices with increasing group index. ng=32, 50 and 93. The fundamental mode of an unmodified W1 PhC waveguide is shown for comparison by red curve.

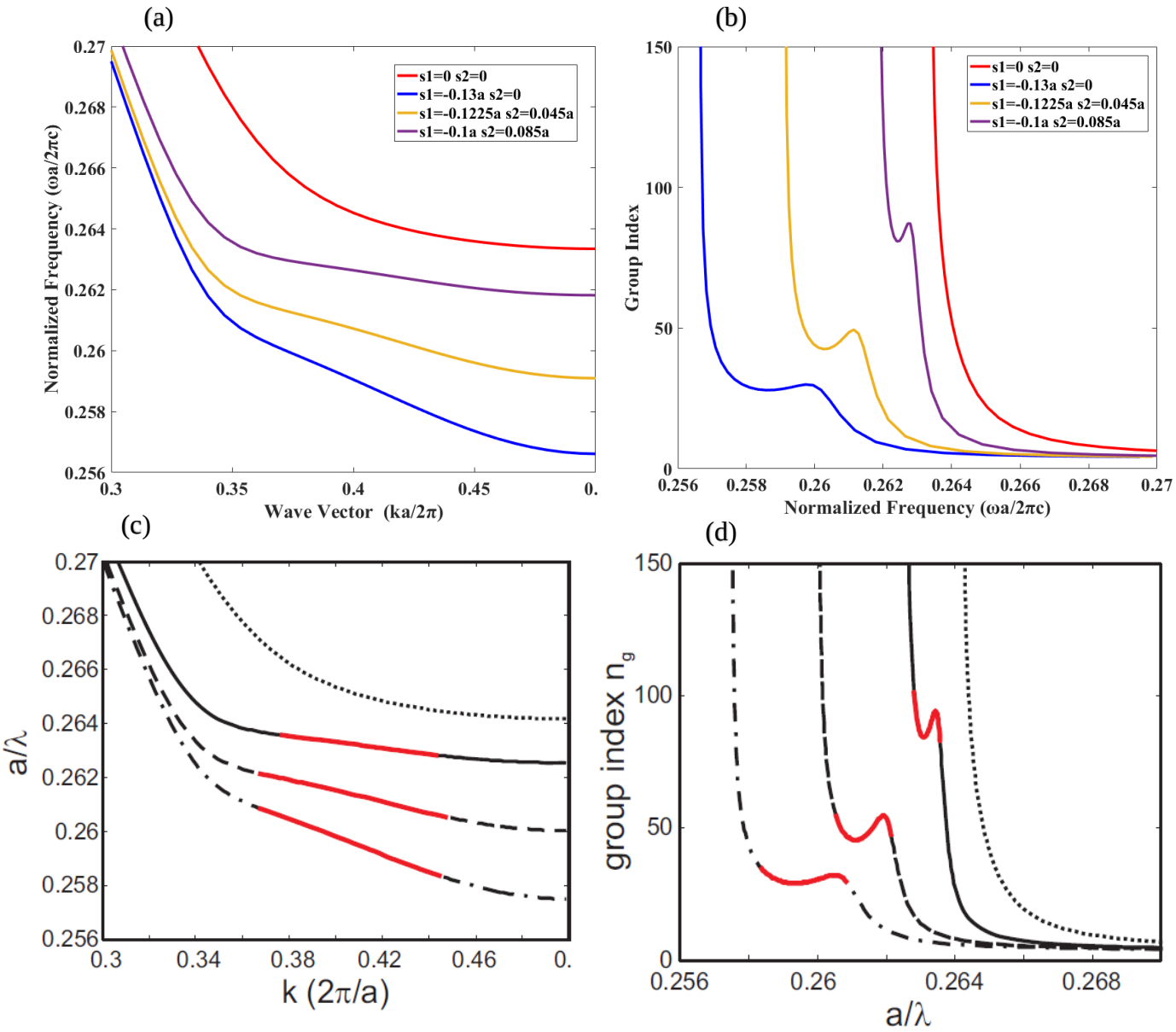

Figure 40 (a) Calculated dispersion curves using Rsoft software and (b) group indices, for the fundamental mode of the modified PhC waveguides (c) and (d) are the results which calculated MPB from ref [61] presented for comparison .

We performed a comparison between our results using a 3D plane wave expansion (PWE) by Rsoft software as shown in figure 40 (a) and (b) and the results from the ref [61] which use a 3D plane wave expansion (PWE) by the MIT's freely available software MPB as shown in figure 40 (c) and (d) [70] the results are totally equivalent.

II.5 The normalized delay bandwidth product NDBP

An essential performance factor for slow light is the delay-bandwidth product (DBP), which is defined as the product of time group delay Δt and bandwidth $\Delta\lambda$ in slow light:

$$DBP = \Delta t \cdot \Delta\lambda \qquad \text{II.5}$$

However, the time group delay Δt of a PCW can be extended by increasing its device length *L* without the need to perform resonance matching. Therefore, the expression of the DBP is usually modified to normalized DBP (NDBP), which is more useful for comparing devices that have different lengths and different operating frequencies. The NDBP is given by

$$NDBP = n_g \times \frac{\Delta\omega}{\omega_0} \qquad \text{II.6}$$

Where $\Delta\omega/\omega_0$ is the normalized bandwidth of a slow light region and n_g is the average group index. The NDBP indicated the obtained compromise between a wide operating bandwidth and a high group index of slow light. It is independent of *L*, and therefore independent of the technological realization and the acceptable loss [71].

II.6 Group Velocity Dispersion

Another important issue for slow light devices is the signal distortion caused by dispersion. Generally, the second order dispersion, also known as group velocity dispersion (GVD), is characterized by β parameter and is very important as it controls the signal distortion and pulse broadening in the slow light region. Low value of GVD parameter is desired so that high group index values are not obtained at the cost of increase in signal distortion [64]. Therefore, low GVD is very important to maintain the transmission signal stable and undistorted in slow light devices. Moreover, the group index in a PCW is strongly dependent on the frequency (or wavelength) as quantified by the GVD parameter β, which is given by [72]:

$$\beta = \frac{d^2k}{dw^2} = \frac{1}{c}\frac{dn_g}{dw} \qquad \text{II.7}$$

Where w is the frequency, k is the wave vector, c is the light velocity in vacuum, $n_g$is the group index.

As shown in Figure 41 the GVD parameter as function of normalized frequency, we notice that the GVD values are in the order of 10^6 ps^2/km.

What is the meaning of 10^6 ps^2/km?

In slow light waveguide of 1 mm for 1 ps pulse you will accumulate approximately 1ps pulse broadening in a waveguide with 10^6 ps^2/km. Which is rather low for such a short pulse.

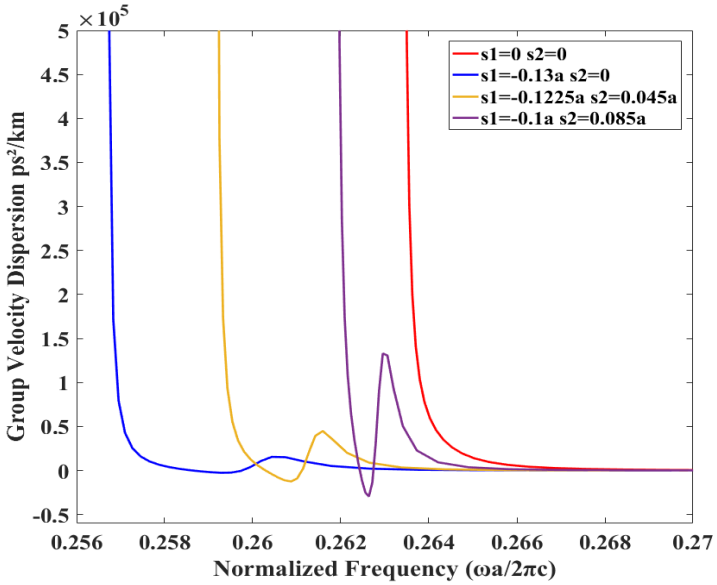

Figure 41 The group velocity dispersion GVD as function of the normalized frequency.

Figure 42 shows the group index curve and GVD curve of W1 PCW when shifting the air holes in both side of the waveguide with s1=-0.1225a and s2=0.045a. we can see that for ng=50, the GVD value stays within 10^5 ps^2/km in the slow light regime, which can be considered as a low dispersion region.

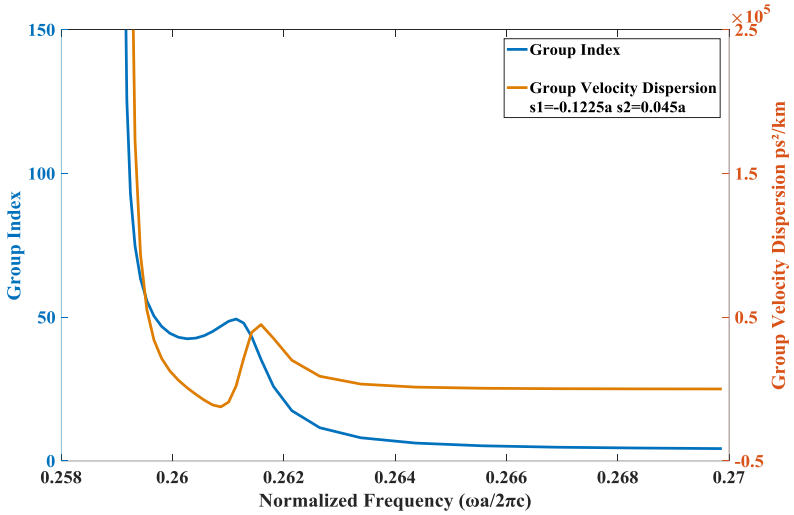

Figure 42 Group index and group velocity dispersion curves of the PhCW when s1=-0.1225a and s2=0.045a.

II.7 Propagation loss

Propagation loss in W1 waveguides is an important aspect that cannot be neglected when discussing slow light devices, as all the exciting advantages of slow light waveguides become pointless if only a tiny fraction of light is transmitted through the structure. Photonic crystal waveguides are intrinsically lossless, because the modes of interest lie inside the band gap and below the light line. They do exhibit extrinsic loss due to fabrication disorder (fabrication imperfections), which leads to scattering into radiation modes (out-of-plane loss) and into the backward propagating mode (backscattering loss) as demonstrated in figure 43. The out-of-plane loss depend linearly on the group index n_g and the backscattering loss depend on its square n_g^2 [73] [74]. This n_g^2 dependence was first discussed by Hughes *et al* [75] and confirmed experimentally by Kuramochi *et al* [76] on state-of-the-art structures. These scaling relations are in agreement with most research on this topic, making it a serious issue for the practical use of slow light photonic crystals. The loss can be expressed as follows [73] :

$$\alpha = c_1 n_g \gamma + c_2 n_g^2 \rho$$

Out of plane **Back-scatter**

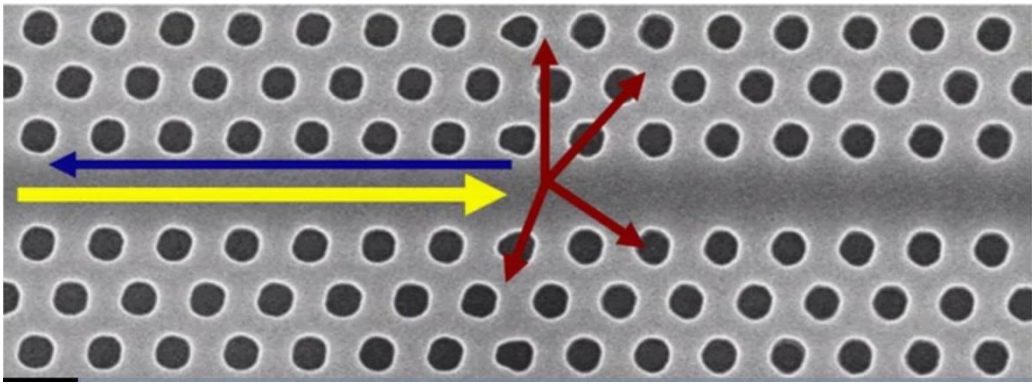

Figure 43 Schematic demonstrate the out-of-plane loss red color and backscattering loss blue color.

To understand the loss engineering we consider two different waveguide designs as shown in figure 44. Where the dispersion engineering realized by altering the position of individual rows of holes figure 44 (a) changed the hole position perpendicular to the waveguide and achieved a group index ng=37 [61] and as we see in figure 44 (b) by shifted the rows of holes in the propagation direction achieved similar performance with ng=40. The structure (a) formed by etching holes with

radius r=0.27a and lattice constant a=410 nm and shifting the two rows of holes with S1=-42 nm and S2=16 nm. The structure (b) formed by etching holes with radius r=0.286 a and lattice constant a=414 nm and shifting the two rows of holes in the propagation direction with P1=83 nm and P2=104 nm [77]

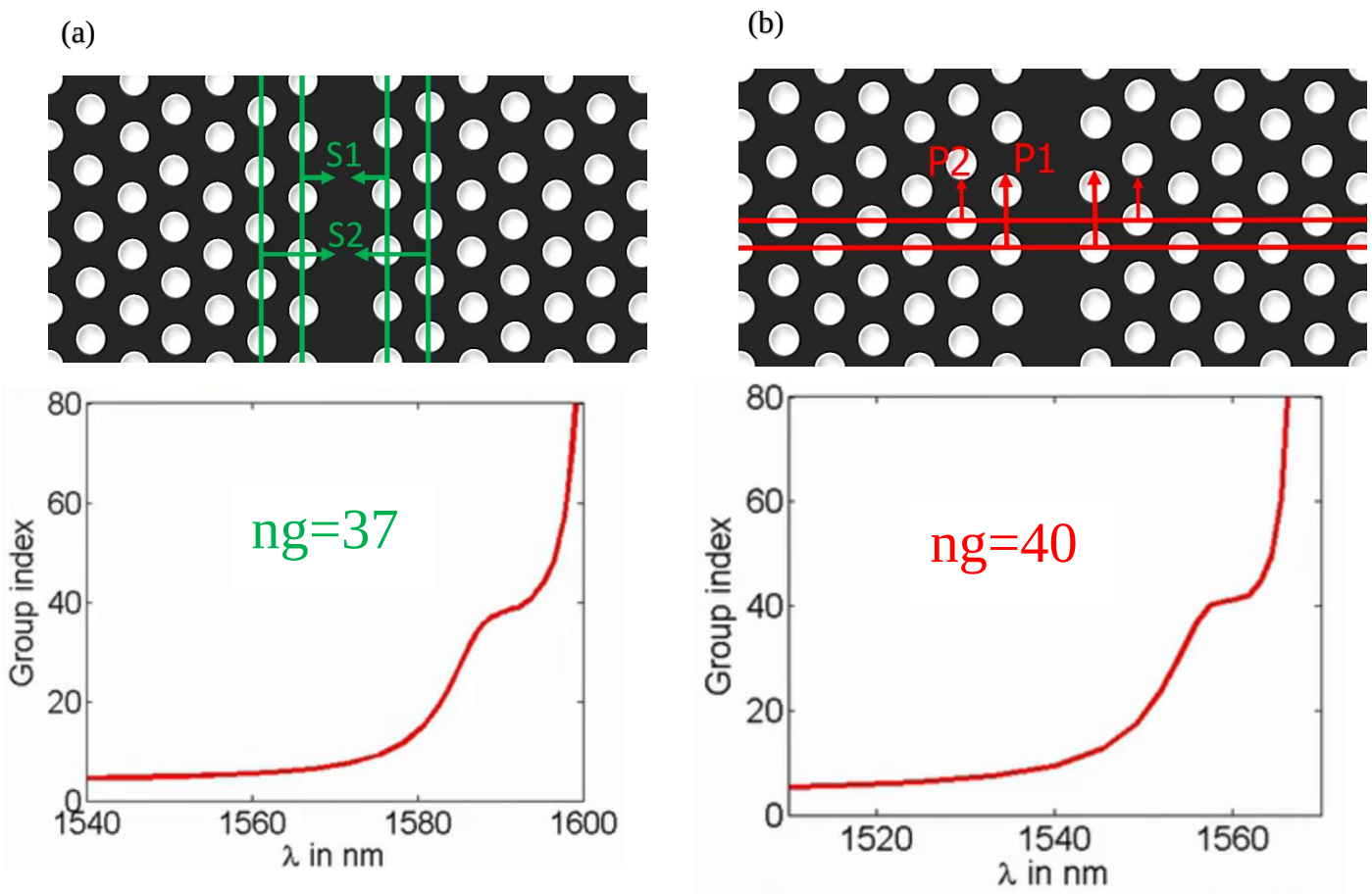

Figure 44 (a) Dispersion engineering through lateral hole position shift, With group index ng=37 (b) Longitudinal hole position shift, with group index ng=40 [79].

The figures above illustrate the dispersion engineering so what is the difference between loss engineering and dispersion engineering?

When we engineered the dispersion of different waveguides and we need to compare theme, we need to make sure that they have a comparable group index curve with very similar values of the group index and very similar bandwidth. In the figure 45(a) we can notice two things. The loss engineered waveguide starts off with a higher loss. But it increases slower and by the time we get the group index where we care about, close to 40, where it's flat band, it has a lower loss than the other waveguide in figure 45 (b) [78] [79].

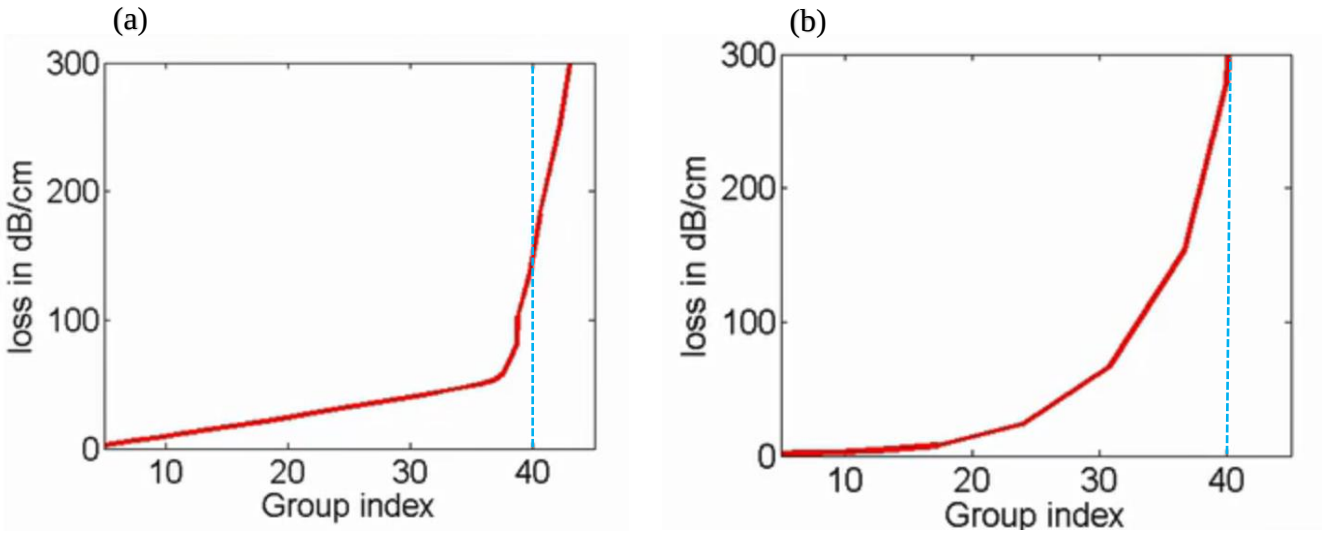

Figure 45 Propagation loss as a function of group index for a waveguide designed to exhibit a constant group index of (a) ng=37 (b) ng=40 [78].

II.8 Other methods of slow light photonic crystals

The most common approaches to flatten the mode dispersion rely on the alteration of the first two rows of holes by changing the hole size [80] or altering the position of holes adjacent to the line defect along the normal [61] or along the propagation direction [81] as shown in figure 46 respectively.

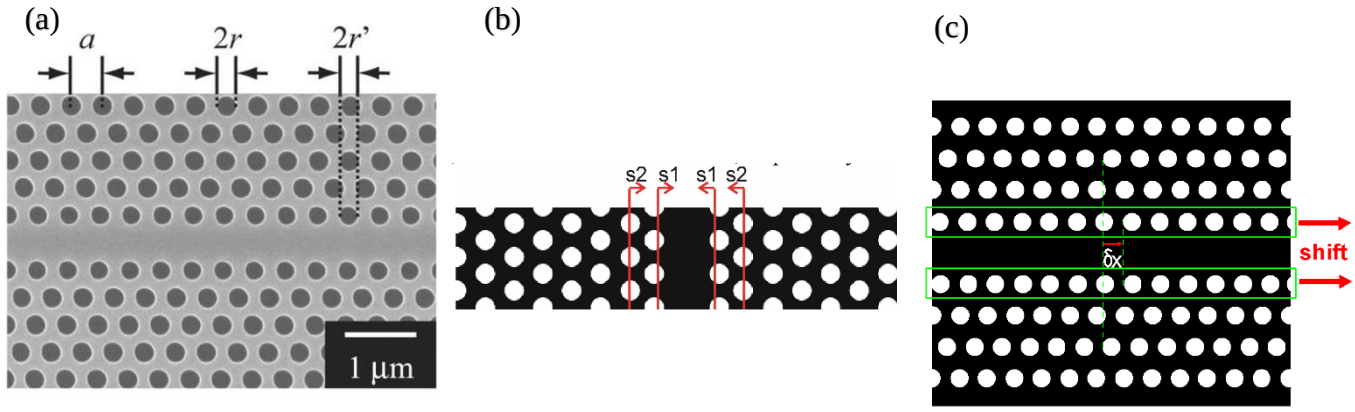

Figure 46 The common approaches to generate slow light regime in photonic crystals (a) reduce holes (b) shifting two rows of holes in the normal direction of the waveguide (c) shifting row of holes in the propagation direction.

It is difficult however, to control the hole size of a photonic lattice accurately and reproducibly. Instead, changing the position of the first two rows of holes in order to modify the dispersion curve it is an approach that is technologically preferred. In addition, shifting of rows is a convenient method for generation of slow light due to providing a single parameter to produce efficient slow light and enabling more accurately and reproducibly fabrication control ability [82] [61] [83].

There is other way to achieve a flat-band slow light in photonic crystals such as infiltrating fluid with suitable refractive index into the first row of air holes adjacent to the waveguide (a) [84] or by introducing extrinsic defect rods in the photonic crystal waveguide (b) [85] or using ring shaped (c) [86] or using alternative row of ellipse-hole photonic crystal waveguide (d) [87] as shown respectively in figure 47.

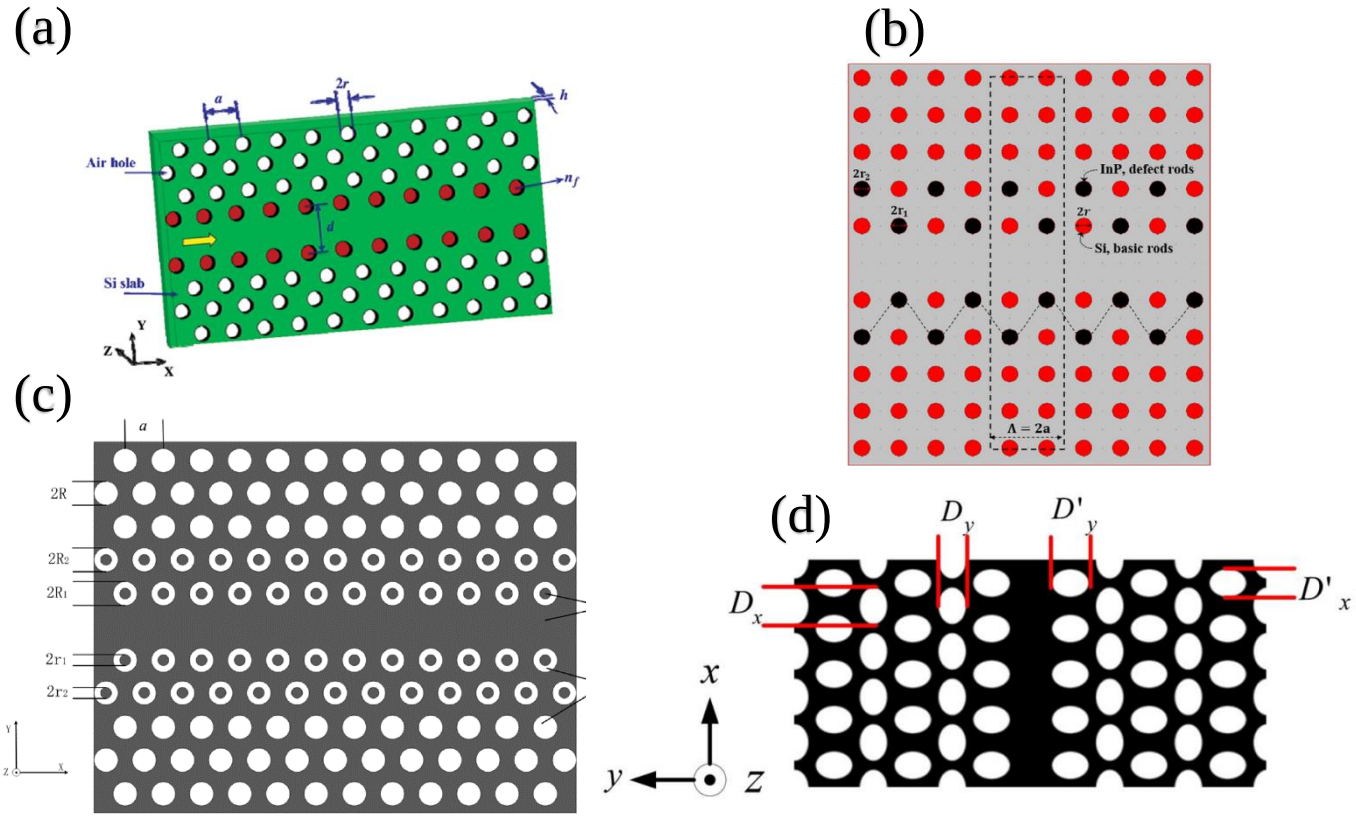

Figure 47 Some structural-based schemes to optimize the slow light properties (a) infiltrating liquid in holes (b) introducing extrinsic defects rods (c) ring shaped PhC (d) ellipse hole.

All of these structural-based optimization schemes depend on the technological capability to realize some specific designs, which require very careful engineering and stringent fabrication processes. Besides, by using these optimization schemes, the working wavelength of slow light (with constant group index) can only be located within a small range and cannot be altered after the fabrication of PCW. Instead, the slight fabrication deviations will bring serious deteriorations to the PC fabricated [84].

II.9 Dispersion compensation

Another approach to suppress higher-order dispersion in slow light devices is that of dispersion-compensated structures: [8] figure 48 shows practical structures and photonic band diagrams of two waveguides with a background index of 2.963. Waveguide A has a channel of width w´ of 0.85 times the normal width w of single line missing airholes. waveguide B has smaller airholes with normalized diameter r´ at the center of the channel.

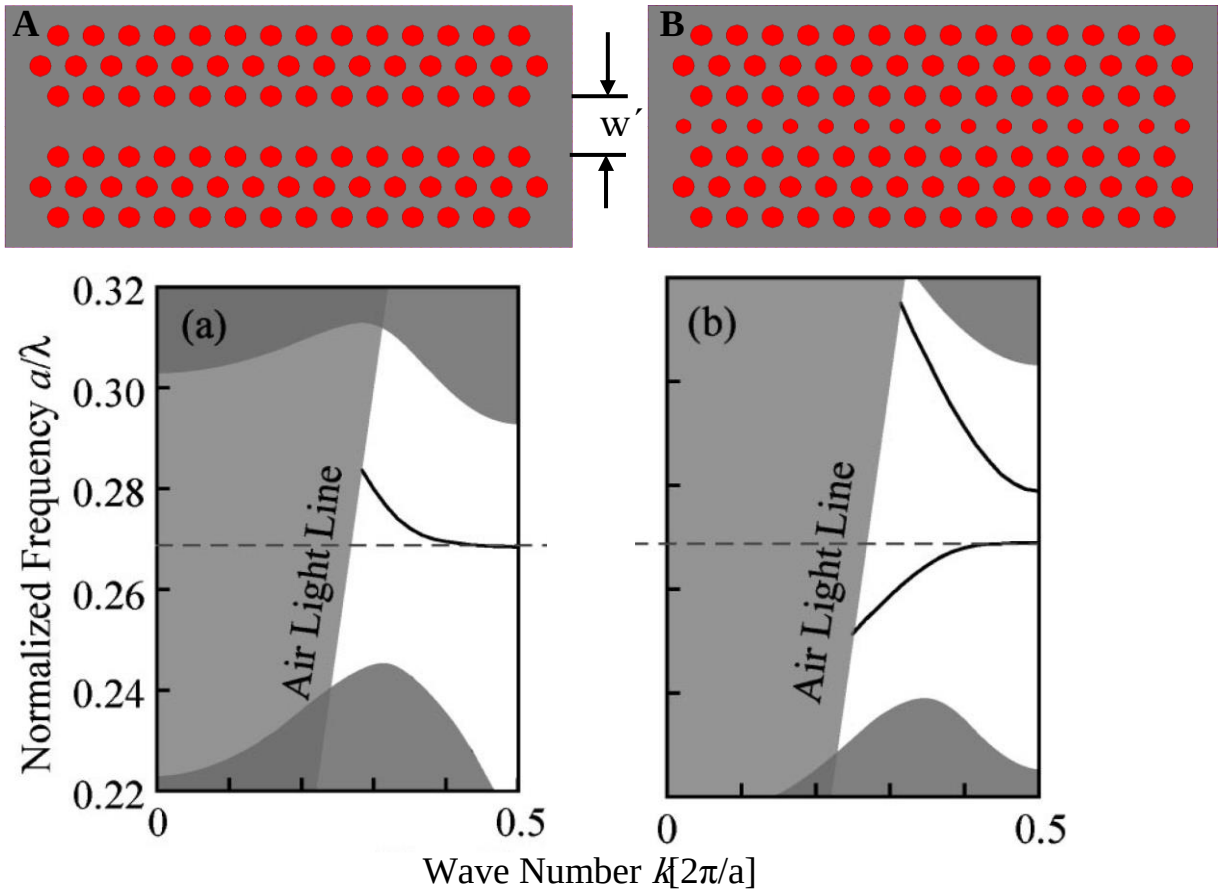

Figure 48 Waveguide structures and photonic band diagrams calculated by the plane wave expansion method.

The Two waveguides, A and B, have different structures and characteristics; A and B have upward and downward band profiles, respectively, but their band edges are always equal. The two waveguides A and B coupled to each other as shown in figure 49.

The guided light in waveguide A reaches the band-edge condition and is localized. Under this condition, the frequency v and the wave number k in the propagation direction agree between the waveguides. Therefore, efficient directional coupling occurs and localized light moves to waveguide B. This time, light is not reflected but rather moves forward in waveguide B with increasing v_g due to the chirping. The delay by localization takes place for any frequencies at

different positions. If the upward band profile of A and the downward band profile of B, are symmetric, the GVD near the band edge is completely canceled. The lower two bands with opposite dispersion characteristics are used for dispersion compensation as shown in figure 50 [88].

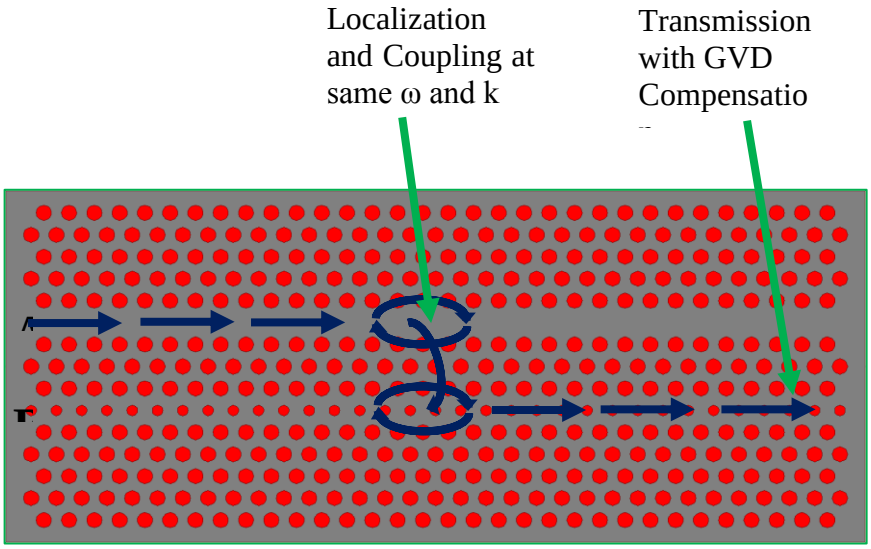

Figure 49 Schematic diagrams of index-chirped PC waveguide devices.

When these bands are shifted by a chirped structure and the band edge frequencies of these bands are maintained to be equal, directional coupling from A to B occurs within a very short length due

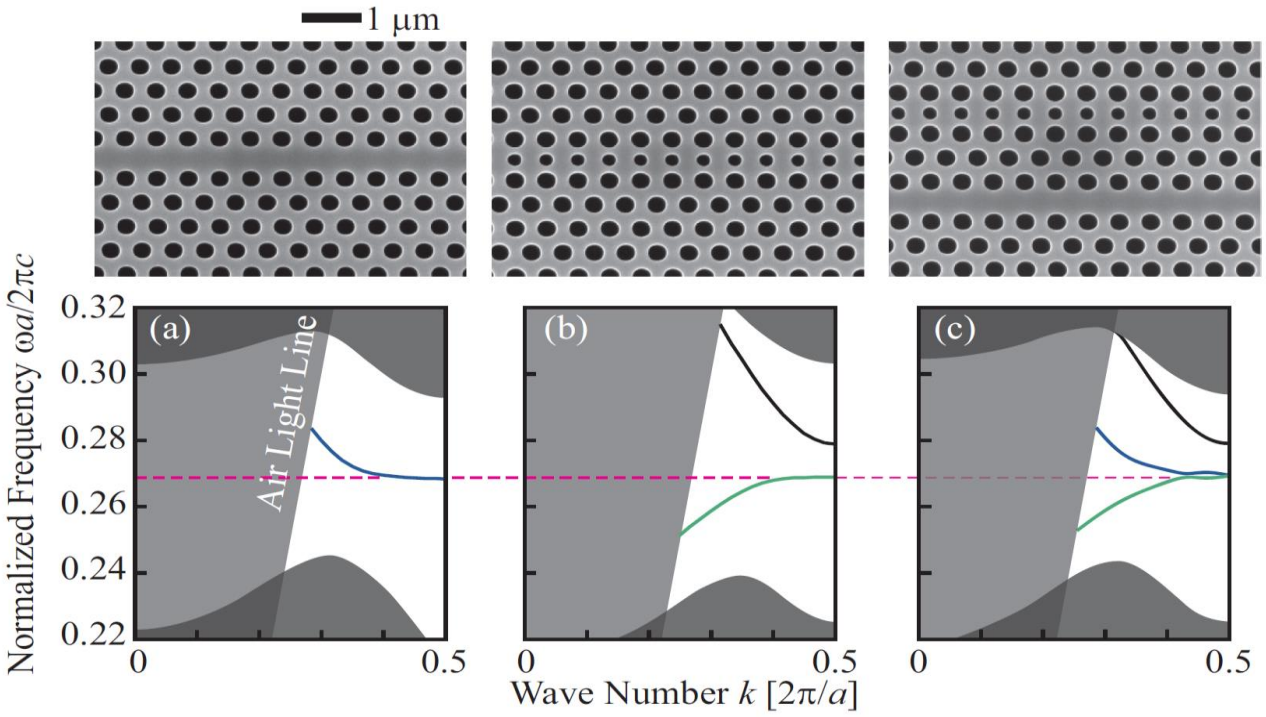

Figure 50 Schematics of PC waveguide and corresponding bands calculated by plane wave expansion method. (a) A, (b) B, (c) directional coupler and the opposite dispersion characteristics of two waveguide A and B blue and green respectively [89].

to the $v_g = 0$ condition. As a result, a transmission-type group delay device for an ultrashort pulse is realized. Not only zero GVD, but also any desired GVD, can also be given for the pulse by designing the band profiles to be asymmetric [89]. One important requirement was for the waveguides to match exactly their band edges, making the final device very sensitive to fabrication tolerances.

II.10 Coupled resonator optical waveguides (CROW)

Another type which play a key role in slow light engineering and various types of light-matter interaction enhancement, is the coupled micro-resonators with small and high-quality factor cavities [90]. As light propagates through A sequence of coupled cavities (coupled resonators optical waveguide, CROW) it is localized at each cavity, in introducing a time delay [91]as shown in figure 51. There are a lot of researchers interested of the dispersion of these slow light using coupled resonators [92] [93] [94]. One issue of CROWs in photonic crystals, however, is that the regular spacing of the cavities introduces a second periodicity on the lattice, corresponding to an additional folding of the bands in the k-space, and as a consequence light can easily couple to the radiation modes above the light line. More importantly, the precise control of both the inter-cavity coupling and the optical resonances of each cavity (which should be identical) at the same time is a huge challenge in photonic crystals, once again due to disorder and non-idealities introduced during the fabrication process, even in some of the best reported results [91], oscillations in the transmission band on the order of 20–30 dB are unavoidable. This type of slow light structures is therefore probably more suited for use with ring resonators, where the control of individual resonances is more straightforward and reliable than in photonic crystals [95] [96].

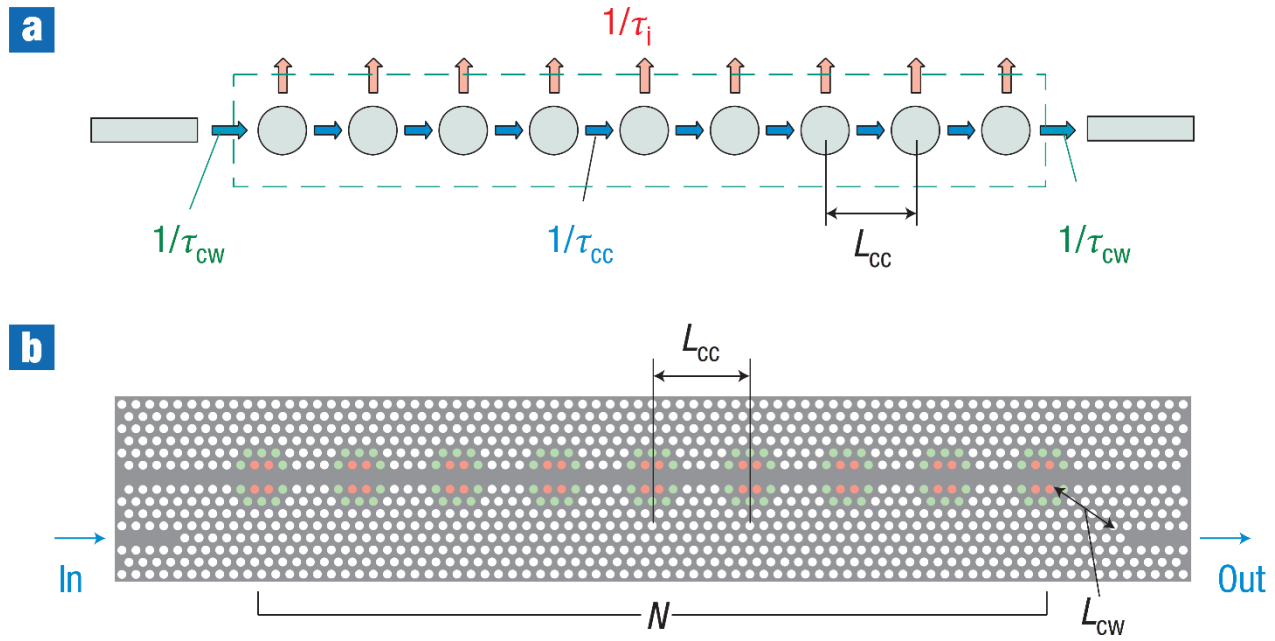

Figure 51 Examples of CROWs (a) Schematic of a coupled resonator loaded to input/output waveguides (b) Design of coupled resonators based on width-modulated line-defect [91].

II.11 Comparison of cavities and slow light waveguides

Cavities and slow light waveguides both enhance the electric field at the expense of bandwidth. So, what is the differences between theme. We compare the performance of two structures in terms of intensity enhancement and bandwidth as follow [63]:

II.11.1 Intensity enhancement

In a cavity, the intensity builds up because the light makes multiple round-trips; On resonance, the fraction of light lost then equals the fraction of light coupled into the cavity from the outside.

Let's consider light of intensity I_0 hit a loss-less Fabry-Perot cavity from the left as we see in figure 52. The two mirrors create a cavity with reflectivity R . When light with intensity I_0 comes to the first mirror in the left part of this light intensity reflected RI_0 and the other part transmitted inside the cavity (cavity intensity I_{cav}) and this I_{cav} in turn hit the second mirror in the right also a part of transmitted $(1-R)I_{cav}$ and the other part reflected RI_{cav} also same operation so we expected $R(1-R)I_{cav}$ in the left which is π out of phase with RI_0 so they cancel each other if these two intensities are equal, the cancellation is complete and no reflection of I_0 occurs at all. This is what is observed for a cavity on resonance. This condition is met when the two intensities are equal, $RI_0 = R(1-R)I_{cav}$.

$I_{cav} = \frac{I_0}{1-R} = I_0 \times \frac{1}{1-R}$ if $R = 1$ so $I_0 = I_{cav}$ if $R = 0$ $I_{cav} = \infty$ so, $\frac{1}{1-R}$ enhanced the intensity inside the cavity on resonance.

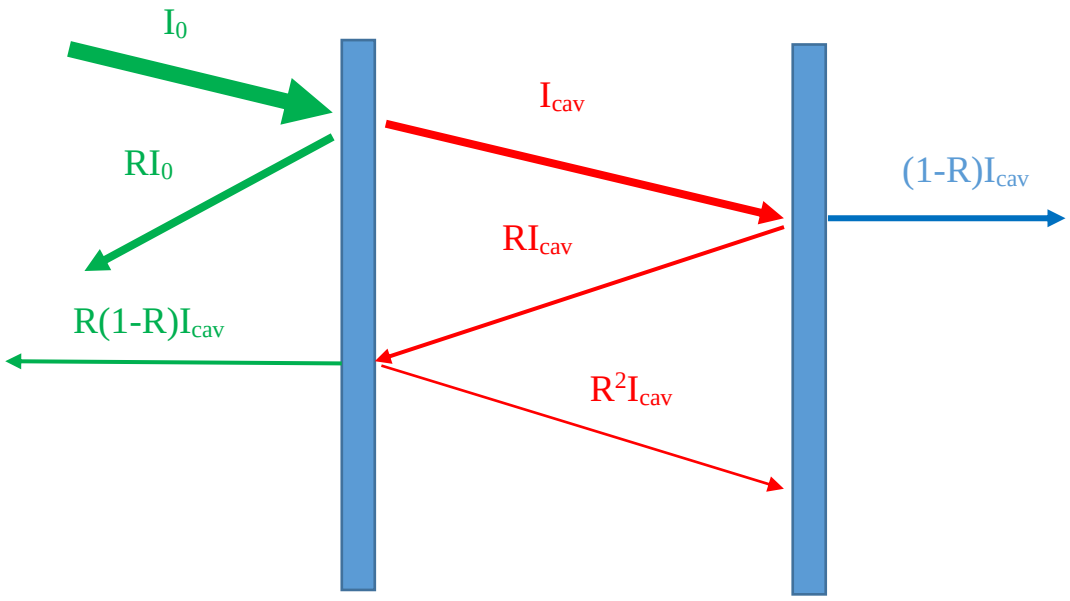

Figure 52 The intensity enhancement in a cavity on resonance.

The quality factor Q is a measure of the losses in the cavity. Since the reflectivity of the crystal surrounding the defect increases with the number of rods, we expect that Q will also increase with the size of the crystal. To compute Q, we choose to use an approach which first involves pumping energy into the cavity, then monitoring its decay. We recall that the quality factor is defined as [30]:

$$Q = 2\pi \frac{Energy\ stored}{Energy\ lost\ per\ cycle} \qquad \text{II.8}$$

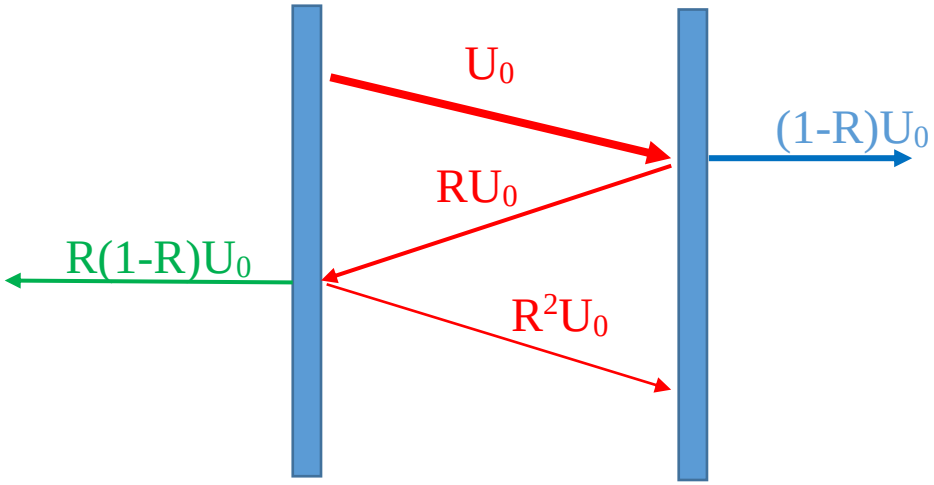

Figure 53 Dependence of the cavity quality factor on the mirror reflectivity.

As shown in figure 53 we relate the precedent enhancement with the quality factor. Assuming that the energy stored is U_0 , we find that the energy lost per cycle, in a single mode cavity, is given by $(1-R)U_0 + R(1-R)U_0 \cong 2(1-R)U_0$. In a multimode cavity of mode order *m*, the loss per cycle is reduced by *m*, since the mirror loss occurs only once in *m* cycles. The quality factor becomes

$$Q = 2\pi m \frac{U_0}{2(1-R)U_0} = \frac{m\pi}{1-R} \qquad \text{II.9}$$

We see before that $I_{cav} = \frac{I_0}{1-R}$ thus $I_{cav} = I_0 \frac{Q}{m\pi}$ so the intensity in the cavity is enhanced by a factor $\frac{Q}{m\pi}$.

Slow light structures are characterized by the slowdown factor S, which is defined as the group index over the phase index,$S = n_g/n_\varphi$ [97]. If an optical pulse enters a slow light medium, and assuming a complete transfer of energy, the front of the pulse is slowed down with respect to the

tail and the pulse compress overall [98]. This effect is illustrated in Figure 54 It is easily understood that in the absence of dispersion and nonlinearities, the shape of the incident pulse is not affected. Given also that the slowdown is not caused by the excitation of material resonances.

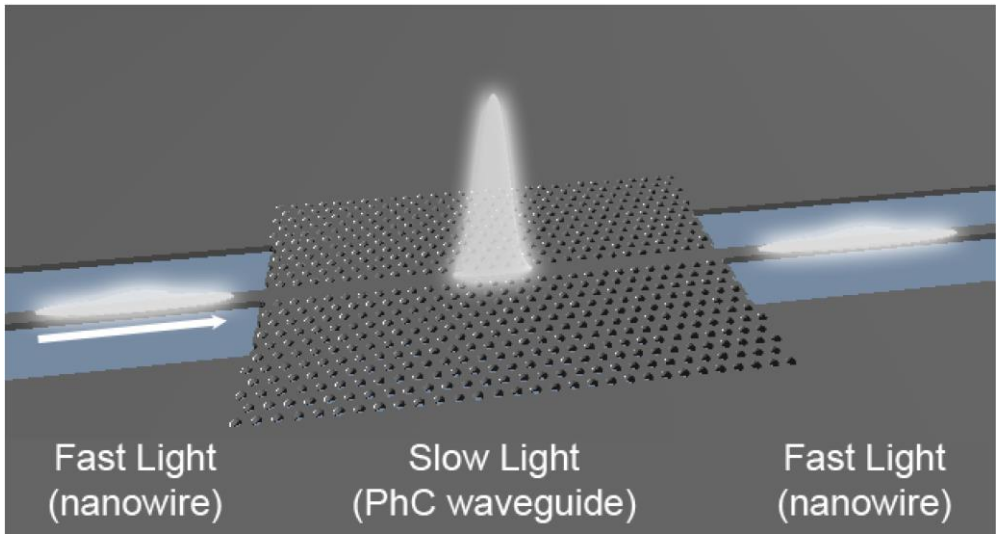

Figure 54 Sketch of a pulse of light entering a slow light waveguide; the pulse enters from the top left and is spatially compressed in the slow light regime, thereby increasing in intensity [98].

The intensity of a pulse in slow light structure is I_{SL}. Therefore, scales as the slowdown factor,

$$I_{SL} = I_0 S \qquad \text{II.10}$$

The in intensity of a cavity and slow light waveguide can be written as follows:

$$\begin{cases} \frac{I_{cav}}{I_0} = \frac{\mathrm{Q}}{\mathrm{m}\pi} \\ \frac{I_{SL}}{I_0} = S \end{cases} \qquad \text{II.11}$$

II.11.2 Bandwidth comparison

A slow light waveguide and a cavity achieve the same bandwidth for a given intensity enhancement. For a larger cavity, the figure of merit grows, which indicates that the slow light waveguide can accommodate more bandwidth for a given intensity enhancement. Therefore, the slow light waveguide behaves like a single mode cavity of arbitrary length.

II.12 Slow light applications

Slow light allows optical scientists turning their attention toward developing useful applications, they are categorized into those using tunable delays as shown in figure 55 (a) and enhanced light-matter interaction as shown in figure 55 (b) [99]. Tunable delay has been anticipated to achieve optical buffer [86]. Retiming and multiplexing demultiplexing (MUX/DEMUX) [100] re-timing and synchronization components [101]. On the other hand, the enhanced light-matter interaction occurs due to the elongated duration of light propagation as well

as enhanced peak intensities of pulses. He interaction strength of light and target analyte would significantly influence the sensitivity of RI sensor [102] and improve the efficiency of phase modulation and optical amplification [103] [104] the examples mentioned here are illustrative rather than exhaustive.

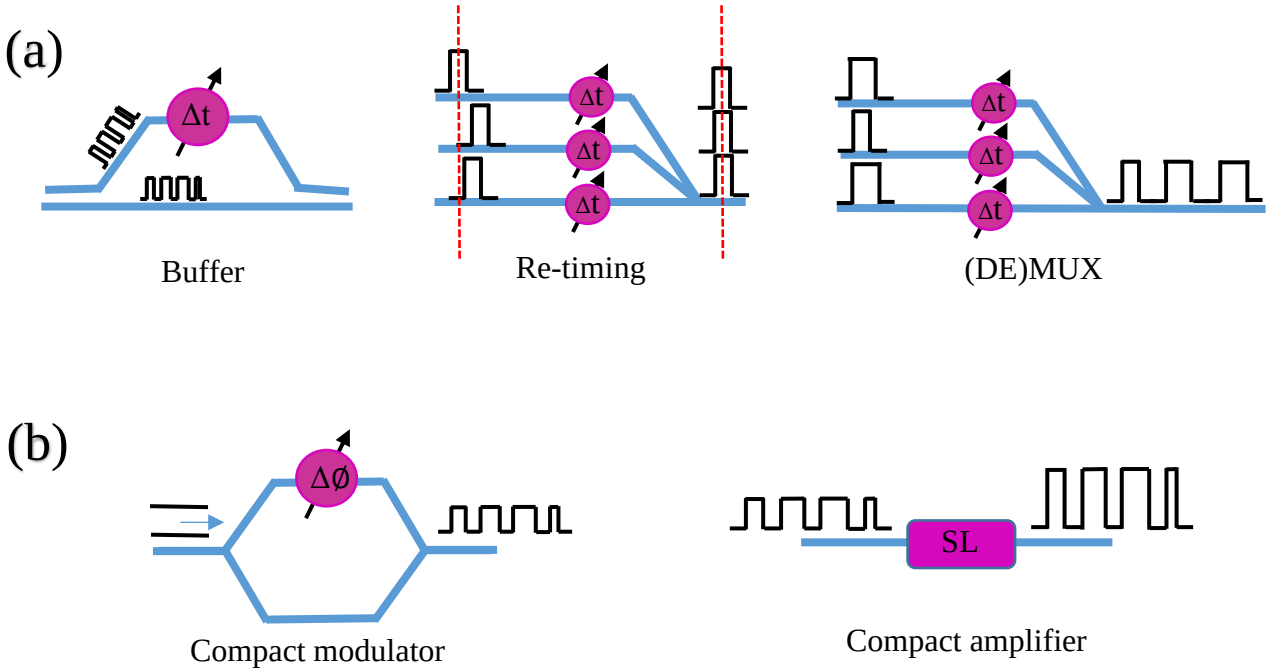

Figure 55 Some slow light applications.

II.13 Buffer

In recent years, optical buffering and time-domain signal processing are key technologies in the future optical networks, and have been a research focus in optical communications. Compared with previous methods, optical buffer based on photonic crystal slow light has many advantages such as nanostructure, very low group velocity and high controllability [105].

One of the proposed applications of slow light is for the process of optical buffering, as illustrated in the figure 56. Any of the input ports can be dynamically switched to any of the output ports. However, a serious problem can arise with this sort of architecture if two data packets arrive simultaneously at the router, because the switch can only deal with one packet at a time. This problem is known as data packet contention in this case, information will be lost, the solution is to build a buffer, which in one of these branches, one of the pulses is delayed while the other clears the switch. In this case, no collision occurs [106] [107].

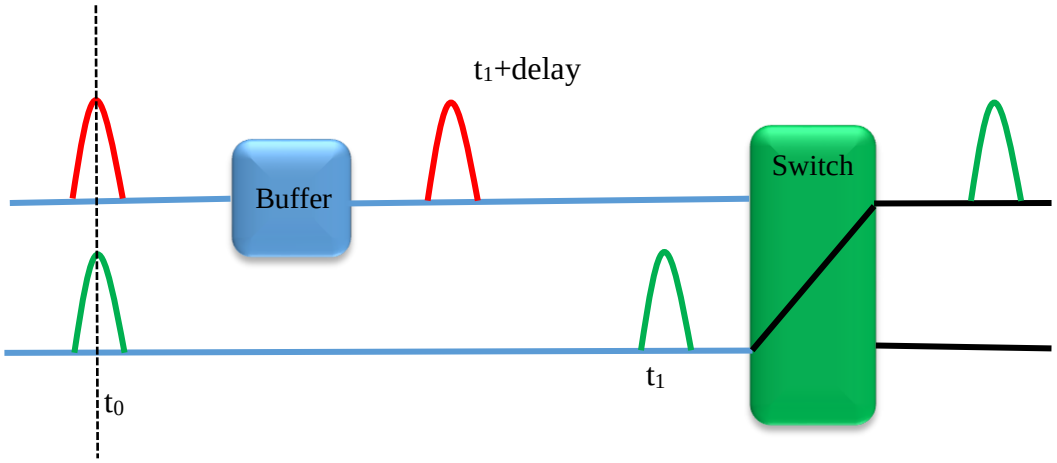

Figure 56 Optical buffer can be used to ensure that two data packets are not incident simultaneously on the switch.

II.14 Sensors

Slow light in photonic crystals took a crucial step for the application in the sensor fields. Researchers found that the slow light could greatly enhanced light-matter interaction, thereby enabling the realization of miniature and highly sensitive sensors such as gas sensor [108] [109]. antibody detection using the slow light regime in photonic crystal waveguide [110] And a lot of RI sensors [111]. Let us take as an example the RI sensor designed by Ya-nan Zhang,in ref [112] as shown in figure 57 (a) The schematic diagram of RI sensor based on slow light engineered PhC cavity constructed on a silicon-on-insulator (SOI) substrate (n=3.48) by replacing the central row of air holes in the triangular lattice PhC with one pair of two air holes as two reflectors (red holes), the radius of air holes is chosen as r=0.30a, and the slot thickness is defined as h=0.7a, where a=340 nm is the lattice constant. When fluid with refractive index n_f of 1.9 is selected to infiltrate into the first two rows of air holes (green holes). Figure 57 (b) shows the normalized transmission spectrum of the conventional PhC cavity (nf=1.0) The linear relationships between the resonant wavelength and the relative refractive index of 66.3 nm/RIU. After that the PCW infiltrated in two rows of holes with nf=1.9 which lead to constant group index of 14.5 over 52 nm bandwidth as shown in figure 57 (c) as we see in figure 57 (d) the measured sensitivity of RI can be enhanced by 7 times when slow light is introduced in PhC cavity to become 469.4 nm/RIU.

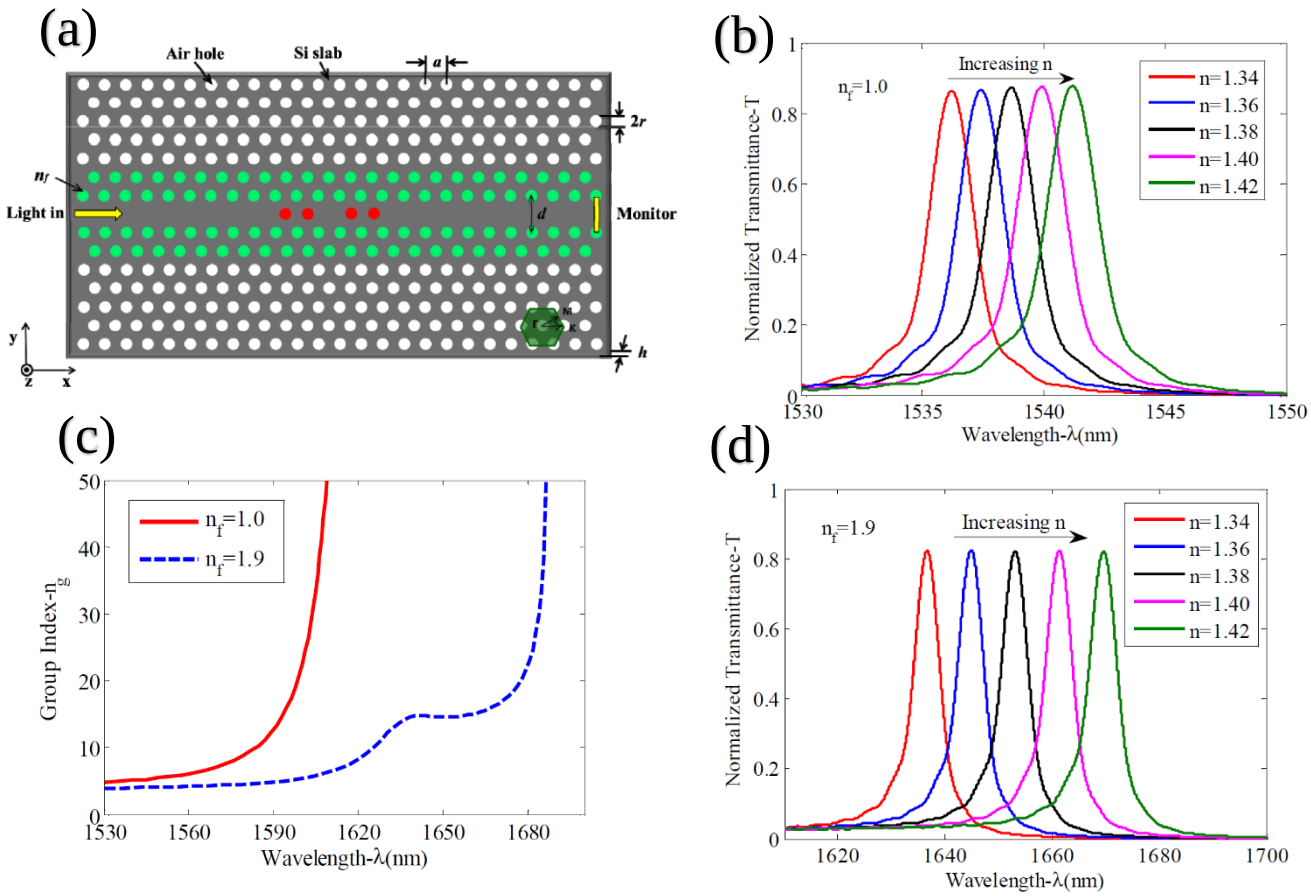

Figure 57 Example of RI sensor based on slow light engineered photonic crystal cavity.

II.15 Conclusion

In this chapter, we concentrate on slow light in photonic crystal waveguides. The first part of chapter is devoted to the basic concepts of slow light and how do we slow a wave with some examples. We talk also about the propagation loss and the effect of fabrication disorder. We mentioned that there are many ways to slow light in photonic crystals such as changing the hole size or altering the position of holes adjacent to the line defect along the normal or along the propagation direction. But all of these structural-based optimization schemes depend on the technological capability to realize some specific designs. We explained and compered between the cavity and slow light waveguides in two terms “intensity enhancement” and “bandwidth” and we saw that the slow light waveguide behaves like a single mode cavity of arbitrary length. In the last of this chapter we explored some application of slow light and we give some example such as buffer and sensors.

Chapter III

Simulation Methods and Tools

Chapter III Simulation Methods and Tools

III. Introduction

Simulation and modelling using numerical methods running on computers is today one of the key approaches in scientific work within practically all fields of research. In particular, in the field of photonics, a wide range of numerical methods are needed for studying both fundamental optics and applied branches such as the design, development, and optimization of photonic components. The topic of numerical modelling is thus becoming an increasing priority in photonics researches. Numerical simulations allow us to solve the Maxwell equations exactly without the limitations of analytical approximations, whose regimes of validity are often difficult to assess [113] [114].

Since the physical behavior in the nanoscale is very difficult and expensive to measure in real experiments, numerical simulations play a fundamental role in understanding such processes. There are many numerical methods that are used in photonics for the modelling of propagation and scattering of light in micro and nano-structures. The propagation and interaction of light at optical wavelengths with such structures is governed by Maxwell's equations, and thus the theoretical methods presented in this chapter are techniques that either directly solve Maxwell's equations or solve equations deduced from those. We will focus only on the methods that we used

to simulate our work such as Plane wave expansion (PWE) [15] [115] and The Finite Difference Time Domain Method (FDTD) [116] [117].

In this chapter we will describes all necessary mathematical operations and notations and provides a basic introduction to optics and Maxwell's equations. We will also review the simulation methods used in our work and the various tools and softwares.

III.1 Maxwell's Equations

In 1864, James Clerk Maxwell wrote the equations to describe all phenomena in electric and magnetic field. Maxwell's equations are the fundamental laws that govern behavior of all electromagnetic energy. They are based on a macroscopic view of how waves interact with matter and may take many forms.

$$\nabla \times \vec{E}(\vec{r},t) = -\frac{\partial \vec{B}(\vec{r},t)}{\partial t} \quad \text{III.1}$$

$$\nabla \cdot \vec{D}(\vec{r},t) = \rho \quad \text{III.2}$$

$$\nabla \times \vec{H}(\vec{r},t) = \vec{J}(\vec{r},t) + \frac{\partial \vec{D}(\vec{r},t)}{\partial t} \quad \text{III.3}$$

$$\nabla \cdot \vec{B}(\vec{r},t) = 0 \quad \text{III.4}$$

Originally there is no free electric charge and current in the dielectric materials. Therefore, the photonic crystal does not have the resources for electromagnetic wave.

So, we consider the electric current density $\vec{J}$ and the electric charge density ρ have zero values ($\vec{J} = 0, \rho = 0$) Then the Maxwell's Equations in time domain described by [118]:

$$\nabla \times \vec{E} = -\frac{\partial \vec{B}}{\partial t} \quad \text{III.5}$$

$$\nabla \cdot \vec{D} = 0 \quad \text{III.6}$$

$$\nabla \times \vec{H} = \frac{\partial \vec{D}}{\partial t} \quad \text{III.7}$$

$$\nabla \cdot \vec{B} = 0 \quad \text{III.8}$$

Where:

$\vec{E}$ is the electric field (Volts/m),

$\vec{B}$ is magnetic flux density (Webers/m^2).

$\vec{H}$ is the magnetic field strength (Ampers/m).

$\vec{D}$ electric displacement (coul/ m^2).

the parameters $\vec{E}$, $\vec{D}$, $\vec{B}$, and $\vec{H}$ meet the following relations:

$$\vec{D} = \varepsilon_0 \varepsilon \vec{E} \quad \text{III.9}$$

$$\vec{B} = \mu_0 \mu \vec{H} \quad \text{III.10}$$

By replacing equations 3.9 and 3.10 into 3.5, 3.6 respectively, we assume that ε is a pure real value function and consider a nonmagnetic material only which means μ=1 we find:

$$\nabla \times \vec{E}(\vec{r}, t) = -\mu_0 \frac{\partial \vec{H}(\vec{r}, t)}{\partial t} \quad \text{III.11}$$

$$\nabla \times \vec{H}(\vec{r}, t) = \varepsilon_0 \varepsilon \frac{\partial \vec{E}(\vec{r}, t)}{\partial t} \quad \text{III.12}$$

We apply plane wave solutions into eq 3.7 and 3.8

$$\vec{E}(\vec{r}, t) = \vec{E}(\vec{r}) e^{i\omega t} \quad \text{III.13}$$

$$\vec{H}(\vec{r}, t) = \vec{H}(\vec{r}) e^{i\omega t} \quad \text{III.14}$$

We have

$$\nabla \times \vec{E}(\vec{r}) + i\omega \mu_0 \vec{H}(\vec{r}) = 0 \quad \text{III.15}$$

$$\nabla \times \vec{H}(\vec{r}) + i\omega \varepsilon_0 \varepsilon \vec{E}(\vec{r}) = 0 \quad \text{III.16}$$

Divide equation III.16 by ε and then take the curl. Then use the equation III.15 to eliminate $\vec{E}(\vec{r})$ we know also that $c = 1/\sqrt{\varepsilon_0 \mu_0}$ the result equation is:

$$\nabla \times \frac{1}{\varepsilon} \nabla \times \vec{H}(\vec{r}) = \left(\frac{\omega}{c}\right)^2 \vec{H}(\vec{r}) \quad \text{III.17}$$

This is the master equation describing the propagation properties of an electromagnetic wave in a photonic crystal. This equation is determined by the field component $\vec{H}(\vec{r})$ [37].

III.2 Electromagnetism as an Eigenvalue Problem

The equation 3.13 is an eigenvalue problem. Because the results of a series of operations $\nabla \times \nabla \times$ on a function $\vec{H}(\vec{r})$ is just the function $\vec{H}(\vec{r})$ itself multiplied by some constant $(\frac{\omega}{c})^2$ the function $\vec{H}(\vec{r})$ is an eigenvector and the constant $(\frac{\omega}{c})^2$ is and eigenvalue.

$$\nabla \times \frac{1}{\varepsilon} \nabla \times \vec{H}(\vec{r}) = (\frac{\omega}{c})^2 \vec{H}(\vec{r})$$

Eigen-operator — Eigenvalue — Eigenvector

In this case, we identify the left side "the eigen operator" of the master equation as an operator Φ acting on H(r) to make it look more like a traditional eigenvalue problem [11]:

$$\Phi \vec{H}(\vec{r}) = (\frac{\omega}{c})^2 \vec{H}(\vec{r}) \qquad \text{III.18}$$

The eigenvectors $\vec{H}(\vec{r})$ are the spatial patterns of the harmonic modes, and the eigenvalues $(\frac{\omega}{c})^2$ are proportional to the squared frequencies of those modes. An important thing to notice is that the operator Φ is a linear operator. That is, any linear combination of solutions is itself a solution; if $\overrightarrow{H_1}(\vec{r})$and $\overrightarrow{H_2}(\vec{r})$are both solutions of III.18 with the same frequency ω, then $\alpha\overrightarrow{H_1}(\vec{r}) + \beta\overrightarrow{H_2}(\vec{r})$, where α and β are constants. For example, given a certain mode profile, we can construct another legitimate mode profile with the same frequency by simply doubling the field strength everywhere ($\alpha = 2, \beta = 0$). For this reason, we consider two field patterns that differ only by an overall multiplier to be the same mode.

III.3 The Bloch Theorem

The Bloch Theorem tells us that, for a Hermitian eigenproblem whose operators are periodic functions of position, the solutions can always be chosen of the form << $e^{i\vec{k}\cdot\vec{r}} \times$ ***Periodic function*** >>.

A periodic function $\vec{f}(\vec{r})$ is one such that$\vec{f}(\vec{r} + \overrightarrow{R_l}) = \vec{f}(\vec{r})$ for any primitive lattice vector $\overrightarrow{R_l}$ of the crystal. The field inside a periodic structure takes on the same symmetry and periodicity of that structure according to the Bloch theorem as shown in figure 58 [119].

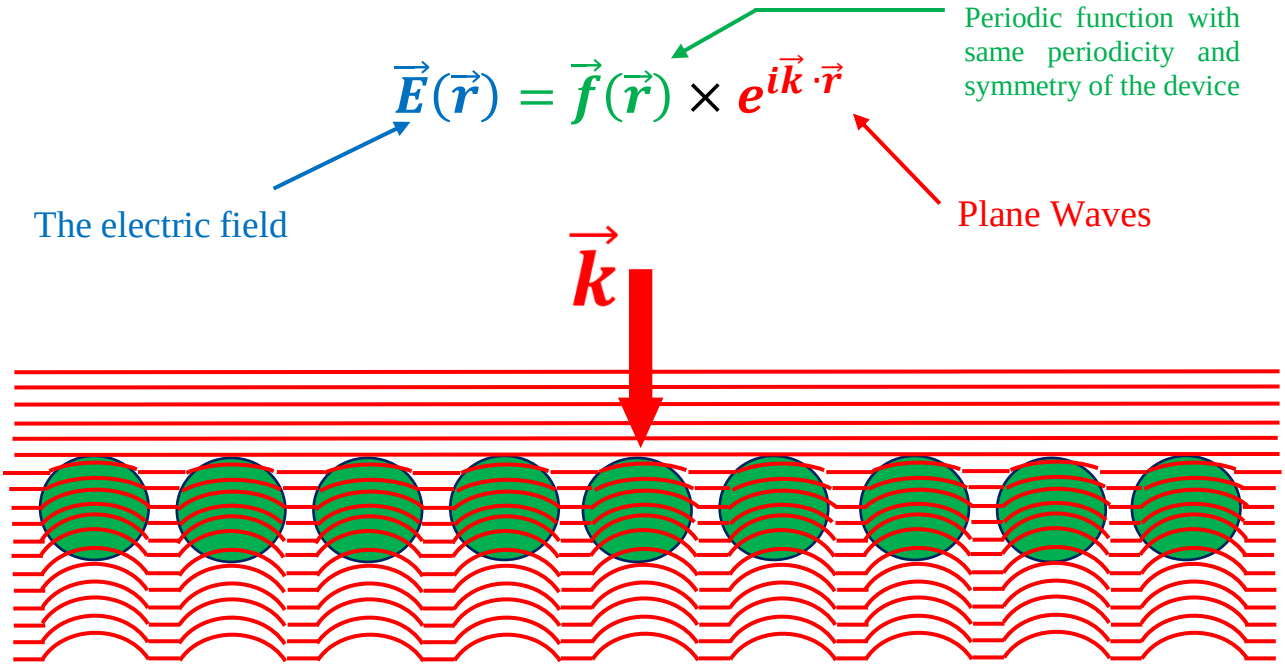

Figure 58 A schematic illustration of plan wave passes a periodic structures.

III.4 Plane wave expansion method PWE

In order to obtain the most general idea of PhCs characteristics as well as to effectively design PhC-based devices, it is convenient to use band structures. Band structures give full information about radiation behavior when propagating within the specific direction inside the PhC. Thus, the plane wave expansion method (PWE) may be the most popular method for calculating dispersion diagrams of periodic structures like photonic crystals. PWE is best suited to analyze periodic structures with low to moderate index contrast where size of the unit cell is less than a wavelength. Using the supercell method or absorbing boundary conditions. The problem of the band structure computation of a PhC is finding the dispersion relation, that is, the dependence of eigen-frequencies or resonant frequencies of the PhC on the wave vector of the radiation passing through it. In order to obtain the dispersion relation, it is necessary to solve the eigen-problem formulated for the Helmholtz equation "III.18" inside infinite periodic structure [25] [12].

III.4.1 Photonic band gap calculation using PWE

Assuming we impose a field oscillating sinusoidally with time, i.e, we can write the mode as: $\vec{E}(\vec{r},t) = \vec{E}(\vec{r})e^{i\omega t}, \vec{H}(\vec{r},t) = \vec{H}(\vec{r})e^{i\omega t}$ and by using

$\vec{D} = \varepsilon_0\varepsilon\vec{E}$, $\vec{B} = \mu_0\vec{H}$ and $\frac{\partial}{\partial t} \rightarrow j\omega$

$$\nabla \times \vec{E}(\vec{r}) = -j\omega\mu_0\vec{H}(\vec{r}) \qquad \text{III.19}$$

$$\nabla \times \vec{H}(\vec{r}) = j\omega\varepsilon_0\varepsilon\vec{E}(\vec{r}) \quad \text{III.20}$$

For H, we get the next eigen value equation:

$$\nabla \times \frac{1}{\varepsilon}\nabla \times \vec{H}(\vec{r}) = (\frac{\omega}{c})^2\vec{H}(\vec{r}) \quad \text{III.21}$$

For E, we get the next eigen value equation:

$$\nabla \times \nabla \times \vec{E}(\vec{r}) = (\frac{\omega}{c})^2\varepsilon\vec{E}(\vec{r}) \quad \text{III.22}$$

According to Bloch theorem, a plane wave in a periodic structure will be modulated by the periodicity. So, the complex-valued magnetic field H can be expressed as:

$$\vec{H}(\vec{r}) = e^{i\vec{k}\cdot\vec{r}} \times h(\vec{r})\hat{e}_k \quad \text{III.23}$$

$$h(\vec{r}) = h\left(\vec{r} + \overrightarrow{R_l}\right) \quad \text{III.24}$$

where $\overrightarrow{R_l}$ is an arbitrary lattice vector, $\hat{e}_k$ is a unit vectors perpendicular to the vector $\vec{k}$ and parallel to the H vector.

Any periodic function can be expanded using Fourier series, so is for ε and h:

$$\varepsilon(\mathrm{r}) = \sum_{\overrightarrow{G_l}} \varepsilon(\overrightarrow{G_l})e^{i\vec{G}\cdot\vec{r}} \quad \text{III.25}$$

$$\frac{1}{\varepsilon(\mathrm{r})} = \sum_{\overrightarrow{G_l}} \varepsilon^{-1}(\overrightarrow{G_l})e^{i\vec{G}\cdot\vec{r}} \quad \text{III.26}$$

$$\mathrm{h}(\mathrm{r}) = \sum_{\overrightarrow{G_l}} \mathrm{h}(\overrightarrow{G_l})e^{i\overrightarrow{G_l}\cdot\vec{r}} \quad \text{III.27}$$

$$\vec{H}(\vec{r}) = \hat{e}_k e^{i\vec{k}\cdot\vec{r}} \times \sum_{\overrightarrow{G_l}} \mathrm{h}\left(\overrightarrow{G_l}\right)e^{i\overrightarrow{G_l}\cdot\vec{r}} = \sum_{\overrightarrow{G_l},\lambda} \mathrm{h}\left(\overrightarrow{G_l},\lambda\right)e^{i(\vec{k}+\overrightarrow{G_l})\cdot\vec{r}}\hat{e}_{\lambda,\vec{k}+\overrightarrow{G_l}} \quad \text{III.28}$$

In equation III.28, the transverse property is used to decompose the wave into sum of a set of plane waves, which is the heart of this method. $\hat{e}_{\lambda,\vec{k}+\overrightarrow{G_l}}$ is the unit vector perpendicular to $\vec{k} + \overrightarrow{G_l}$ and $\mathrm{h}\left(\overrightarrow{G_l},\lambda\right)$ is the component amplitude along the unit vector. $\vec{k} + \overrightarrow{G_l}$, $\hat{e}_{1,\vec{k}+\overrightarrow{G_l}}$,. $\hat{e}_{2,\vec{k}+\overrightarrow{G_l}}$ forms a Cartesian triad. $\overrightarrow{G_l}$ is the frequency component, λ represents the two axes in the perpendicular plane and $\hat{e}_\lambda$is the unit vector along the axis. All the $\overrightarrow{G_l}$ forms the reciprocal lattice. All the $\overrightarrow{R_l}$ forms the crystal lattice:

$$\overrightarrow{R_l} = l_1\overrightarrow{a_1} + l_2\overrightarrow{a_2} + l_3\overrightarrow{a_3} \quad \text{III.29}$$

l_1, l_2, l_3 are any integers, $\overrightarrow{a_1}, \overrightarrow{a_2}, \overrightarrow{a_3}$ are called the primitive lattice vectors to describe the lattice.

$$\overrightarrow{G_h} = h_1\overrightarrow{b_1} + h_2\overrightarrow{b_2} + h_3\overrightarrow{b_3} \quad \text{III.30}$$

Where, $\overrightarrow{b_1}, \overrightarrow{b_2}, \overrightarrow{b_3}$ are called the primitive reciprocal lattice vectors and $h_1, h_2, h_3$are any integers. Substitute (3.29) and (3.27) into eigen equation (3.22):

$$\nabla \times \frac{1}{\varepsilon} \nabla \times \vec{H}(\vec{r}) = (\frac{\omega}{c})^2 \vec{H}(\vec{r}) \quad \text{III.31}$$

$$\frac{1}{\varepsilon(\mathrm{r})} = \sum_{\overrightarrow{G_l}} \varepsilon^{-1}(\overrightarrow{G_l}) e^{i\vec{G}\cdot\vec{r}} \quad \text{III.32}$$

$$\vec{H}(\vec{r}) = \hat{e}_k e^{i\vec{k}\cdot\vec{r}} \times \sum_{\overrightarrow{G_l}} \mathrm{h}(\overrightarrow{G_l}) e^{i\overrightarrow{G_l}\cdot\vec{r}} = \sum_{\overrightarrow{G_l},\lambda} \mathrm{h}(\overrightarrow{G_l},\lambda) e^{i(\vec{k}+\overrightarrow{G_l})\cdot\vec{r}} \hat{e}_{\lambda,\vec{k}+\overrightarrow{G_l}} \quad \text{III.33}$$

$$\nabla \times \sum_{\overrightarrow{G_l}} \varepsilon^{-1}(\overrightarrow{G_l}) e^{i\vec{G}\cdot\vec{r}} \; \nabla \times \sum_{\overrightarrow{G_l},\lambda} \mathrm{h}(\overrightarrow{G_l},\lambda) e^{i(\vec{k}+\overrightarrow{G_l})\cdot\vec{r}} \hat{e}_{\lambda,\vec{k}+\overrightarrow{G_l}} = (\frac{\omega}{c})^2 \sum_{\overrightarrow{G_l},\lambda} \mathrm{h}(\overrightarrow{G_l},\lambda) e^{i(\vec{k}+\overrightarrow{G_l})\cdot\vec{r}} \hat{e}_{\lambda,\vec{k}+\overrightarrow{G_l}} \quad \text{III.34}$$

By applying the transverse condition, Helmholtz's equation can be transformed to an algebraic form [120] :

$$\sum_{G'} |k+G||k+G'| \varepsilon^{-1}(\mathrm{G}-G') \begin{bmatrix} \hat{e}_2 \hat{e}_2^{'} & -\hat{e}_2 \hat{e}_1^{'} \\ -\hat{e}_1 \hat{e}_2^{'} & \hat{e}_1 \hat{e}_1^{'} \end{bmatrix} \begin{bmatrix} h_1' \\ h_2' \end{bmatrix} = (\frac{\omega}{c})^2 \begin{bmatrix} h_1 \\ h_2 \end{bmatrix} \quad \text{III.35}$$

This is a standard eigenvalue problem. Which can be implemented by numerical method.

A photonic band diagram is constructed by lining up the eigen-values computed over a sequence of Bloch wave vectors. The sequence contains values of β that progress around the perimeter of the IBZ connecting all key points of symmetry as shown in figure 59. The PWE calculates all the modes the eigen-values contain the frequencies and the eigen-vectors contain the fields [25].

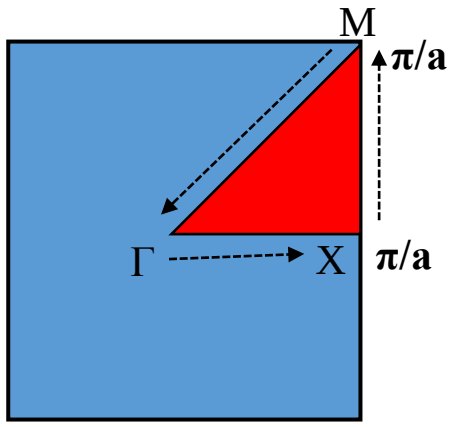

$$\vec{\beta} = \begin{bmatrix} 0 & \pi/a & \pi/a & 0 \\ 0 & 0 & \pi/a & 0 \\ \Gamma & \chi & \mathrm{M} & \Gamma \end{bmatrix}$$

Figure 59 Schematic of all key points of the perimeter of the IBZ

Now we use the PWE method we set up a loop that iterates over a list for each Bloch wave vector we calculate a whole list of eigen values to obtain the band gap diagram as an example we consider a rectangular structure with air hole radius r=0.2a and lattice constant a=1 nm the structure is in silicon n_{si}=3.48 as shown in figure 60.

Γ	0	0	0	0.54	0.55	0.55
X	π/a	0	0.24	0.42	0.55	0.71
M	π/a	π/a	0.28	0.49	0.49	0.68
Γ	0	0	0	0.54	0.55	0.55

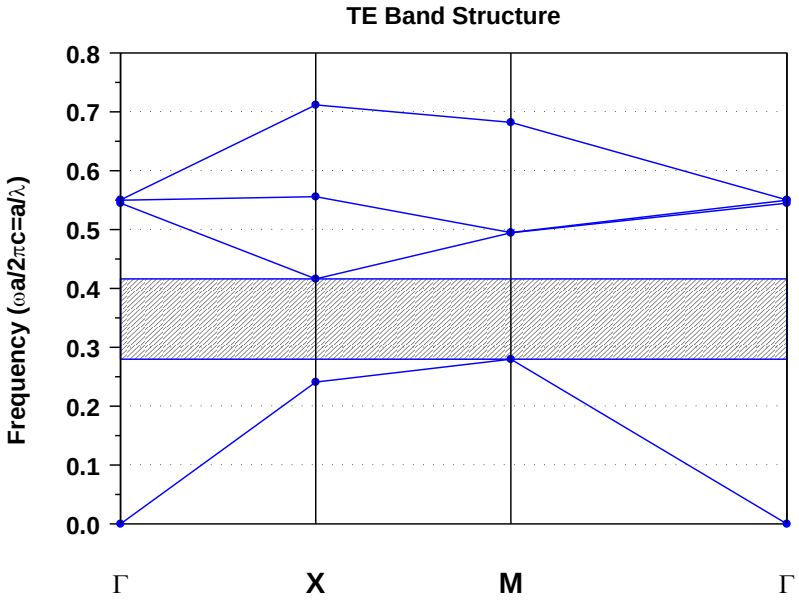

Figure 60 Bloch wave vector with the eigen values to create a band gap diagram

III.5 The Finite difference time-domain (FDTD) method

The FDTD method is widely used, and it is considered one of the most applicable for the problems. It is universal, robust, methodologically simple and descriptive. The wave propagating through the structure is found by direct integration in the time domain of the Maxwell's equations in discretized form. in FDTD an incident electromagnetic wavefield is propagated in discretized space and discretized time, according to both Maxwell equations and the constitutive relations (which state how materials respond to the EM field). This information is then post-processed to obtain the EM response of the considered system. This method was originally proposed in 1966 by K. Yee, and has been developed over the years [121] [122] Maxwell's equations in an isotropic medium can be expressed as follows [123]:

$$\frac{\partial \vec{B}}{\partial t} + \nabla \times \vec{E} = 0 \implies -\mu \frac{\partial \vec{H}}{\partial t} = \nabla \times \vec{E} \qquad \text{III.36}$$

$$\frac{\partial \vec{D}}{\partial t} - \nabla \times \vec{H} = J \ , \ J = 0 \implies \varepsilon \frac{\partial \vec{E}}{\partial t} = \nabla \times \vec{H} \qquad \text{III.37}$$

$$B = \mu H \qquad \text{III.38}$$

$$D = \varepsilon E \qquad \text{III.39}$$

The below figure 61 shows the Yee grid and illustrates the $\vec{E}$ and $\vec{H}$ components in 3D space. in a rectangular coordinate system, III.36 and III.37 are equivalent to the following system of scalar equations:

$$\begin{cases} -\mu \frac{\partial H_x}{\partial t} = \frac{\partial H_z}{\partial y} - \frac{\partial H_y}{\partial z} \\ -\mu \frac{\partial H_y}{\partial t} = \frac{\partial E_x}{\partial z} - \frac{\partial E_z}{\partial x} \\ -\mu \frac{\partial H_z}{\partial t} = \frac{\partial E_y}{\partial x} - \frac{\partial E_x}{\partial y} \\ \varepsilon \frac{\partial E_x}{\partial t} = \frac{\partial H_z}{\partial y} - \frac{\partial H_y}{\partial z} \\ \varepsilon \frac{\partial E_y}{\partial t} = \frac{\partial H_x}{\partial z} - \frac{\partial H_z}{\partial x} \\ \varepsilon \frac{\partial E_z}{\partial t} = \frac{\partial H_y}{\partial x} - \frac{\partial H_x}{\partial y} \end{cases} \quad \text{III.40}$$

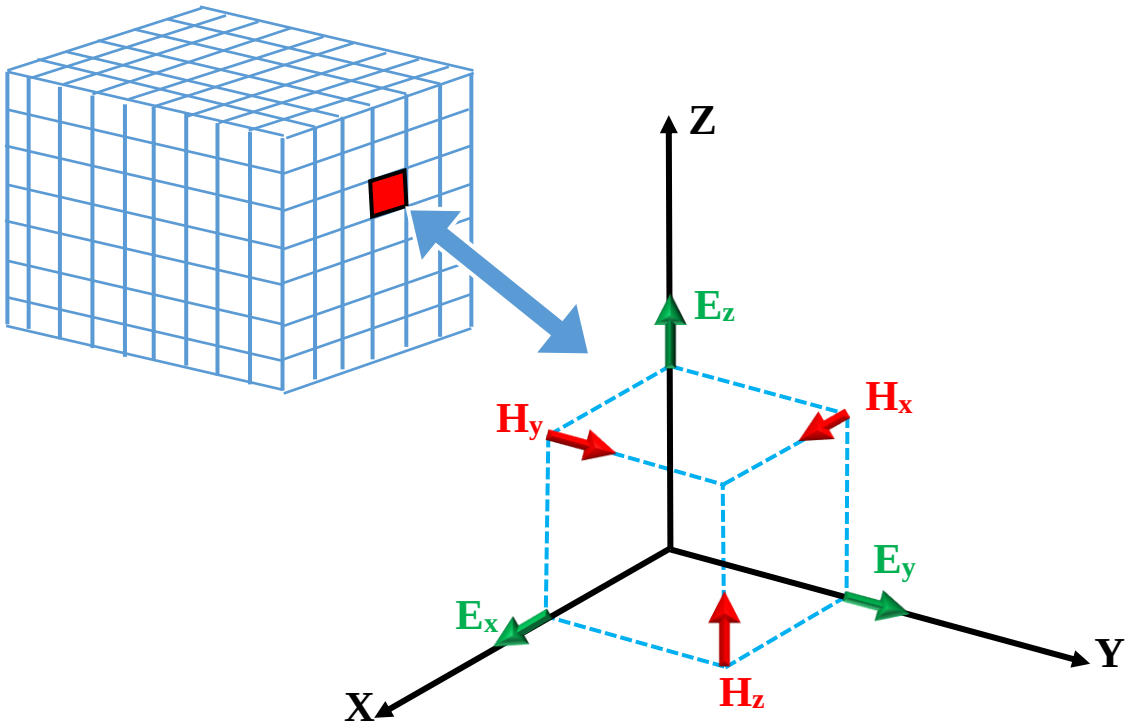

Figure 61 Positions of various field components electric field (red color) magnetic field (red color) reprinted with permission from lecture 11 of EE 5337 computational electromagnetics by Pr. Raymond Rumpf.

Yee used centered finite difference expression for the space and time derivates. With Yee algorithm, we re-write 3D Maxwell's equations for example the first equation from 3.47 become $-\mu \frac{\partial H_x}{\partial t} = \frac{\partial H_z}{\partial y} - \frac{\partial H_y}{\partial z}$ become:

$$H_x^{n+\frac{1}{2}}\left(i,j+\frac{1}{2},k+\frac{1}{2}\right)=H_x^{n-\frac{1}{2}}\left(i,j+\frac{1}{2},k+\frac{1}{2}\right)-\frac{\Delta t}{\mu}\left\{\frac{1}{\Delta y}\left[E_z^n\left(i,j+1,k+\frac{1}{2}\right)-E_z^n\left(i,j,k+\frac{1}{2}\right)\right]-\frac{1}{\Delta z}\left[E_y^n\left(i,j+\frac{1}{2},k+1\right)-E_y^n\left(i,j+\frac{1}{2},k\right)\right]\right\} \quad \text{III.41}$$

$\varepsilon\frac{\partial E_x}{\partial t}=\frac{\partial H_z}{\partial y}-\frac{\partial H_y}{\partial z}$ become:

$$E_x^{n+1}\left(i+\frac{1}{2},j,k\right)=E_x^n\left(i+\frac{1}{2},j,k\right)+\frac{\Delta t}{\varepsilon}\left\{\frac{1}{\Delta y}\left[H_z^{n+\frac{1}{2}}\left(i+\frac{1}{2},j+\frac{1}{2},k\right)-H_z^{n+\frac{1}{2}}\left(i+\frac{1}{2},j-\frac{1}{2},k\right)\right]-\frac{1}{\Delta z}\left[H_y^{n+\frac{1}{2}}\left(i+\frac{1}{2},j,k+\frac{1}{2}\right)-H_y^{n+\frac{1}{2}}\left(i+\frac{1}{2},j,k-\frac{1}{2}\right)\right]\right\} \quad \text{III.42}$$

Where *n* is an integer representing the compute step.

III.5.1 grid size and stability criterion

To ensure the accuracy of the computed results, the spatial grid must be small enough to resolve the smallest feature of the field to be simulated. This means that, to have meaningful results, the linear dimension of the grid must be only a fraction of the wavelength. We shall choose Δx=Δy=Δz. For computational stability, it is necessary to satisfy a relation between the space increment and time increment Δt. To obtain a stable simulation, one must adhere to the Courant condition which relates the spatial and temporal step size [124] [116]:

$$c\Delta t<\frac{1}{\sqrt{(1/\Delta x^2+1/\Delta y^2+1/\Delta z^2)}} \quad \text{III.43}$$

where *c* is the velocity of light.

III.5.2 Boundary conditions

The perfectly matched layer PML technique theoretically allows the electromagnetic waves to be absorbed with a reflection as short as needed. Thus, absorbing layer which does not activate any reflection at an interface with first vacuum described in figure 62, Finite-difference experiments have shown that a small amount of numerical reflection occurs in practical computations, but with a magnitude that can be reduced by tuning some parameters of the layer, especially its thickness. So, using the PML technique allows us to obtain a better accuracy in some problems and a release of computational requirements in some others [125].

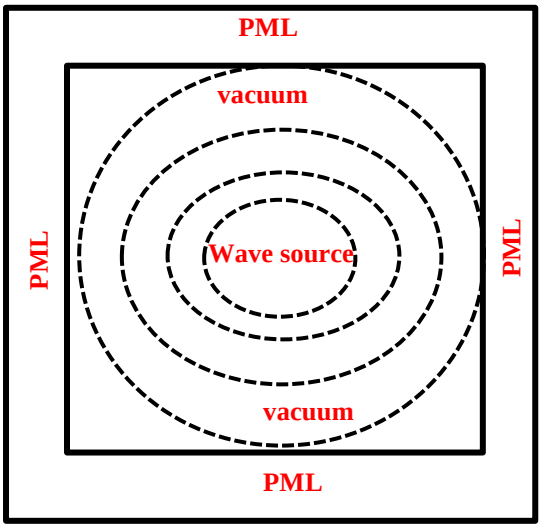

Figure 62 The PML technique.

III.6 Simulation software

Simulation software is based on the process of modeling a real phenomenon with a set of mathematical formulas. Scientific laws give algorithms, or procedures, for determining how systems behave. The computer program is a medium in which the algorithms can be expressed and applied. Physical objects and mathematical structures can be represented as numbers and symbols in a computer, and a program can be written to manipulate them according to the algorithms. When the computer program is executed, it causes the numbers and symbols to be modified in the way specified by the scientific laws. It thereby allows the consequences of the laws to be deduced [126]. There are commercial software packages available for many electromagnetic modeling techniques such as Rsoft, Lumerical, COMSOL, MPB from MIT, Optiwave.

III.6.1 Rsoft

The RSoft Photonic Component Design Suite allows users to design and simulate both passive and active photonic devices for optical communications, optoelectronics, and semiconductor manufacturing. The RSoft CAD Environment is the core program of the RSoft Passive Device Suite, and allows researchers and engineers to create systems for the design of waveguide devices, optical circuits, and other photonic devices. It acts as a control program for the RSoft passive device modules, including BeamPROP, FullWAVE, BandSOLVE, ModePROP, DiffractMOD, GratingMOD, and FemSIM, and defines the important input required by these programs: the material properties and structural geometry of the device to be studied [127]. In this work we used two modules, BandSOLVE and FullWAVE.

III.6.1.1 BandSOLVE

BandSOLVE is a simulation module for generating and analyzing photonic band structures. This simulation engine employs the Plane Wave Expansion (PWE) algorithm to perform band computations, and also provides a graphical display of the electromagnetic fields and other quantities of interest for further analysis. It is ideal for producing band structures for classic photonic bandgap structures such as 2D and 3D photonic crystal waveguides and defect sites. In addition, it can be applied to a wide range of PC components, including but not limiting to: 2D and 3D PC slab and waveguides, 2D and 3D cavity problems, Photonic crystal fibers, both band-gap guiding and conventional, Defect modes of non-strictly periodic structures, Metallic and anisotropic structures guiding. To review the strength and accuracy of this module we re-simulated some important published papers.

The first paper is in ref [80] which cited by 170 times. In this paper, a photonic crystal slab consisting of circular holes in a triangular lattice.

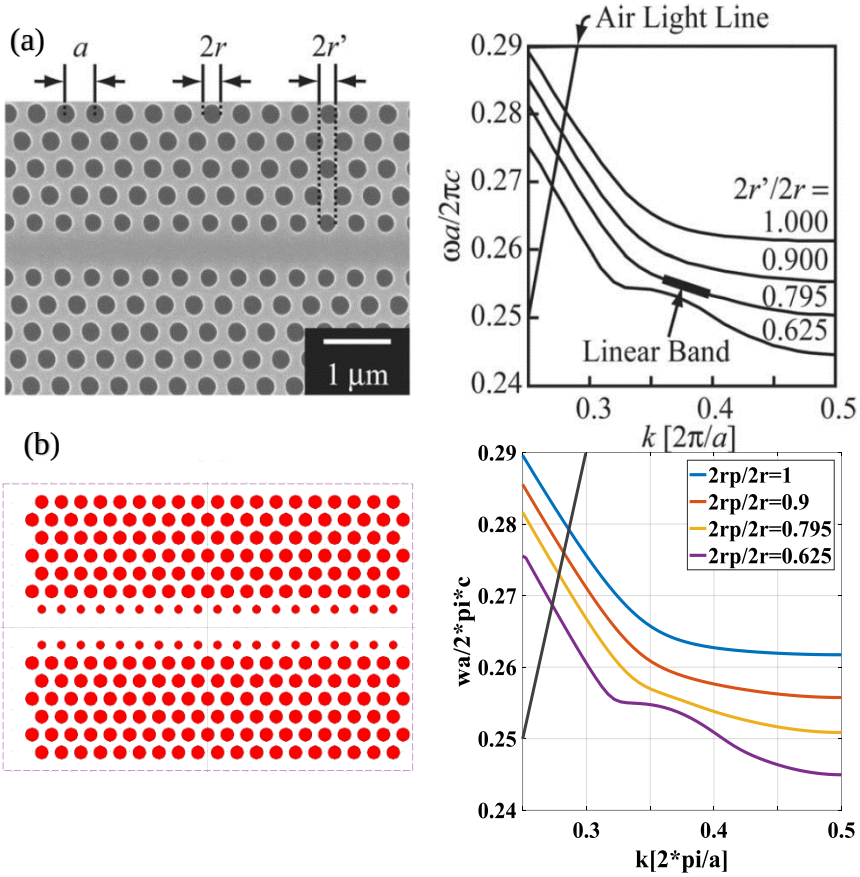

Figure 63 Photonic band of the main propagation mode of PCW (a) ref [80] (b) re-simulated structure with BandSOLVE Rsoft.

We present the photonic band of the main propagation mode of the single-line-effect PCW when the polarization is assumed to be transverse electric the results from the paper and our results using

BandSOLVE in figure 63 (a) (b) respectively. The 2D analysis performed with an effective index of n_{eff}= 2.9.

Also, we calculated the group index n_g characteristics obtained from the photonic bands above. We obtained the same results of the ref [75] as shown in figure 64.

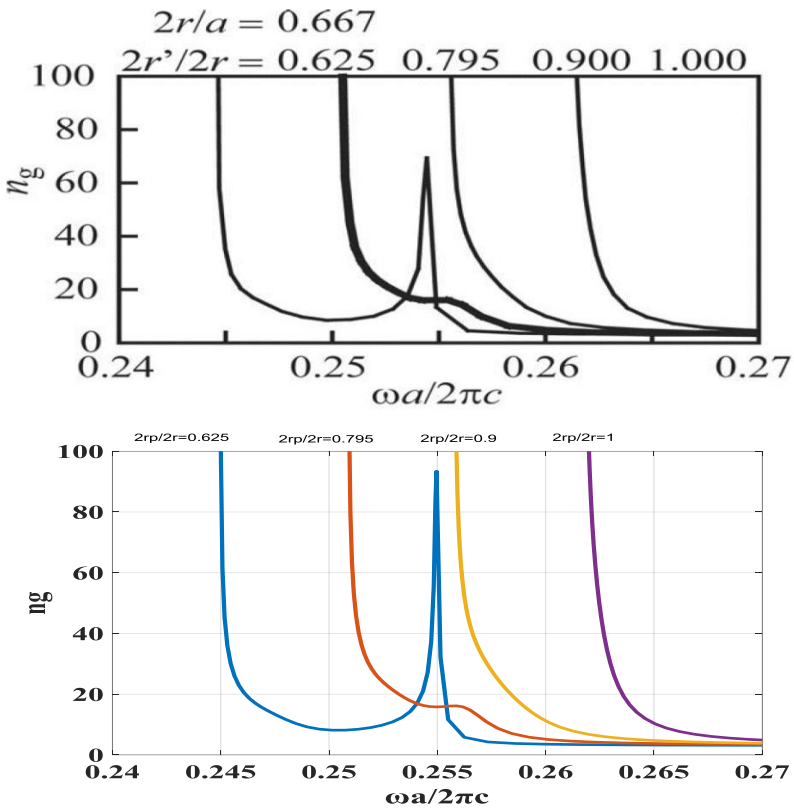

Figure 64 Comparison between the group index results from ref [75] and our results using BandSOLVE Rsoft.

We also re-simulated the paper in ref [61] which have 543 citations and we obtained the same results as we illustrated it in chapter 2.

III.6.1.2 Fullwave

FullWAVE is a highly sophisticated simulation tool for studying the propagation of light in a wide variety of photonic structures. In addition it's ideal for the design of complex photonic devices including integrated and fiber-optic waveguide devices as well as circuits and nanophotonic devices such as photonic crystals. The software employs the finite difference time-domain (FDTD) method for simulation, which allows analysis of devices, such as photonic bandgaps and ring resonators.

Fullwave has applications in a wide range of integrated and nano-optic devices including, but not limited to: WDM devices such as ring resonators, Photonic bandgap circuits & applications,

Grating structures, surface normal gratings, and other, diffractive structures, Cavity computations and extractions, Biophotonics, Light scattering, Sensor and bio-sensor designs, Plasmon propagation effects, Surface plasmons, Negative refractive index materials [128].

We discuss in this section the transmission spectra and resonance cavity. Let's consider a square lattice of dielectric circles of silicon with refractive index of 3.4 and in a background of air. The constant lattice a=0.6 um and rod radius is r=0.3*a as shown in figure 65 the PhC exhibit a three band gaps. Now we use the Fullwave to calculate the transmission of light through our photonic crystal structure. As we see in figure 66 the PhC crystal prevent the transmission of light in three places exactly as in band gap structure calculated with Bandsolve.

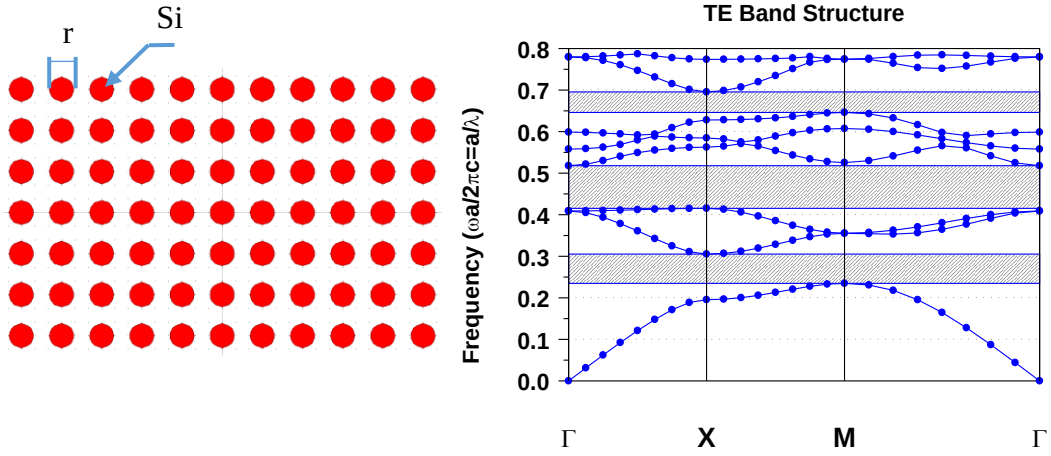

Figure 66 Square lattice and the corresponding band gap.

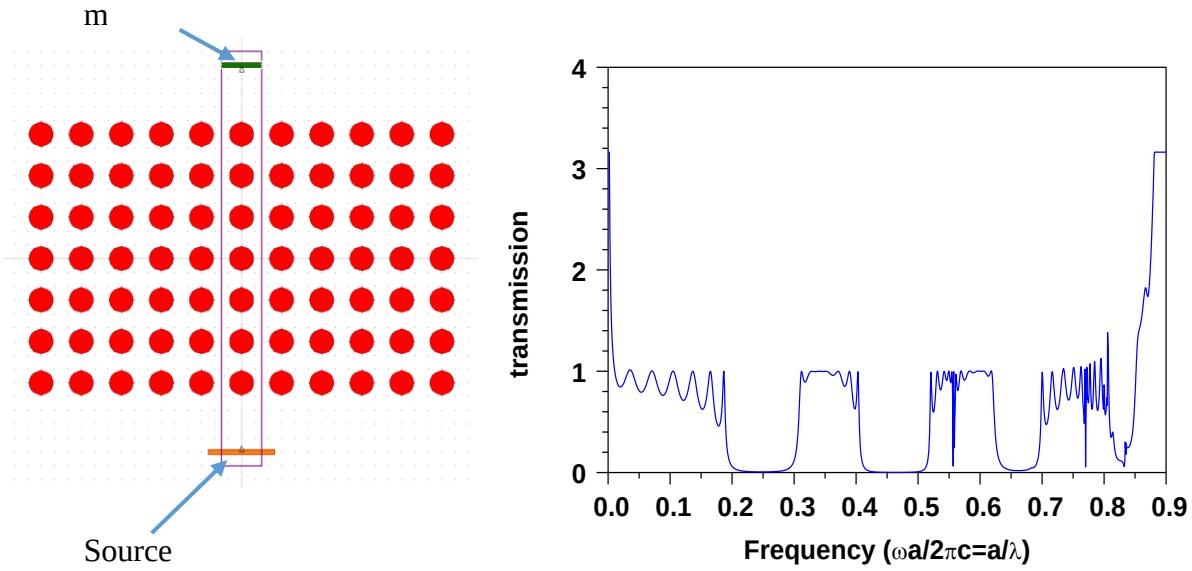

Figure 65 The computed transmission of the PhC.

Now we calculate the transmission again but we create a defect in the PhC by removing the center rod. As expected, the defect creates a resonant cavity which open two peaks in two different places inside the band gap as shown in figure 67.

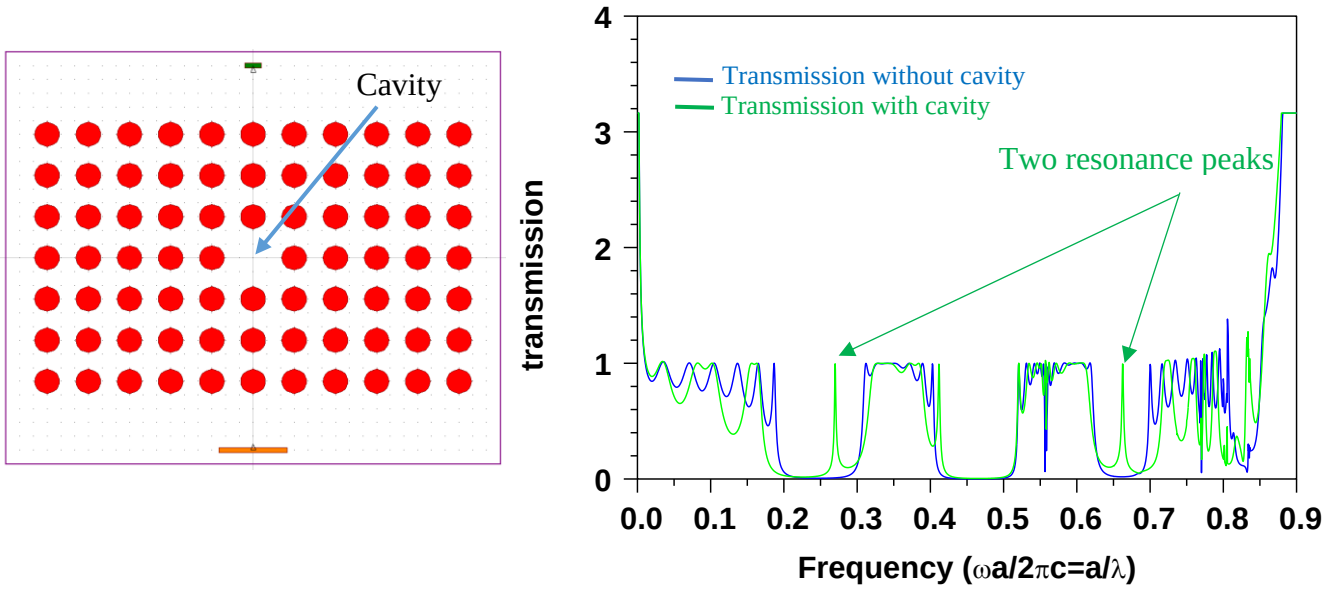

Figure 67 The resonance of the cavity in the PhC.

We re-simulated a paper published in nature with more than 1200 citations in ref [129] as shown in figure 68 (a) the structure proposed in the paper and (b) the simulated structure using Rsoft. We use layer table editor to create the structure. The results are summarized in the figure 69.

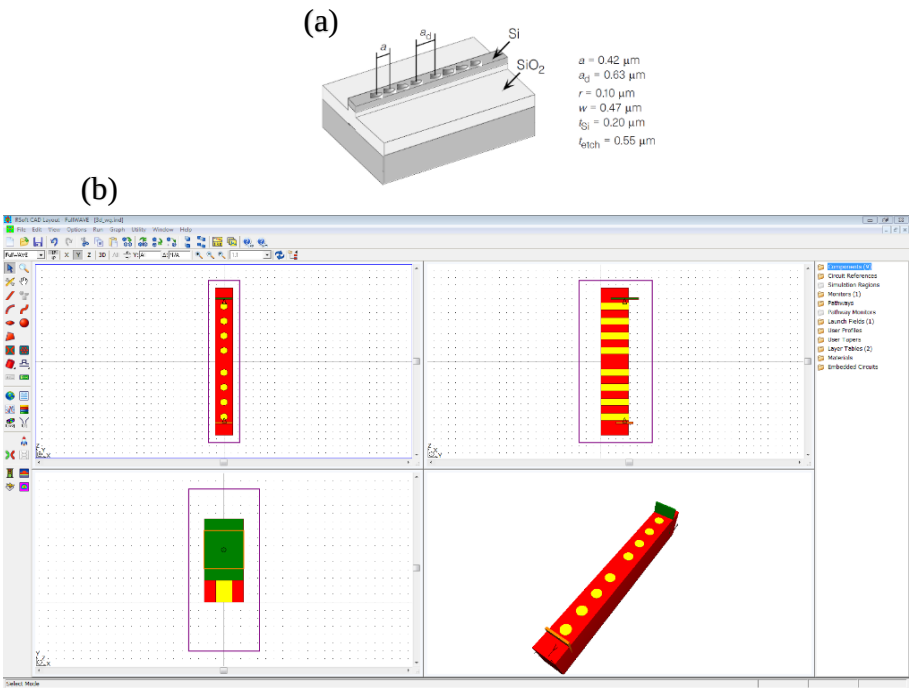

Figure 68 Structure (a) nature paper (b) re-simulated structure using Rsoft.

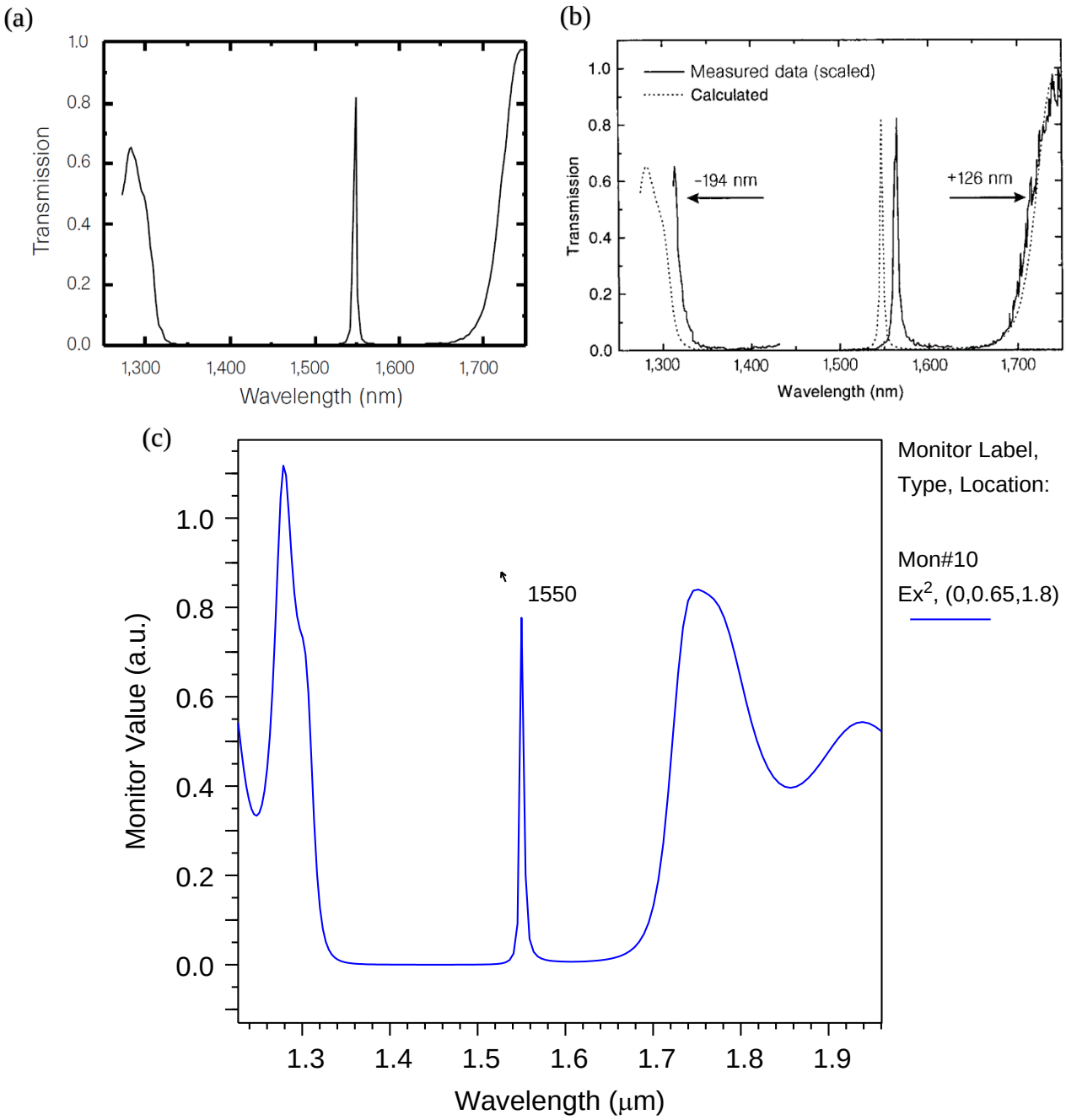

Figure 69 Computed Transmission spectrum of the PhC cavity structure (a) simulation (b) measured transmission [129](c) simulation with Fullwave Rsoft.

The simulation results with Fullwave are in remarkable agreement with the results from the paper of ref [129].

III.7 The effective index method EIM

When designing planar photonic crystal (PhC) devices, the most reliable calculations to describe the experiments are obtained with a three-dimensional (3D) discretization of the device, which are very demanding in terms of time and memory requirements. Therefore, an effective index approximation of PhC has been used in this study for relieving these requirements by reducing the full 3D calculations to simpler 2D calculations. Thus, the computational efforts needed in the design were significantly reduced. The PCS is replaced by a 2D system with the background dielectric medium having the effective refractive index of the fundamental guided mode of the slab system. For different structures of photonic crystal devices, the effective indexes are totally different because this approximation takes into account the Si slab thickness, the resonant wavelength and the polarization (TE, TM) type. Therefore, each designed structure presents a specific effective refractive index according to its initial predefined properties [130] [131].

Let's consider the structure published in the ref [132] which demonstrated the validity of the two-dimensional approximation by the effective index method for heterostructure slab waveguide based two-dimensional photonic crystals tested against the full-vectorial three-dimensional finite-difference time-domain calculations. This paper is cited more than 360 times, it is an important paper. We re-simulated the structure mentioned in this paper and we compared the results.

The proposed structure is photonic crystal slab waveguide with SiO2 /Si/SiO2 system with $n_{SiO2} = 1.5$, $n_{Si} = 3.6$ and the core layer thickness 0.4a as shown in figure 70.

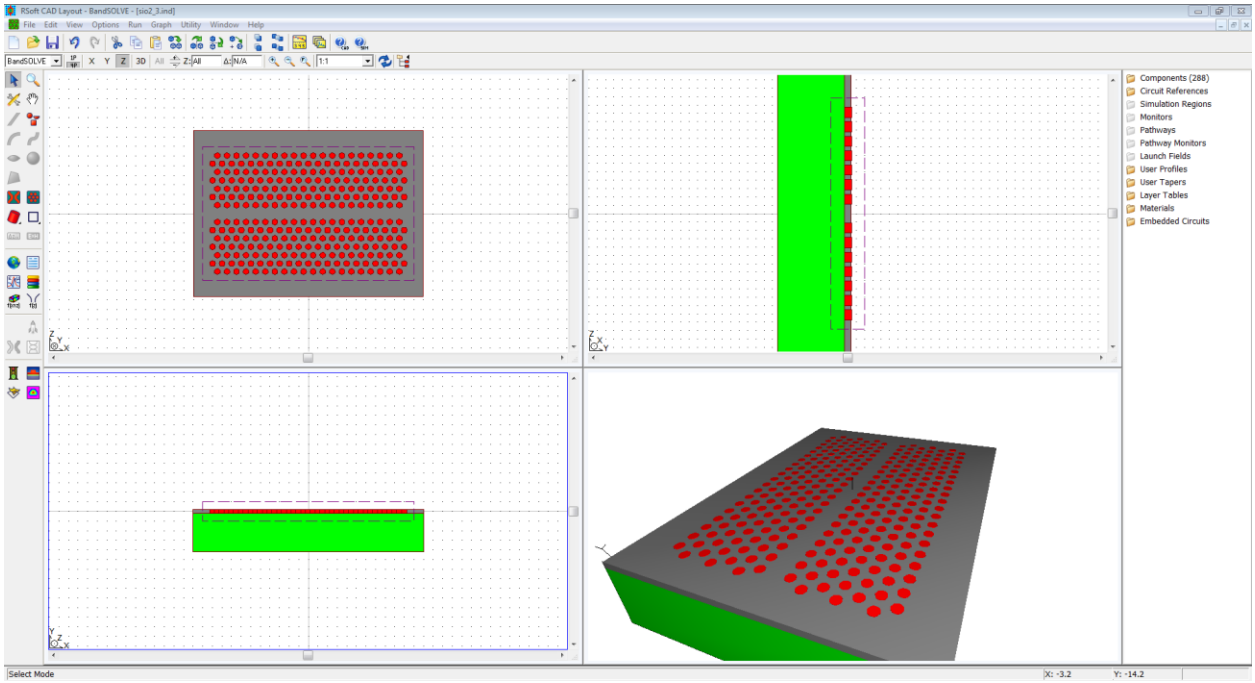

Figure 70 The proposed structure using Rsoft software, with 3 layers SiO2 /Si/SiO2.

We calculated the guided modes inside the band gap using 3D plane wave expansion method for three dimensional calculations and 2D PWE for 2D photonic crystal waveguide with the calculated effective refractive index n_{eff}=2.73. The refractive effective index calculated by Rsoft software. we found the results in the figure 71.

(a) (b)

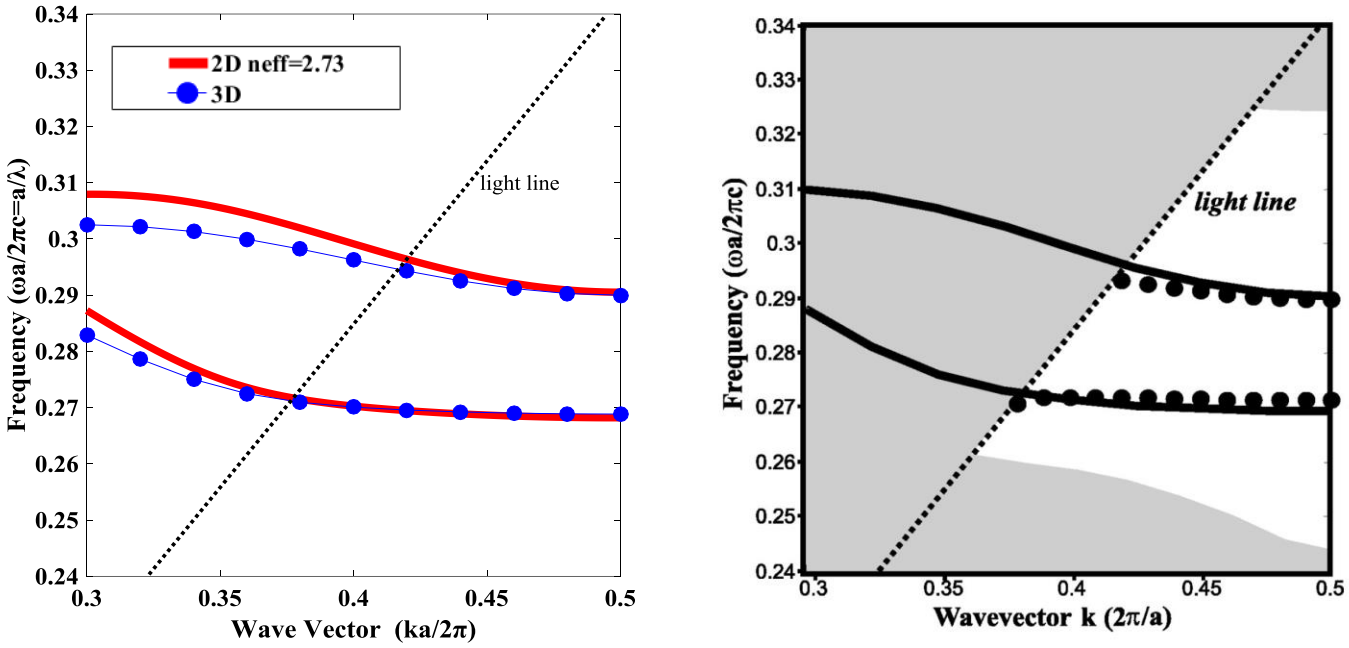

Figure 71 (a) The Calculated guided modes of the photonic crystal slab waveguide using Rsoft software, 2D PWE (red curve) 3D PWE (the blue dot) and (b) the computed guided modes in a PC waveguide of the ref [132].

the effective index method is still valid, our results are totally equivalent with the obtained results in the paper on ref [132].

III.8 Conclusion

In this chapter, we first presented Maxwell's Equations which describe all phenomena in electric and magnetic field then we explain the electromagnetism as an eigenvalue problem. Then, we outline the numerical methods that were used in our calculations such as Plane wave expansion method PWE and how we use it to calculate Photonic band gap with an example, and The Finite difference time-domain (FDTD) method with stability criterion to ensure the accuracy of the computed results. Finally, we present the RSoft CAD and the two important modules which used in this work (Bandsolve and Fullwave) with examples to review the strength and accuracy of this modules.

Chapter IV

Results and Discussions

Chapter IV Results and Discussions

IV. Introduction

Photonic crystals (PhCs) have evoked a lot of research interest in recent years, since their wavelength-scale periodic nature allows us to manipulate light in a way that has not been possible in conventional (not periodically structured) materials [133]. Photonic Crystals are periodically structured electromagnetic media, generally possessing photonic band gaps: certain frequencies do not pass through the structure. The PBG structures have several scientific and technical areas and various devices. A few years ago, the photonic crystals waveguides (PhCWs) can have a low group velocity away from the band edge, this property which named "Slow light" attracts a wide attention due to its wide applications. Slow light promotes stronger light–matter interaction, it offers additional control over the spectral bandwidth of this interaction and it allows us to delay and temporarily store light in all-optical memories. It is also anticipated to enhance linear and nonlinear effects and so miniaturize functional photonic devices because slow light compresses optical energy in space, as a light pulse enters a photonic-crystal waveguide operating in the slow-light regime, the pulse length is compressed resulting in increased intensity [134] [135] [136] [7] [5] [137]. In this chapter we investigated the optical properties of the resonance modes such as,

group delay, group velocity and normalized-bandwidth-delay product (NBDP), in photonic crystal waveguides. It can be seen by suitable design of the photonic crystal structure, the interested parameters such as, group index, delay time and the normalized delay-bandwidth product can be tuned to any desired values. We explore a simple and technologically preferable method to achieve slow light. Shifting air holes is one of the simplest methods in terms of control and fabrication, therefore, we have two photonic crystal waveguides designs PCW1 and PCW2: the first proposed method lies on inserting reduced air holes with a half period in the middle of the waveguide and shifting only the second rows of air holes adjacent to the center waveguide, and keep the position of the first rows unchanged. The second design obtained by enlarging the entire holes of the PhC and shifting the first and second rows adjacent to the line defect in the propagation direction of light, we focused on reducing the unwanted dispersion by engineering the dispersion curve with the aim of achieving a constant group index over a broad wavelength range and low group velocity dispersion (GVD).

IV.1 The first proposed structure of slow light PCW1

The first design of modified photonic crystals waveguide is proposed and shown in figure 72 (a). It is a triangular lattice photonic crystal slab consisting of circular air holes of radius r=0.3a, where a=400 nm is the lattice constant, embedded in a silicon-on-insulator (SOI) substrate (n_{si} = 3.48) with a 410 nm thickness. The silicon slab has been bounded by an upper cladding layer of air and a lower cladding layer of silica (SiO_2). The x-axis is parallel to the line defect and the y-axis is perpendicular to the line defect of the waveguide.

The waveguide is formed by replacing the central row of air holes in the triangular lattice photonic crystal along the Γ-K direction with successively reduced air holes with a half lattice constant (a/2). Three-dimensional photonic crystals (PC) with a complete band gap are ideal candidates for these applications, but their fabrication is challenging. An alternative solution is the photonic crystal slab PCS because of their relative ease of fabrication, their photonic band gaps lie in the x-y plane, and the index differences are used to confine the light vertically (total internal reflection). But full three-dimensional calculation and simulation of such complex devices are very time consuming and extreme demands on computer memory. To deal with this drawback, the effective index method (EIM) [130] has been widely used to reduce the actual 3D problem shown in figure 72 (b) to a 2D one. The effective refractive index for our photonic crystal slab has been calculated to be 3.2.

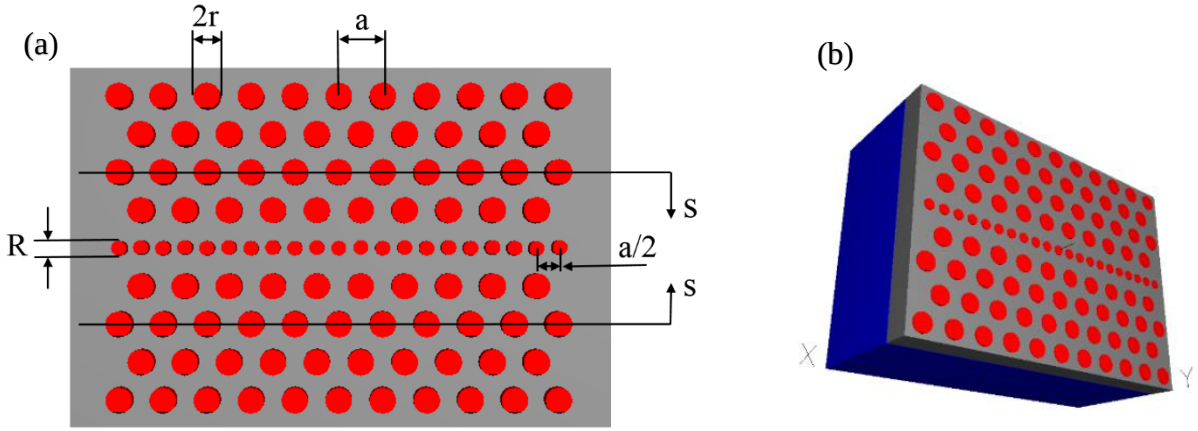

Figure 72 Schematic representation of the proposed modified photonic crystal waveguide with reduced air holes in the middle of the waveguide, (a) the 2D modified photonic crystal waveguide with neff=3.2, (b) photonic crystal slab on 3D.

The most important property of the photonic crystals is the band gap. Figure 73 shows the calculated band diagram for the initial PhC structure consisting of circular air holes; it has been calculated along the Γ-K-M-Γ edge for the BZ by employing a 2-D PWE method of the RSoft (BandSOLVE) software. The structure exhibits a photonic band gap for TE polarization in the normalized frequency range of 0.2241 (ωa/2πc) and 0.2926 (ωa/2πc). Using the triangular PhCs is very valuable, since they have a large bandgap with the TE polarization, and it is a good platform for photonic integrated circuits, optical sensors, and miniaturized optical devices [138]

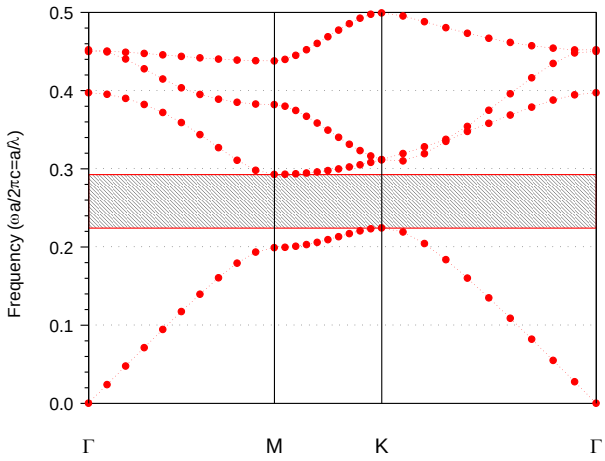

Figure 73 Dispersion diagram and band gap for TE polarization for the 2D triangular lattice of air holes without defects.

Preliminary, we study the simplest form of a waveguide line-defect waveguide as shown in figure 74 (a), which obtained by removing a row of holes along the Γ-K direction of 2D triangular lattice photonic crystals with cylindrical air holes in silicon. Figure 74 (b) shows the selected

supercell, since the photonic crystal structure is still perfectly periodic in the X direction, we use one row of air holes along the X-axis, but we need to include more rows along the Y-axis then 8 rows of air holes in the Y direction which adequate for eigenmodes calculation.

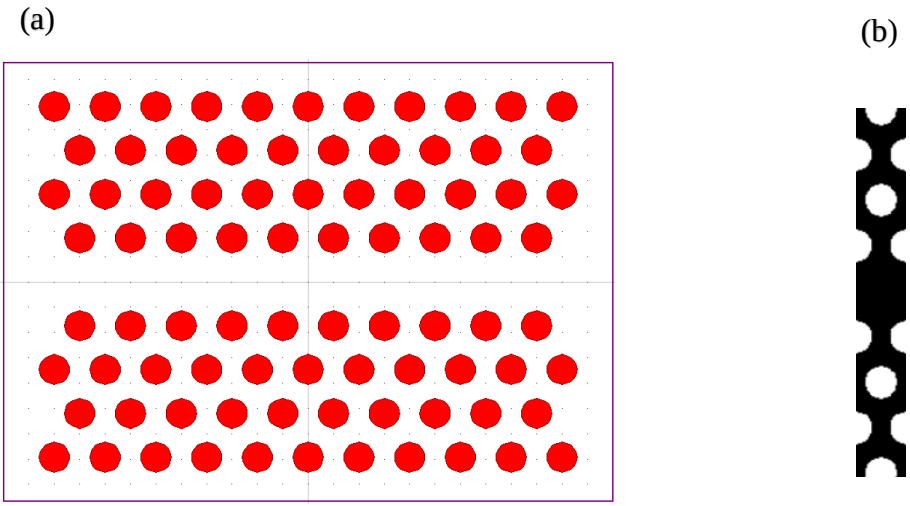

Figure 74 Schematic picture of the W1 line-defect waveguide with r=0.3a and lattice constant a=0.4. (b) The periodic supercell for simulation analysis.

The dispersion diagram for the w1 has been shown in figure 75 (a) which exhibits two guided modes, the odd and even modes by solid blue and red curve, respectively, existing below the silica light line. Only the dispersion region below the light line could confine light well in the vertical direction of the slab, whereas modes above the light line become leaky. The linear dispersion curve of the even mode has a wide range of wave vectors, therefore, in this paper we discussed only the vertically even transverse electric like modes.

By using the 2D finite difference time domain (FDTD) method we obtained the electric field distribution of the even mode shown in figure 75 (b), it is clear that the energy is concentrates in the line defect of the waveguide due to symmetric constraint.

The group velocity $v_g = d\omega/dk = c/n_g$ of the light wave can be calculated from the slope of the dispersion curve, where k and ω are the wave vector and the light frequency, respectively. ng and c are the group index and the speed of light in vacuum, respectively. The group velocity dispersion GVD is defined as the derivative of the inverse group velocity $d(vg^{-1}) = d^2k/d\omega^2$.

In the figure 75 (a) we see that the normalized frequency of the even mode at the band edge is $\frac{\omega a}{2\pi c} = 0.23042$ which means that the wavelength at the band edge is λ=1735 nm ($\frac{\omega a}{2\pi c} = \frac{a}{\lambda}$ where λ is the wavelength) so the group index will extremely increase at this frequency.

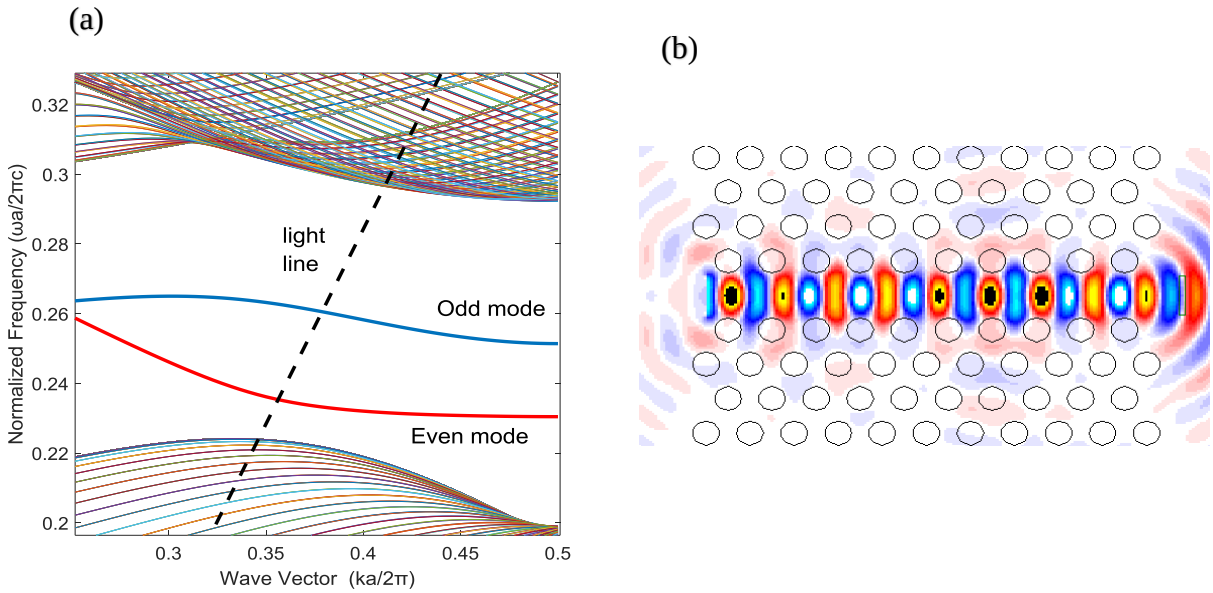

Figure 75 Calculated dispersion diagram of the basic w1 (b) The electric field distribution of the basic w1.

The speed of the light wave is slowing very dramatically. The group index has been calculated for the basic photonic crystal waveguide w1 as shown in Fig. 76 (a).

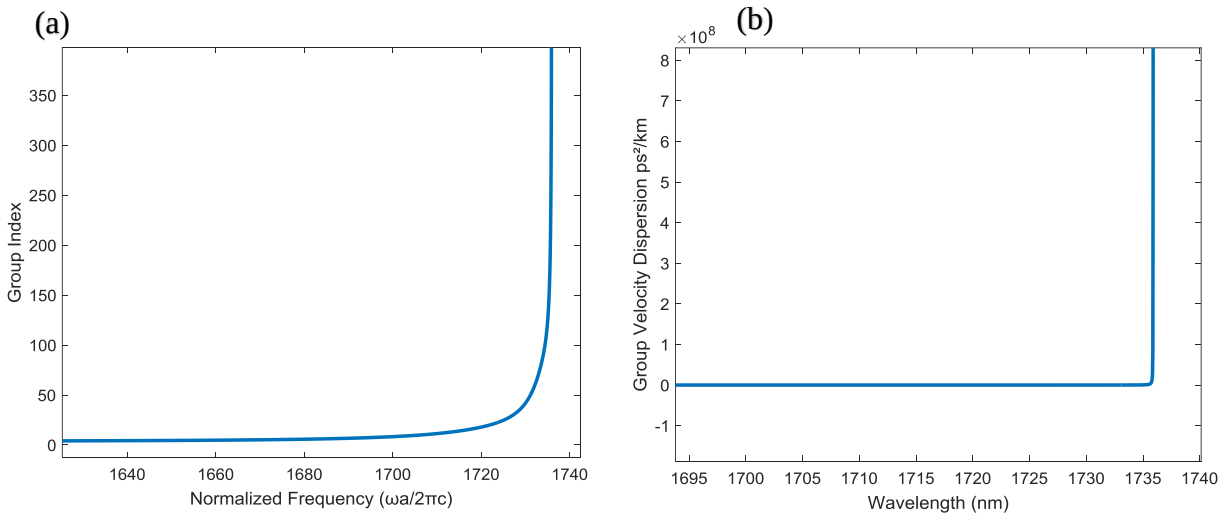

Figure 76 (a) The group index curve of basic waveguide w1 (b) The group velocity dispersion versus the wavelength.

As we can see the group index varies rapidly in the slow light region, which means that we have a narrow bandwidth and large group velocity dispersion GVD in the order of 10^8 ps^2 /km near the band edge as we see in figure 76 (b), the optical signals propagating through such waveguides will experience a broadening.

Figure 77 (a) presents the modified photonic crystal waveguide; we removed the middle row of holes of the waveguide and replaced it with a row of air holes separated by a distance of half lattice constant $a/2\ nm$, we need to find a guided mode near the 1550 nm at the band edge

($ka/2\pi = 0.5$) this ensures a wideband of slow light in the vicinity of the operation wavelength 1550 nm , to achieve this we have changed the radius of the air holes in the center of the waveguide in order to obtain the required guided mode.

Figure 77 (b) Shows the supercell selected with one row of air holes in the X direction and 8 rows of air holes in the Y direction for calculating the dispersion diagrams.

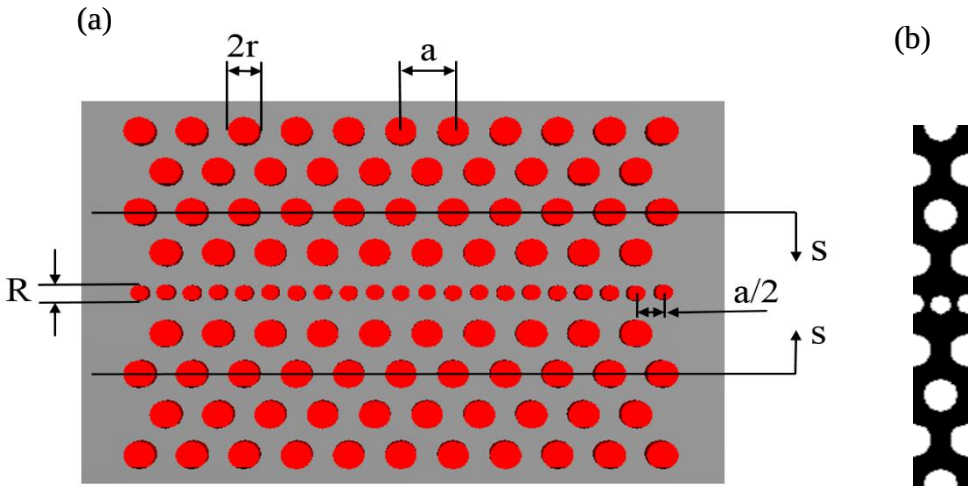

Figure 77 (a) The modified photonic crystal waveguide (b) The supercell of the modified waveguide with 1 row of air holes in the X direction and 8 rows of air holes in the Y direction.

Figure 78 shows the variation of the guided modes versus the radius of the reduced air holes in the middle of the modified photonic crystal waveguide. It has been observed that the even mode shift towards the higher frequency when the reduced air holes in the waveguide center along the propagation direction increases from R1=0.105a to 0.2325a. we found that the radius R1=0.17a is an optimum value of the reduced air holes which lead to the guided mode (even mode for the optimized structure) in the vicinity of the wavelength 1550 nm at the band edge ($ka/2\pi = 0.5$) as shown in Figure 79. The solid red curve within the gap illustrates the even mode propagating along the waveguide, whereas the dash black line is showing the photonic crystal light line .

By taking R1=0.17a nm, the group index and the group velocity dispersion parameter has been calculated and plotted as shown in Figure 80 (a). It is evident that the group index in the slow light region lies at the wavelength 1550 nm area, and as expected the corresponding group velocity dispersion GVD shown in Figure 80 (b) is lower than the photonic crystal waveguide w1 and it is in order of 10^6 ps^2/km.

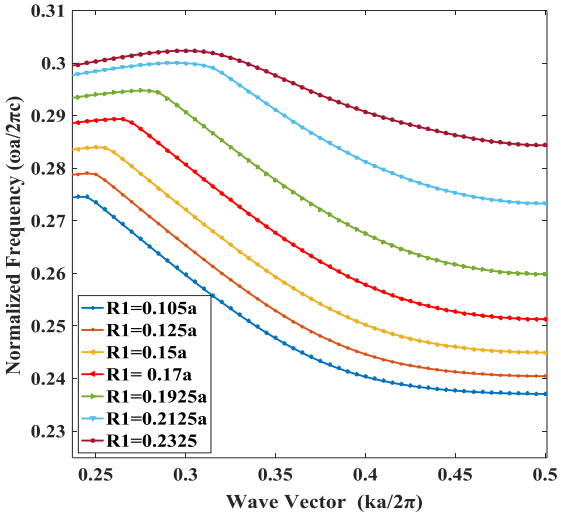

Figure 78 Variation of dispersion curve with the radius R1 from 0.105a to 0.2325a of the reduced air hole in the middle of the modified photonic crystal waveguide.

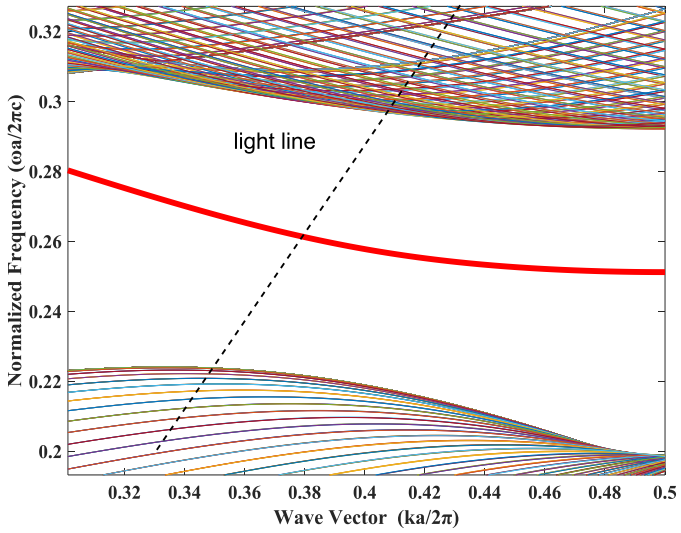

Figure 79 Dispersion curve of the even mode for the optimized structure with R1=0.17a.

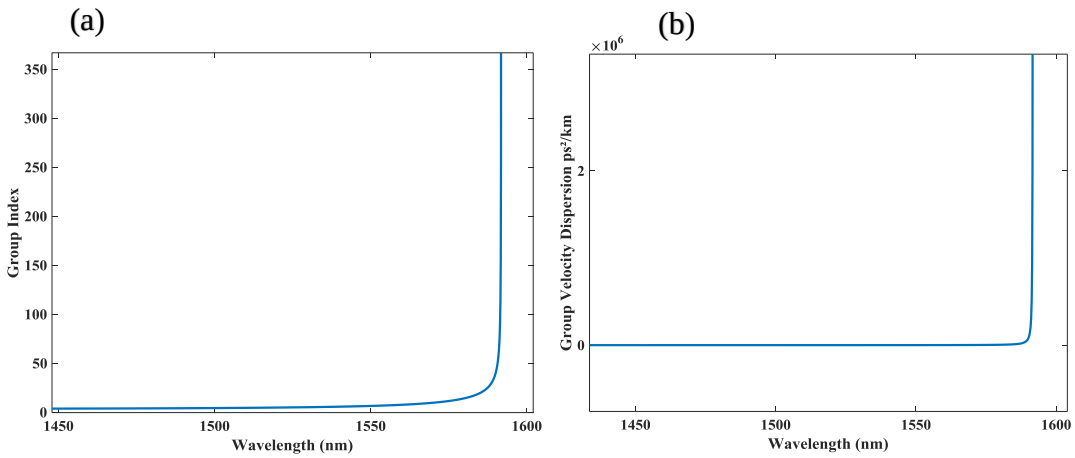

Figure 80 (a) and (b) Group index and group velocity dispersion for the modified

IV.1.1 Simulation, results, and discussion

The aim of our work is to achieve a slow light regime with high group index, wide bandwidth, and low GVD. We have studied the influence of the displacement of air holes position; therefore, we keep the first rows of air holes unchanged and shift the positions of air holes in the second rows on both sides of the line defect in opposite directions toward the center of the waveguide, in order to modify the dispersion curve. As shown in Figure 77 (a), the S parameter describes the deviation relative to the unmodified lattice; we optimized this parameter (S) to tailor the shape of the modified PCW dispersion curve. Figure 81 (a) shows the normalized frequency $\frac{\omega a}{2\pi c}$ as a function of the wavevector $ka/2\pi$ of the even mode when S are varied for optimization. It can be found that there exists a linear region of each curve corresponds to a flatband slow light region with a specific group index ng determined by its slope. The flatband region represented with a thick solid black line. As we see, the dispersion curves shift to lower frequency with S increased and the shift becomes more rapidly near the tail of the dispersion curve. Figure 81 (b) shows the calculated group indices as a function of the wavelength, we can clearly see that the slow light of the modified photonic crystal waveguide possesses a "wideband slow light" region where the group index is nearly constant. In order to evaluate the dispersion bandwidth of the slow light, some previous papers select a bandwidth criterion, where the group index ng considered as constant within ±10% range, the simulation results according to this criterion demonstrate a nearly constant group indices of 21, 20, 35.5 and 65 their corresponding bandwidths can reach 20.3 nm, 15.6 nm, 9.5 nm, 5.3 nm, respectively, which we represent with a thick solid black lines. We also observe that when the S parameter increases the group index decreases and shifts to higher working wavelength besides the slow light bandwidth become wider.

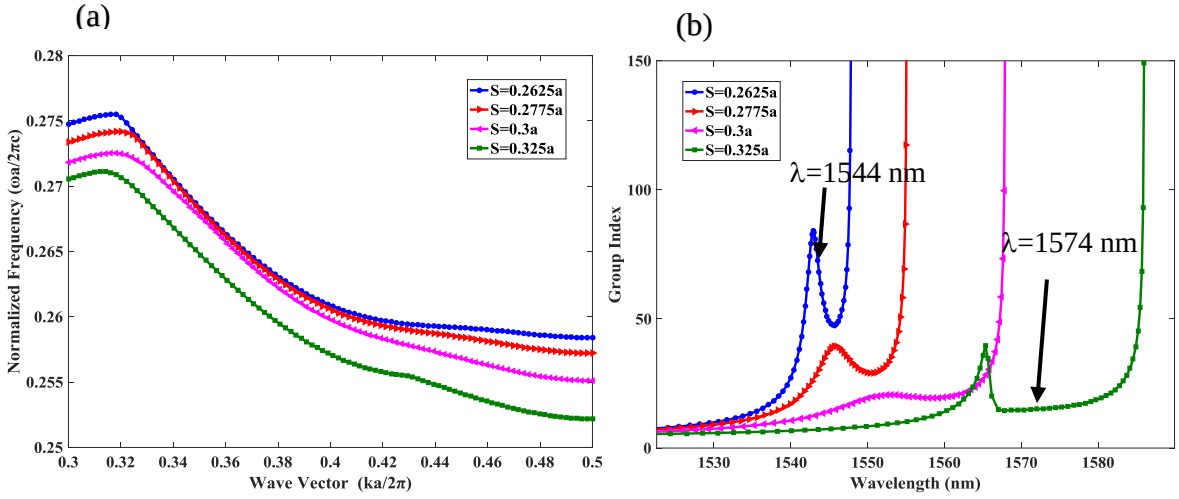

Figure 81 (a) Calculated dispersion curves of the modified photonic crystal waveguide (b) The corresponding group indices for the fundamental mode of the modified PCW for different values of the S parameter, the thick solid black line represents the flat band slow light region.

The second order dispersion, known as the group velocity dispersion GVD ($\beta_2 = d^2 k/d\omega^2$), we have calculated this parameter for two values of the parameter S (0.325a, 0.2775a) as shown in Figure 82 (a) and (b). The group index curve and the corresponding dispersion group velocity curve of the slow light flat region for the modified PCW are lower than 10^5 ps^2/km, which is one order of magnitude smaller than the basic photonic crystal waveguide w1.

The operational wavelength can be tuned over a large range from 1544 nm to 1574 nm, (where the 1544 and 1574 nm are the working wavelengths of the wideband slow light as shown in figure 81 (b)) by shifting only the second rows with the S values calculated previously.

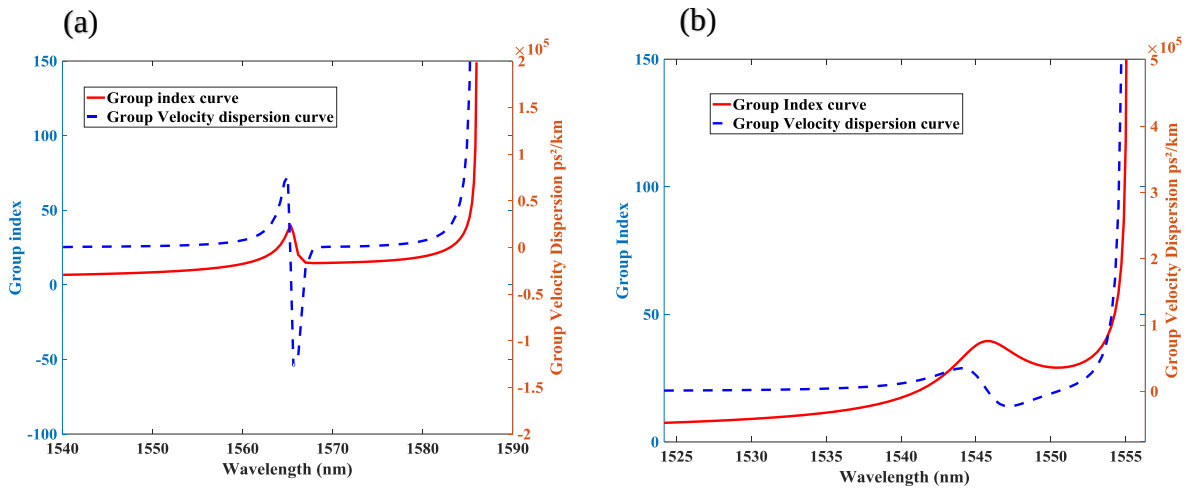

Figure 82 (a) and (b) The group index curve and the corresponding GVD curve of the slow light modified PCW for S=0.325a and S=0.2775a respectively.

Table 1. Group index and bandwidth under different optimized shifting parameters

Optimized shifting parameters		ng	bandwidth centered at 1550 nm
[139] Two-hole diameter variations		34	11
[65] Lateral hole position shifting		32	14.7
[140] Ring-shaped holes' structure		37	8
[141]Longitudinal hole position shifting		26	13.1
[142]liquid infiltration of a slotted PCW		50	7.5
Current work	S=0.325a	21	20.3
	S= 0.3a	20	15.6
	S=0.2775a	35.5	9.3
	S=0.2625a	65.5	5.3

IV.2 The second modified slow light photonic crystal waveguide PCW2

We propose a design of a modified photonic crystal waveguide for achieving high group index, wide bandwidth and low group velocity dispersion (GVD), Therefore, by enlarging the entire holes

of the PhC and shifting the first and second rows adjacent to the line defect in the propagation direction of light,

IV.2.1 Design of the second photonic crystal waveguide PCW2

We proposed the design of a line defect photonic crystal waveguide Figure 83. The PhC structure it is a hexagonal lattice (triangular) of air holes etched in a silicon-on-insulator (SOI) substrate. The air holes radius r=0.4a, where "a" is the lattice constant (a=470 nm), the thickness of the photonic crystal slab is h=200 nm.

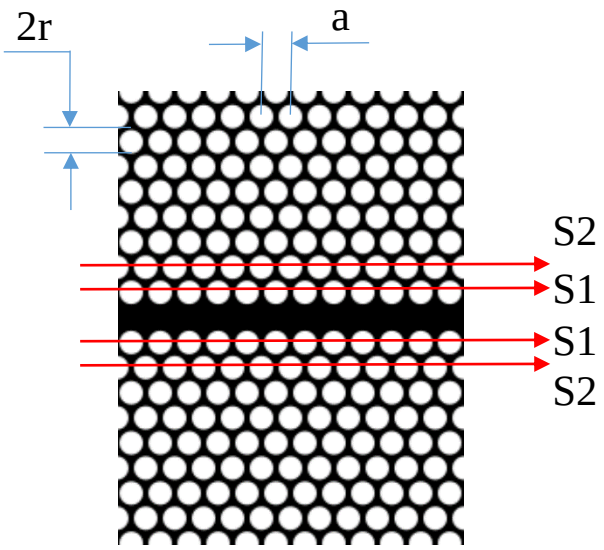

Figure 83 Geometry of the modified W1 PhC waveguide: the first and second rows of holes are shifting by S1, S2 in the light propagation direction.

In this study, the waveguide is formed by removing the middle row of holes of the triangular lattice photonic crystal in the X direction, which create modes propagate along the missing holes. 3D photonic crystal slab (PC) confines light in the x-y plane by the photonic band gap and the index differences is used to confine the light vertically (total internal reflection). To obtain a 2D device from a real 3D device, we use the effective refractive index method (EIM). We performed a 2D analysis with an equivalent index of the slab of 2.76 because the three-dimensional calculation consuming too much time and computer memory. The effective index of the proposed structure has been calculated using RSOFT's commercial software. For a 200 nm of silicon slab thickness [143] [144] n=3.48 on Silicon dioxide layer (n_{SiO2}=1.44) and the top cladding layer is air (n_{air}=1) for TE polarization, the corresponding effective index was n_{eff}=2.76 [145].

We analyzed our basic photonic crystal structure, as shown in figure 84 (a) the domain of the unit cell is hexagonal and the high index (red color) with an effective index of 2.76 and the hole (Purple color) represented by low index 1. We are able to fill a whole 2D space with these translated unit cells. Figure 84 (b) shows the Brillouin zone (BZ) and k-path for a 2D hexagonal lattice, where k is the wave vector inside the BZ. We calculated the band diagram for our structure using the plane wave expansion (PWE) method of the Rsoft (BandSOLVE) software, a large transverse electric TE band gap bet has obtained in the normalized frequency range of 0.3033 (ωa/2πc) and 0.4484 (ωa/2πc) as shown in figure 85.

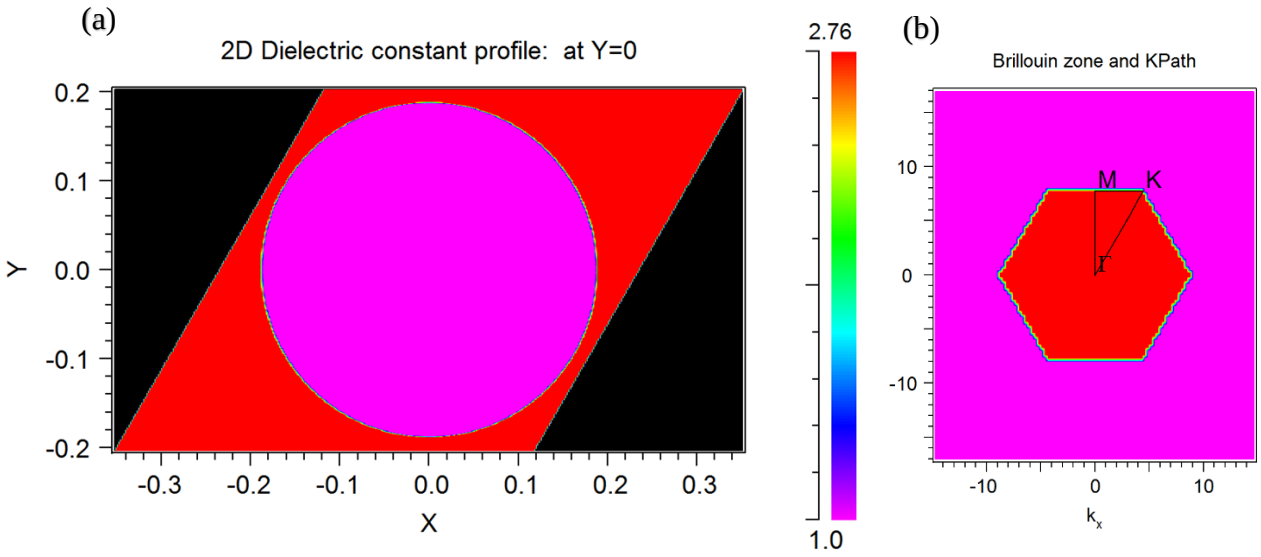

Figure 84 (a) Index profile for the single unit cell b) Brillouin zone

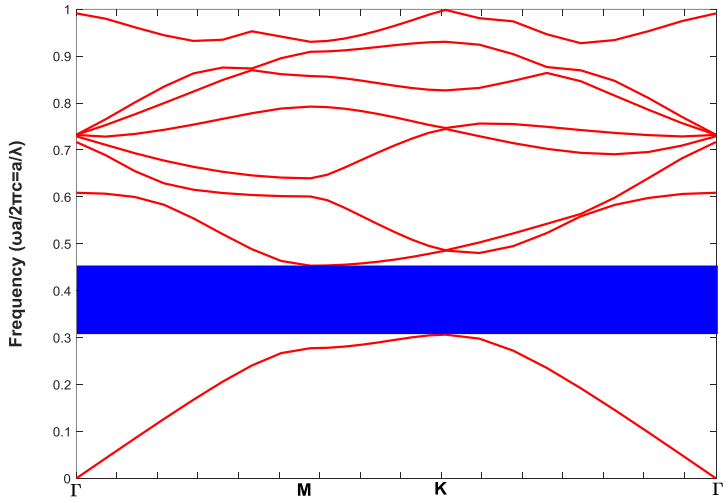

Figure 85 Dispersion diagram and band gap for the TE polarization for the 2D hexagonal lattice.

IV.2.2 Slow light theory

The basic parameter that characterizes the slow light is its group velocity (vg) which is the speed and direction in which the envelope of the wave's amplitude propagates.

$$v_g = \frac{d\omega}{dk} = \frac{c}{ng} \quad \text{IV.1}$$

Where ω the angular frequency, k is the wave vector, c expresses the speed of light in vacuum, ng is the group index.

$$n_g = c\frac{dk}{d\omega} \quad \text{IV.2}$$

The normalized delay bandwidth product NDBP is an important factor for slow light property. Often the NDBP is useful when comparing devices of different length or operating at different frequencies.

$$NDBP = n_g \times \frac{\Delta\omega}{\omega_0} \quad \text{IV.3}$$

Where $\Delta\omega/\omega_0$ is the normalized bandwidth of a slow light region and n_g is the average group index.

IV.2.3 Numerical results and discussion

We created a line defect by removing the entire row of holes in the center of the photonic crystal structure, which give us a simple waveguide W1. To study or describe the properties of this waveguide, we identified a supercell as shown figure 86 (a) since the lattice is still perfectly periodic in the y-direction, we use one air hole along the y-axis but we need to include more air holes along the x-axis. We investigated the effect of the radius of air holes of the Photonic crystal waveguide on slow light properties figure 86 (b) shows the variation of the guided modes versus the radius (r) of air holes of PhC structure. The bands shift to higher frequencies as the radius value increases from r=0.2a to 0.45a nm, this change is caused by the slab mode band below the propagation mode band. As can be seen in figure 86 (b) there is a flat band (slow light region) corresponding to the radius value r=0.4a. The group index parameter has been calculated and plotted, as shown in figure 87 in order to evaluate the dispersion bandwidth of the slow light, we calculate the NDBP with the constant group index criterion in the previous paper [65]. As r=0.4a a group index ng=25, bandwidth $\Delta\lambda$=20 nm and NDBP=0.322 has obtained.

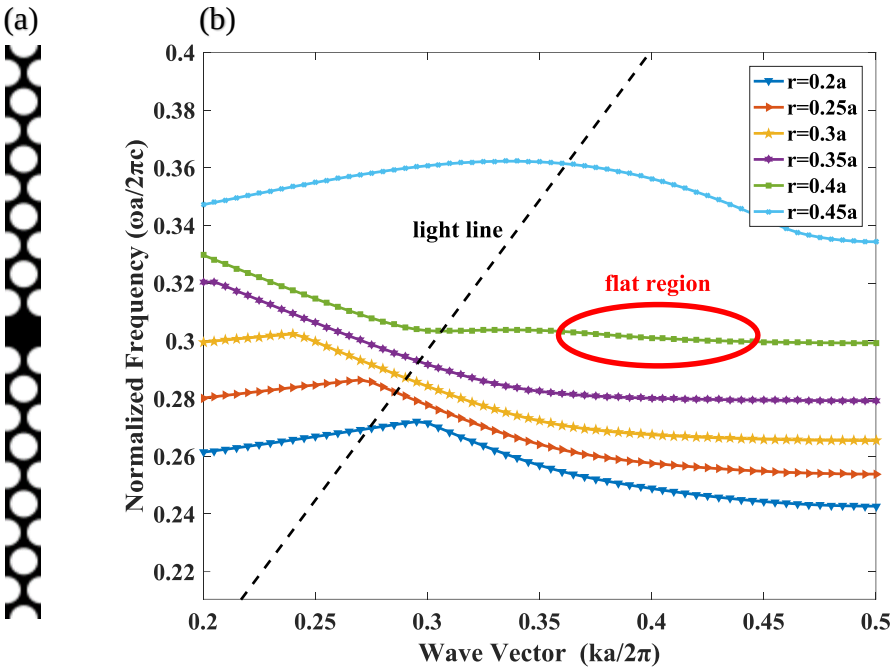

Figure 86 The supercell of w1 with 1 row of air holes in the X direction and 20 rows of air holes in the Y direction (b) guided modes of PCW for r=0.2a to 0.45a nm.

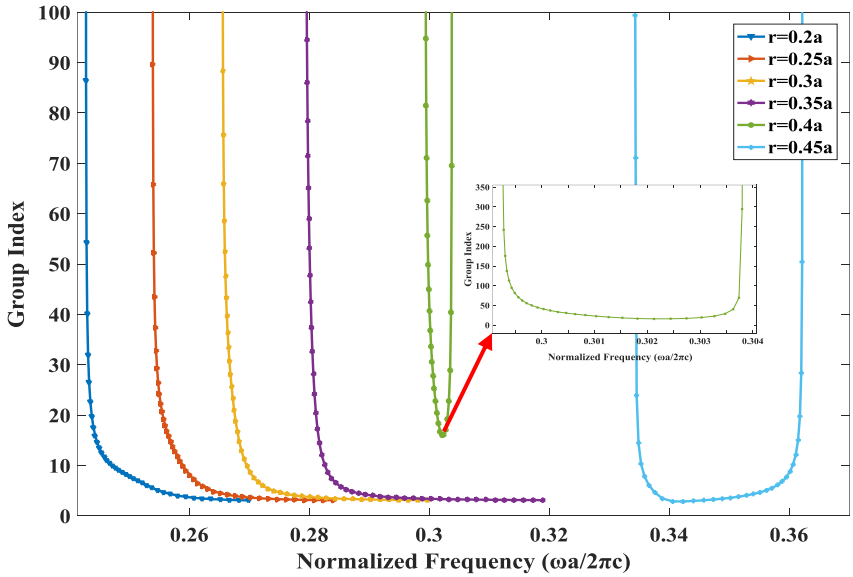

Figure 87 Group index ng characteristics of photonic crystal waveguide.

After selecting the radius value r=0.4a that produced a flat region (slow light), we have studied the effect of changing the position (shift) of the first and second rows on both sides of the line defect in the x-axis direction in order to obtain high group index (ng), low group velocity dispersion (GVD) and high NDBP.

First, we changed the position of the first air holes row along the line defect from S1=0.0212a to S1=0.1276a with step 0.0213a, as we can see in figure 88 (a) we noticed that the guided modes headed towards high frequencies. figure 88 (b) shows the corresponding group index that increased as S1 increased from 16 to 69. On the contrary, as S1 increased the bandwidth decreased from 22.9 to 3.1 nm.

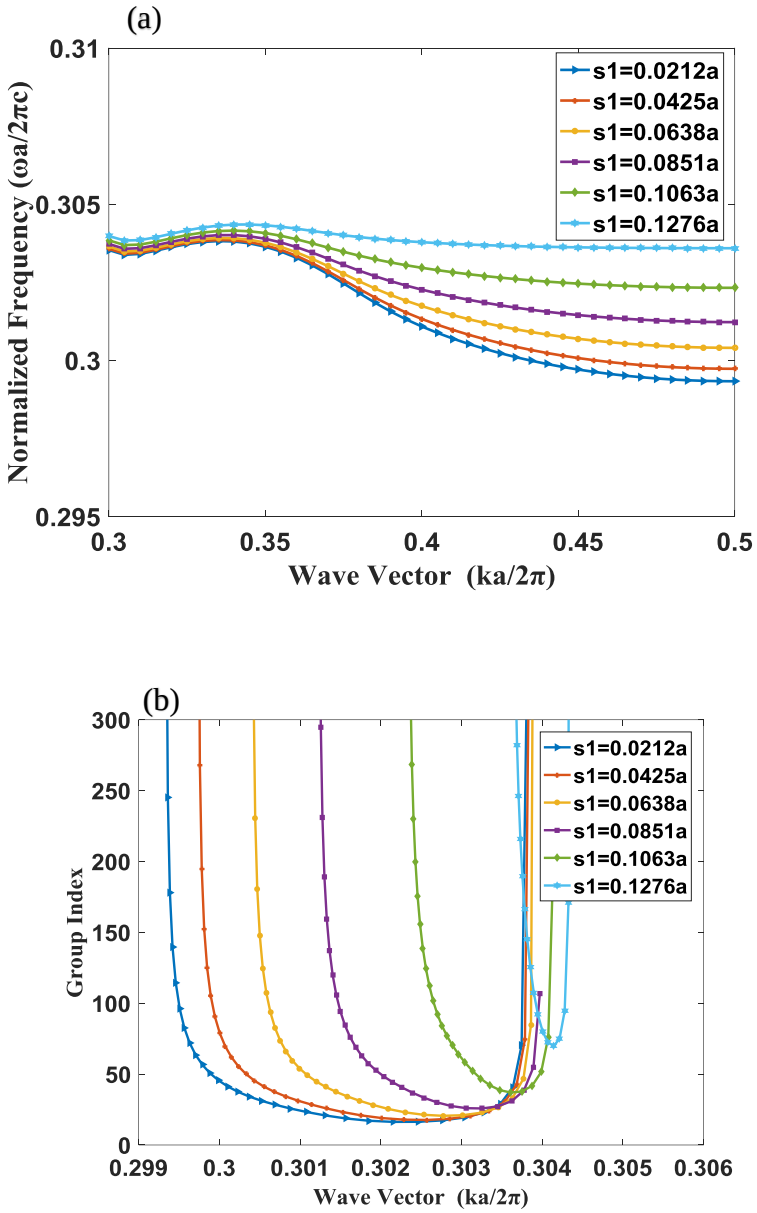

Figure 88 (a) Variation of dispersion curve photonic crystal waveguide by changing S1 from 0.0212a to 0.0.1276a (b) the group index as a function of the position S1 from 0.0212a to 0.01276a.

Second, we changed the position of the second air holes row along the line defect from S1=0.0212a to S1=0.1276a with step 0.0213a. As shown in figure 89 (a) the guided modes shift towards the higher frequency as S2 increased in the same way when we changed S1, but there is a region from 0.35 to 0.45 (ka/2π) turned from the concave to convex when S2 increased, we exploited this

phenomenon to engineer the dispersion. Figure 89 (b) shows the group index, which increases as S2 increases from 16.67 to 46.94, In contrast the bandwidth, decreases from 22.21 to 8.1 as S2 decreases.

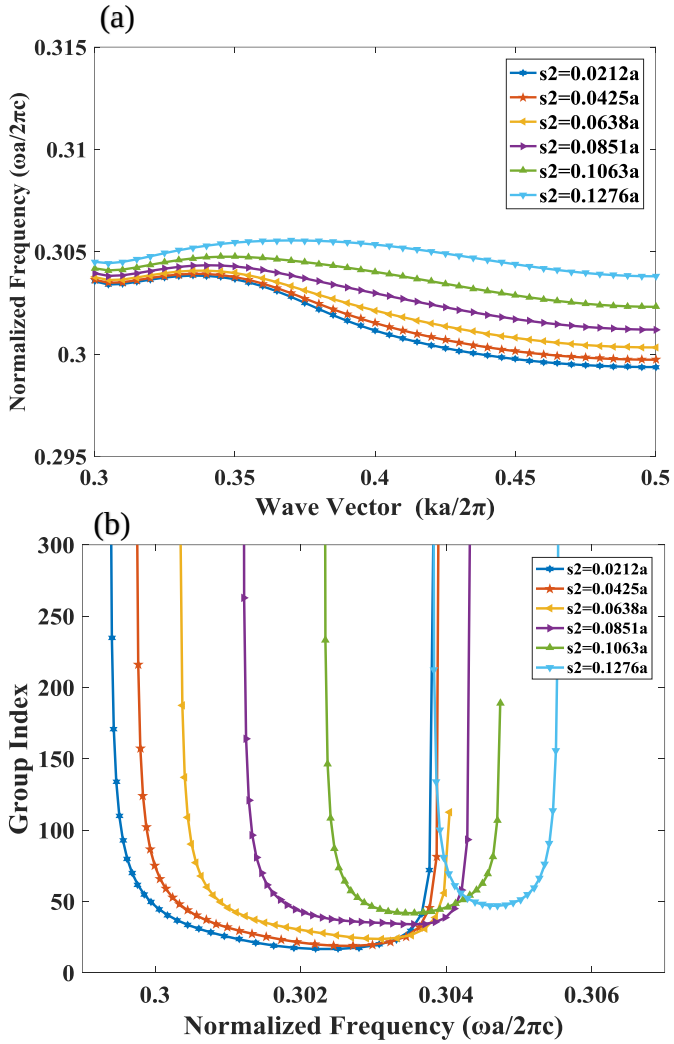

Figure 89 (a) The group index as a function of the position S2 from 0.0212a to 0.0.1276a (b) Variation of dispersion curve photonic crystal waveguide by changing S2 from 0.0212a to 0.0.1276a.

As we have noticed, there is an inverse proportion between the bandwidth and the group index. Therefore, high group index brings forth slow light but a narrow bandwidth and vice versa. To obtain a high group index with wide bandwidth we engineered the dispersion curve.

We tailor the dispersion curve as shown in figure 90 we have selected two dispersion curves corresponding to the shift values S1=S2=0.1063a, we noticed that there is a turning point (A and B) before the curves becomes completely horizontal at the band edge. The turning point A located far away from the band edge, the slope of the dispersion curve (blue) is very small from point A to the band edge on the contrary the turning point B very close to the band edge. Using the

properties of each curve (blue and red), we obtained an extended curve (green) with a long flat band which provide a high group index and large bandwidth.

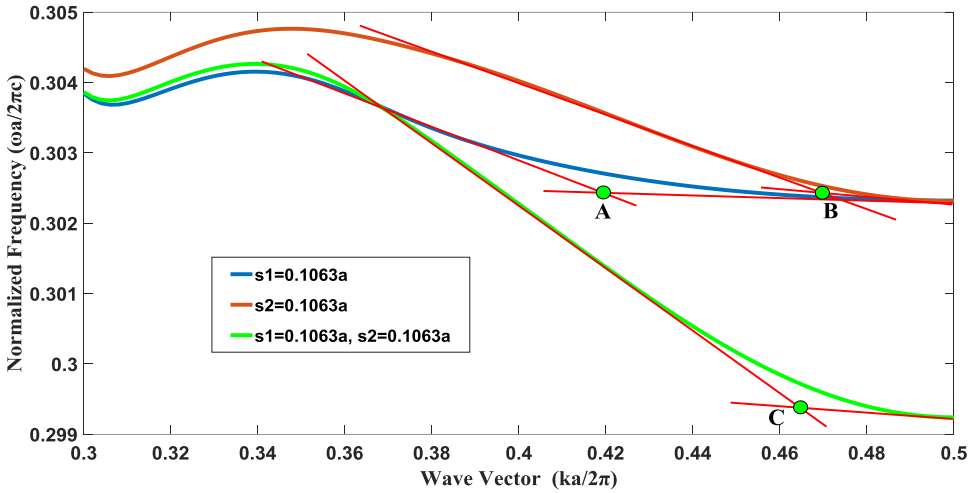

Figure 90 Dispersion engineering of tow curves red curve S1=0.1063a blue curve S2=0.1063a to obtain the green curve S1=S2=0.1063.

We selected an optimum values S1 and S2 to tailor the shape of the dispersion curves to achieve a slow light regime with high group index, low group velocity dispersion and high NDBP, figure 91 (a) shows the normalized frequency as a function of the wave vector of the even mode when S1, S2 is varied for optimization. Figure 91 (b) shows the calculated group indices as a function of the normalized frequency, we observe a wideband slow light region where the average group indices of 18.24 to 41.7 over 11.7 to 24 nm bandwidth, we listed the simulation results in the table 2 and compared it with the results of previous papers.

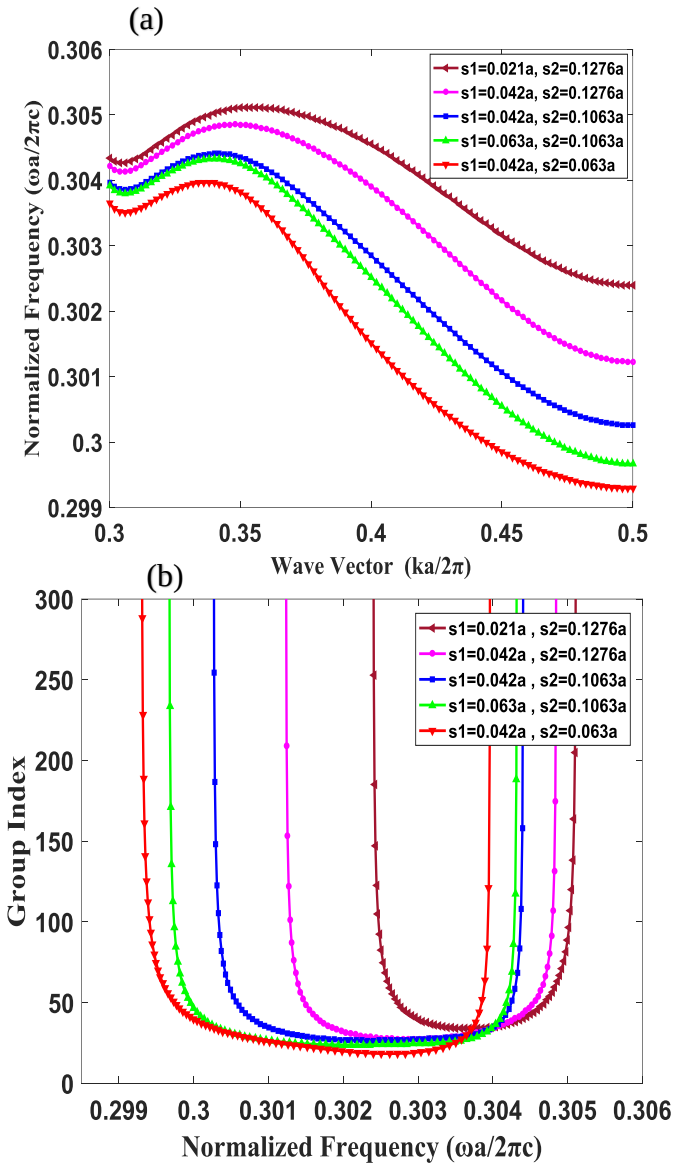

Figure 91 (a) Calculated dispersion curves of the photonic crystal waveguide with the optimum shift s1 and s2. (b) The corresponding group index curves.

Table 2. The comparison between our results and previous results

references	ng	Δλ at 1550 nm	NDBP
Current work			
S1= 0.042a, S2=0.063a	18.24	24	0.282
S1= 0.021a, S2=0.1276a	41.7	11.7	0.315
S1= 0.042a, S2=0.1276a	34.55	16.9	0.377
S1= 0.042a, S2=0.1063a	33	20.3	0.439
S1= 0.063a, S2=0.1063a	30.43	23.7	0.465
[146]	36.6	18.82	0.430
[147]	54.55	9.13	0.320
[148]	46	12.8	0.380
[137]	21	20.3	0.275

The major component of the higher order dispersion is the group velocity dispersion (GVD) is defined by the second order derivative of the dispersion relation $\beta_2 = \frac{d^2k}{d\omega^2}$

This parameter is very important in slow light devices, because high GVD lead to pulse broadening and signal distortion. Figure 92 shows the calculated group velocity dispersion; it is clearly that the GVD have a low value in the order of $10^5 ps^2/km$.

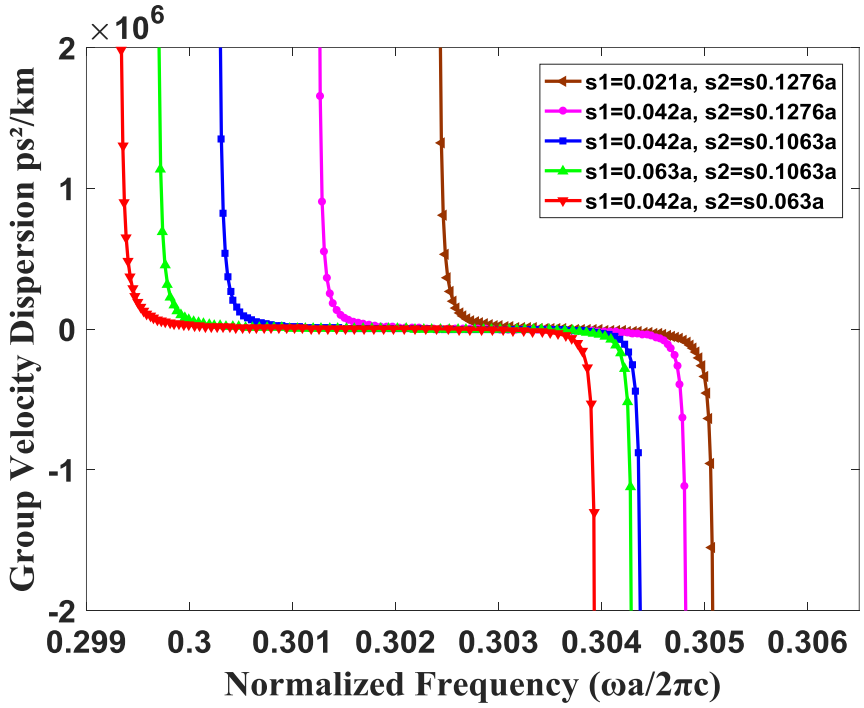

Figure 92 The group velocity dispersion GVD as function of the normalized frequency.

Table 3. The comparison between the group velocity dispersion (GVD) in this paper with the group velocity dispersion (GVD) of previous research.

references	GVD (ps^2/km)
Current work	10^5
[146]	10^4
[147]	10^7
[148]	10^6
[137]	10^5

IV.2.4 Three-dimensional (3D) calculation

For a more accurate estimation, a three-dimensional calculation was used. The silicon slab (n_{Si} =3.48) with thickness h=200 nm has been bounded by a top cladding layer of air (nair=1) and a bottom cladding layer of silica (n_{SiO2}=1.44) as shown in figure 93. The band diagrams of this structure are given in figure 94 the structure exhibits a photonic band gap for TE polarization in the normalized frequency range of 0.3184 (ωa/2πc) and 0.4800 (ωa/2πc). Only the dispersion

region below the light line presented with "green line with square dots" could confine light well in the vertical direction of the slab, whereas modes above the light line become leaky.

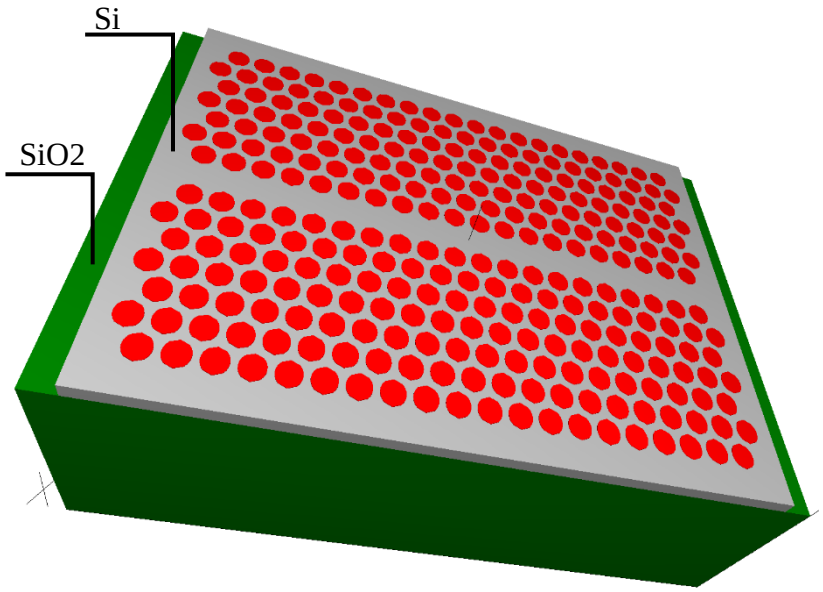

Figure 93 Photonic crystal waveguide slab consisting of a silicon core (Si) sandwiched by a top cladding layer (air) and a bottom cladding layer (SiO2).

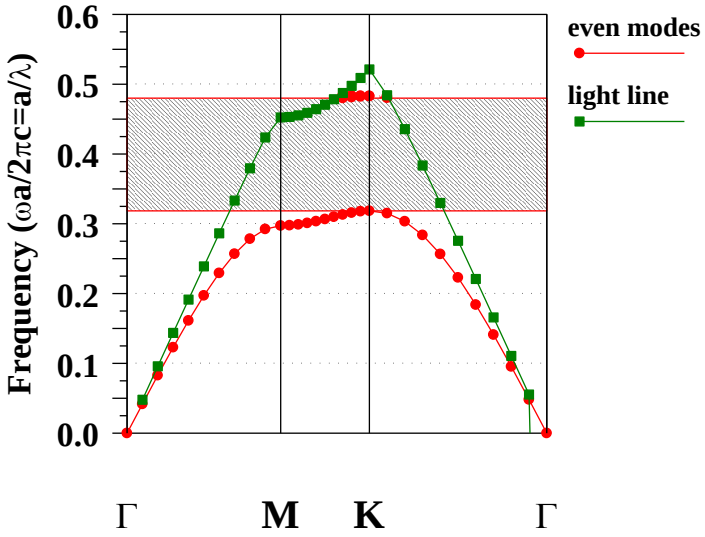

Figure 94 Band structure of such a system having a thickness h = 200 nm and a radius r=0.4a even modes only.

we selected as supercell as shown figure 95 (a) we use one air hole along the y-axis 14 air holes along the x-axis. We recalculated the top three results from Table 1 with "S1= 0.042a, S2=0.1276a", "S1= 0.042a, S2=0.1063a" and "S1= 0.063a, S2=0.1063a we obtained the variation of the guided modes by changing S1 and S2 as shown in figure 95 (b). The corresponding group indices as a function of the normalized frequency shown in figure 96.

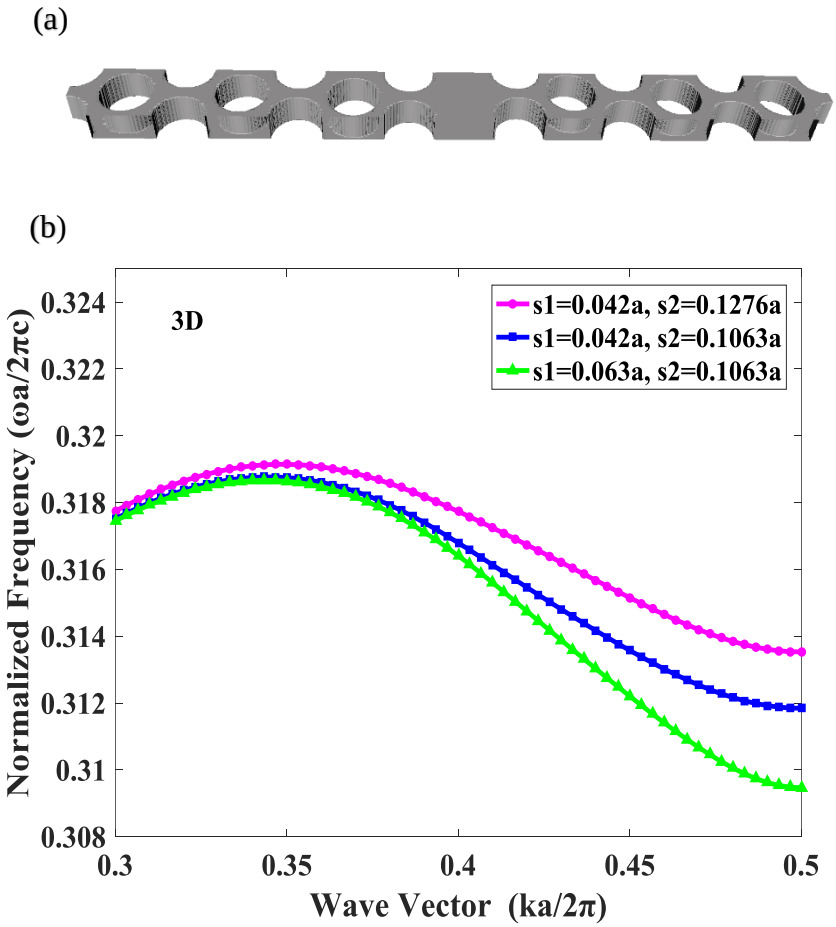

Figure 95 (a) The supercell of w1 with 1 row of air holes in the X direction and 14 rows of air holes in the Y direction (b) guided modes of PCW.

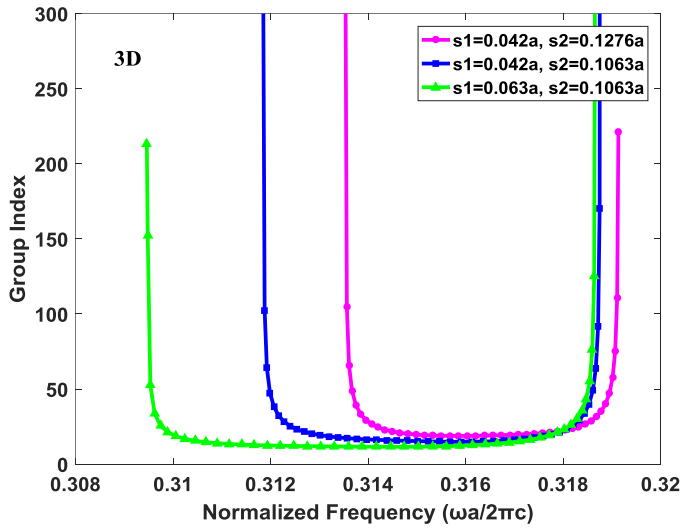

Figure 96 Group indices, for the fundamental mode of PhC waveguide.

The results of three-dimensional and two-dimensional calculation is in good agreement as see in table 3 that the NDPB is almost equal in both cases 2D and 3D, except that the group index and bandwidth are larger and narrower, respectively, for the 2D calculation.

Table 4. The comparison between three-dimensional and two- dimensional calculation.

references	ng 3D	ng 2D	Δλ 3D	Δλ 2D	NDBP 3D	NDBP 2D
Current work						
S1= 0.042a, S2=0.1276a	23.57	34.55	25	16.9	0.380	0.377
S1= 0.042a, S2=0.1063a	21.45	33	32	20.3	0.442	0.439
S1= 0.063a, S2=0.1063a	17.4	30.43	42	23.7	0.471	0.465

IV.2.5 Time-Domain Analysis

In order to demonstrate the results obtained by the PWE method, we use the finite difference time domain (FDTD) method for the proposed structure in figure 97 (a). When S1=0.063a and S2=0.1063a we have obtained a group velocity value ng=30.43 and the group velocity dispersion GVD value $\beta_2 = 10^5 \mathrm{ps}^2/\mathrm{km}$.

For this case, by launch a Gaussian pulse centered at 0.3005 ($2\pi c/a$) with a frequency width 0.0391 ($2\pi c/a$) in the center of photonic crystal waveguide with a length between Input and output monitor L=30a, we observe that the pulse delayed, as we seen in the figure 97 (b) the peak of the normalized field amplitude are located at 2.127 ps and 3.481 ps in the Input and Output monitor, respectively.

The time delay of the pulse in the waveguide Δt =1.354 ps is the time between two pulses (red and blue). We calculated the group velocity using the relation between the length of the waveguide and the slow down factor of the pulse velocity $ng = \Delta t \times c/L$ =28.8 that confirm the value obtained by the PWE calculation. The width of the Gaussian pulse at the output and Input monitor is approximately equal, with very little pulse expansion due to the low GVD.

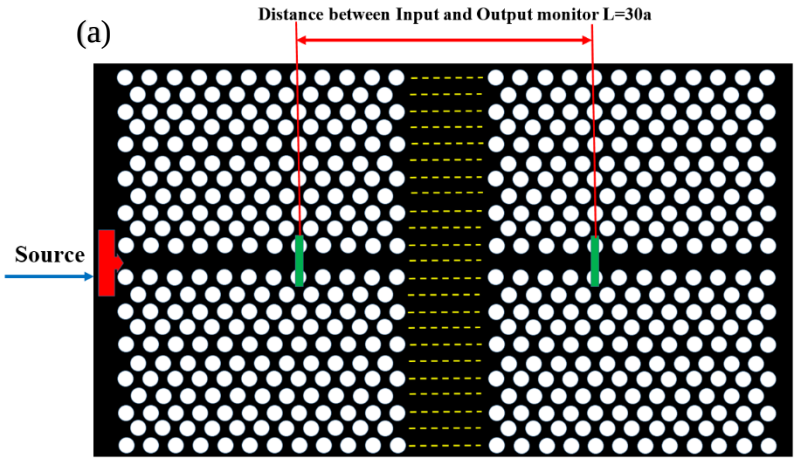

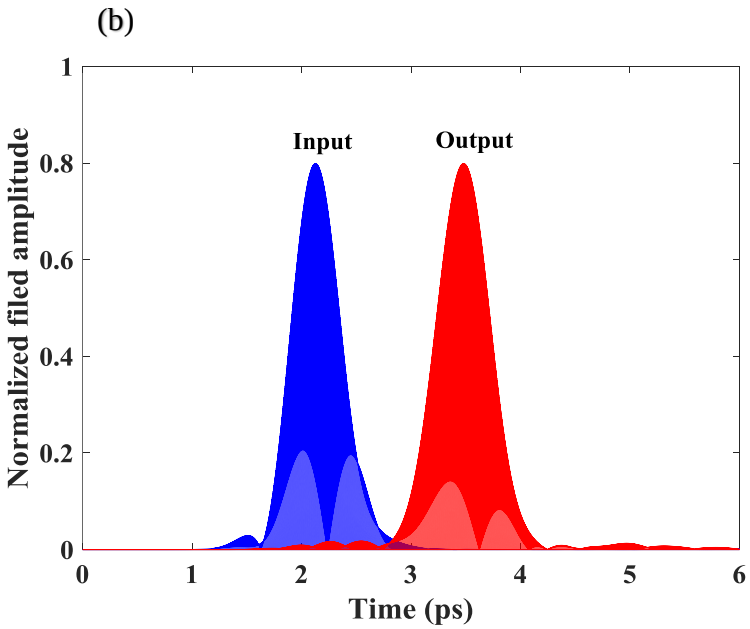

Figure 97 (a) Photonic crystal waveguide of finite-difference time-domain simulation system of the proposed design. (b) Normalized Field amplitude of the Gaussian pulse recorded at the input and output monitor of the photonic crystal waveguide as a function of time.

IV.3 The Application of the PCW2 as a buffer

The photonic crystal waveguide is a very promising method for realizing all-optical buffer in practical applications for its compact physical size and excellent slow light performance [86]. In this section, we study the optical buffer capability of the second modified PCW, the buffer characterized by:

The group delay or the storage time Δt expressed as [106]:

$$\Delta t = \frac{L}{v_g} = L\frac{n_g}{c} \qquad \text{IV.4}$$

Where L is the length of the device, c the speed of light in vacuum and n_g is the group velocity.

Another important parameter is the buffer capacity C And the physical size of the stored bit can be written as follow [149]:

Buffer capacity C

$$C = \frac{L}{2a} \times n_g \Delta\omega \qquad \text{IV.5}$$

the physical size of the stored bit L_{bit}

$$L_{bit} = \frac{L}{C} = \frac{2a}{n_g \Delta\omega} \qquad \text{IV.6}$$

We summarized the slow light parameters and buffer capability of structures in figure 97 (a) for different group indices in the table 5. We selected the length of the device L=1 mm for better contrasting the buffer capability.

Table 5 slow light parameters and buffer capability

S1 and S2	n_g	$\Delta\omega$ (10^{-4} $\omega a/2\pi c$)	$\Delta\lambda$ (nm)	Δt (ps)	NDBP	L_{bit} (μm)	C (bit)
S1= 0.042a, S2=0.063a	18.24	45	24	60.8	0.282	11.45	87.31
S1=0.021a, S2=0.1276a	41.7	25	11.7	139	0.315	9.01	110.90
S1=0.042a, S2=0.1276a	34.55	35	16.9	115.16	0.377	7.77	128.64
S1=0.042a, S2=0.1063a	33	41	20.3	110	0.439	6.94	143.93
S1=0.063a, S2=0.1063a	30.43	46	23.7	101.43	0.465	6.71	148.91

Figure 98 shows that the buffer capacity increase when the NDBP increase. The largest storage time is Δt=139 ps due to the largest group index ng=41.7 but have large bit length also leading to a low capacity C=110.9. thus, the waveguide with shift S1=0.063a, S2=0.1063a have the best buffer capability compared with other waveguides, with a buffer capacity C=148.91 and NDBP=0.465.

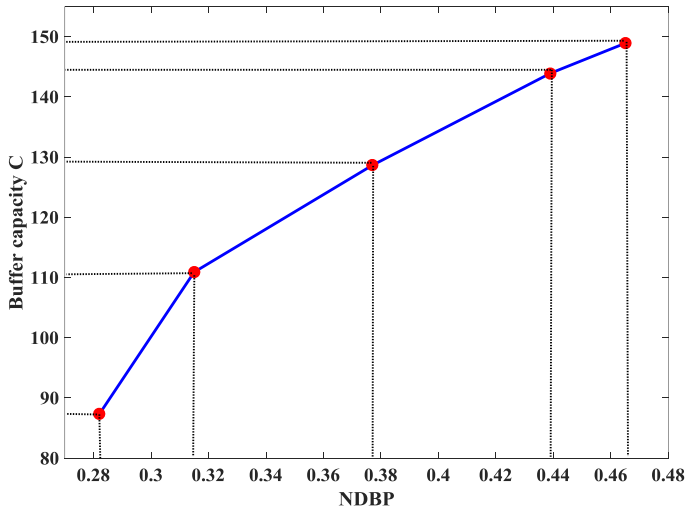

Figure 98 Relation between the normalized delay bandwidth

IV.4 Conclusion

In this chapter. We present the numerical analysis of two types of slow light modified photonic crystal waveguides (PCW1 and PCW2), PCW1 is capable of producing a wideband slow light with high group index and low group velocity dispersion, by only shifting the second rows of air holes adjacent to the center of the modified waveguide. Nearly constant group indices of 21, 20, 35.5 and 65 over 20.3 nm, 15.6 nm, 9.5 nm, 5.3 nm with low group velocity dispersion in the order of 10^5 ps2/km have been achieved. Also, the operational wavelength can be tuned over a wide range span from 1544 to 1574 nm.

The second photonic crystal waveguide PCW2 obtained by enlarging the entire holes of the PhC and shifting the two rows of holes adjacent to the waveguide in the propagation direction; we have obtained a high group index of 18.24, 41.7, 34.55, 33 and 30.43 over 24, 11.7, 16.9, 20.3 and 23.7 nm, respectively. Also, the design featured by a low group velocity dispersion. We achieved a high NDBP value of 0.465.

In order to demonstrate the results obtained by the PWE method, we use the finite difference time domain (FDTD) method for the PCW2, the simulation results with FDTD are in remarkable agreement with the results obtained with PWE. To further test the practical applicability of our waveguide PCW2, the buffering capacity is calculated, which is found to be as high as 148 bits on the assumption that the device length is L=1mm. The reported results can be useful in making on-chip optical buffers and delay lines.

General conclusion

General conclusion

Studies carried out over the last decade on the use of photonic crystals for the production of integrated circuits meeting the requirements of the new lab-on-chip systems have shown that these periodic structures are potential candidates which can offer new perspectives for the development and production of a future generation of all-optical integrated circuits. Optical scientists are turning their attention toward developing useful applications of slow light, including controllable optical delay lines, optical buffers and true time delay methods.

In this thesis, we explore the design, computation, and analysis of photonic crystals waveguides, and how we slow down the light inside it, the exploitation of slow light phenomena has potential for applications ranging from all-optical storage to all-optical switching, we review two different types of dispersion engineered photonic crystal waveguides PCW1 and PCW2 that have been developed for slow light applications such as buffer or sensors.

In the present work, our structures based on triangular lattice photonic crystal slab consisting of circular air holes embedded in a silicon-on-insulator (SOI) substrate, the photonic crystals which evoked a lot of research interest in recent years in particular the photonic crystal slab (PCS) has been proposed that promises easier fabrication using existing techniques, the PCS is two-dimensionally periodic dielectric structures of finite height that have a band gap for propagation in the plane and use index guiding to confine light in the third dimension as mentioned in the chapter1. To obtain a photonic crystal waveguide (PCW) we break the periodicity of the slabs in one direction by creating linear defects. For controlling the velocity of light and slow it down, there are two standard methods. One using material induced dispersion and the other using structural induced dispersion. In our work we focused on the structural induced dispersion one of the most suitable and attractive structures for realizing the slow light effect is the photonic crystal waveguide which can have a low group velocity away from the band edge, this property which named “Slow light” attracts a wide attention due to its wide applications Such as optical delay line and optical switching. The term ‘slow light’ refers to a reduction in the group velocity of light. The basic parameters that characterizes the slow light is its group velocity (vg) which is the speed and direction in which the envelope of the wave’s amplitude propagates and the group velocity dispersion (GVD) is the second order dispersion which causing broadening of the pulses when have a high value. Another important factor for slow light properties is the normalized delay

bandwidth product NDBP, the NDBP is useful when comparing devices of different length or operating at different frequencies all this information is discussed in chapter 2.

Simulation and modelling using numerical methods running on computers is today one of the key approaches in scientific work within practically all fields of research. Since the physical behavior in the nanoscale is very difficult and expensive to measure in real experiments, numerical simulations play a fundamental role in understanding such processes. We use two methods in our work the plane wave expansion method (PWE). The plane wave expansion method, which is a frequency-domain approach based on the expansion of the fields and material parameters into the Fourier (or reciprocal) space. The components of this expansion represent the definite-frequency states and the finite difference time domain method (FDTD), the idea is to simply discretize both in time and space the Maxwell's equations with central difference approximations. We re-simulate some important and famous papers published in this domain we calculated the dispersion diagram and the group index using the PWE method also we calculate the transmission of waveguide structure using FDTD method the results obtained are in a good agreement with the papers mentioned in chapter 3.

Our work is presented in the last chapter of this thesis, the objective was to develop a photonic crystal waveguide by introducing a slow light regime with high group index over a broad wavelength range and reducing the unwanted dispersion by engineering the dispersion curve. We proposed two photonic crystal waveguides designs PCW1 and PCW2: the first design it is a triangular lattice photonic crystal slab consisting of circular air holes embedded in a silicon-on-insulator (SOI) substrate, the waveguide PCW1 is formed by replacing the central row of air holes in the triangular lattice photonic crystal along the Γ-K direction with successively reduced air holes with a half lattice constant (a/2). By selecting a suitable supercell, we calculated the dispersion diagram using the PWE method for the PCW1 which exhibits two guided modes odd and even, we chose the even mode for its wide range of wave vectors. Then, we choose the optimum value of the reduced air holes which lead to the guided mode in the vicinity of the wavelength 1550 nm at the band edge. Then, we have studied the influence of the displacement of air holes position, we keep the first rows of air holes unchanged and shift the positions of air holes in the second rows on both sides of the line defect in opposite directions toward the center of the waveguide, in order to modify the dispersion curve. the simulation results demonstrate a nearly constant group indices of 21, 20, 35.5 and 65 their corresponding bandwidths can reach 20.3 nm, 15.6 nm, 9.5 nm, 5.3 nm, respectively. We also observed that when the shifting of the second rows of air holes increases the group index decreases and shifts to higher working wavelength besides the slow light bandwidth become wider.

The second design it is a hexagonal lattice (triangular) of air holes etched in a silicon-on-insulator (SOI) substrate. The waveguide is formed by removing the middle row of holes of the triangular lattice photonic crystal in the propagation direction, which create modes propagate along the missing holes confined by total internal reflection in the vertical direction and Bragg reflection, due to the PBG, in the lateral direction. We performed a 2D analysis with an equivalent index of the slab of 2.76 using the effective refractive index method (EIM) because the three-dimensional calculation consuming too much time and computer memory. To study the properties of this waveguide, we identified a supercell to investigate the effect of the radius of air holes of the Photonic crystal waveguide on slow light properties. We observed that the bands shift to higher frequencies as the radius value increases, this change is caused by the slab mode band below the propagation mode band. Also, we explored a flat band (slow light region) corresponding to the radius value r=0.4a. by shifting the two rows of holes adjacent to the waveguide in the propagation direction, we observed an inverse proportion between the bandwidth and the group index. Therefore, high group index brings forth slow light but a narrow bandwidth and vice versa. We engineered the dispersion curve to obtain a high group index with wide bandwidth of 18.24, 41.7, 34.55, 33 and 30.43 over 24, 11.7, 16.9, 20.3 and 23.7 nm, respectively. Which lead us to a high NDBP value of 0.465. for more precision, we used a three-dimensional PWE calculation, we found that the results of three-dimensional and two-dimensional calculation are in good agreement. In addition, to demonstrate the results obtained by the PWE method, we used the finite difference time domain (FDTD) method. The time delay of the pulse in the waveguide Δt =1.354 ps which correspond to a group index ng= 28.8 that confirm the value obtained by the PWE calculation. Finally, we proposed an application of our design as a buffer, we calculated the buffer capacity we have found that for a device with 1mm length give us 148 bits.

Currently, optical buffers require conversion to electrical signals as input to computer buffering and then converting electrical signal to optical signals again, by our design we don't need to convert the optical signal to electrical signal also we reduced the size, power and cost requirements of the buffers needed to perform this operation.

References

[1] C. Soukoulis, Photonic Crystals and Light Localization in the 21st Century, Springer Science \& Business Media, 2001.

[2] J. D. Joannopoulos, P. R. Villeneuve and S. Fan, "Photonic crystals: putting a new twist on light," *Nature,* vol. 386, no. 6621, pp. 143-149, 1997.

[3] S. G. Johnson, P. R. Villeneuve, S. Fan and J. D. Joannopoulos, "Linear waveguides in photonic-crystal slabs," *Physical Review B,* vol. 62, no. 12, pp. 8212-8222, 2000.

[4] N. Janrao and V. Janyani, "Slow light photonic crystal waveguide with large quality factor," *Optik - International Journal for Light and Electron Optics,* vol. 127, no. 3, pp. 1260-1264, 2016.

[5] T. Krauss, "Why do we need slow light?," *Nature Photonics,* vol. 2, no. 8, pp. 448-450, 2008.

[6] L. V. Hau, S. E. Harris, Z. Dutton and C. H. Behroozi, "Light speed reduction to 17 metres per second in an ultracold atomic gas," *Nature,* vol. 397, no. 6720, pp. 594-598, 1999.

[7] T. Baba, "Slow light in photonic crystals," *Nature photonics,* vol. 2, no. 8, pp. 465-473, 2008.

[8] T. Baba, J. Adachi, N. Ishikura, Y. Hamachi, H. Sasaki, T. Kawasaki and D. Mori, "Dispersion-controlled slow light in photonic crystal waveguides," *Proceedings of the Japan Academy, Series B,* vol. 85, no. 10, pp. 443-453, 2009.

[9] R. Boyd, "Material slow light and structural slow light: similarities and differences for nonlinear optics," *JOSA B,* vol. 28, no. 12, pp. A38-A44, 2011.

[10] K. Sakoda, Optical Properties of photonic crystals, Springer Science \& Business Media, 2004.

[11] J. D. Joannopoulos, S. G. Johnson, J. N. and Winn and R. D. Meade, Photonic crystals: molding the flow of light, Princeton university press, 2008.

[12] I. A. Sukhoivanov and I. V. Guryev, Photonic Crystals: Physics and Practical Modeling, Springer, 2009.

[13] A. W. Eckert, The world of opals, John Wiley \& Sons, 1997.

[14] E. Armstrong and C. O'Dwyer, "Artificial opal photonic crystals and inverse opal structures--fundamentals and applications from optics to energy storage," *Journal of Materials Chemistry C,* vol. 24, no. 3, pp. 6109-6143, 2015.

[15] K. Ho, C. T. Chan and C. Soukoulis, "Existence of a photonic gap in periodic dielectric structures," *Physical Review Letters,* vol. 65, no. 25, pp. 3152-3155, 1990.

[16] E. Yablonovitch, T. J. Gmitter and K. M. Leung, "Photonic band structure: The face-centered-cubic case employing nonspherical atoms," *Physical Review Letters,* vol. 67, no. 17, pp. 2295-2298, 1991.

[17] K. M. Ho, C. T. Chan, C. M. Soukoulis, R. Biswas and M. Sigalas, "Photonic band gaps in three dimensions: New layer-by-layer periodic structures," *Solid State Communications,* vol. 89, no. 5, pp. 413-416, 1994.

[18] H. S. Sözüer and J. P. Dowling, "Photonic band calculations for woodpile structures," *Journal of Modern Optics,* vol. 41, no. 2, pp. 231-239, 1994.

[19] S. Y. Lin, J. G. Fleming, D. L. Hetherington, B. K. Smith, R. Biswas, K. M. Ho, M. M. Sigalas, W. Zubrzycki, S. R. Kurtz and J. Bur, "A three-dimensional photonic crystal operating at infrared wavelengths," *Nature,* vol. 394, no. 6690, pp. 251-253, 1998.

[20] P. R. Villeneuve and M. Piché, "Photonic band gaps in two-dimensional square lattices: Square and circular rods Pierre," *physical Review B,* vol. 46, no. 8, pp. 4973-4975, 1992.

[21] M. Plihal and A. Maradudin, "Photonic band structure of two-dimensional systems: The triangular lattice," *Physical Review B,* vol. 44, no. 16, pp. 8565-8571, 1991.

[22] P. R. Villeneuve and M. Piche, "Photonic band gaps in two-dimensional square and hexagonal lattices," *Physical Review B,* vol. 46, no. 8, pp. 4969-4972, 1992.

[23] C. Sibilia, T. M. and Benson, M. Marciniak and T. Szoplik, Photonic crystals: physics and technology, Springer, 2008.

[24] B. C. Kress and P. Meyrueis, Applied Digital Optics: from micro-optics to nanophotonics, John Wiley \& Sons, 2009.

[25] R. Rumpf, Design and optimization of nano-optical elements by coupling fabrication to optical behavior, (Doctoral dissertation, University of Central Florida)., 2006.

[26] S. Fan, A. Mekis, S. Johnson and J. Joannopoulos, "Manipulating light with photonic crystals," *AIP Conference Proceedings,* vol. 560, no. 1, pp. 57-76, 2001.

[27] R. Meade, A. Rappe, K. Brommer and J. Joannopoulos, "Nature of the photonic band gap: some insights from a field analysis," *Journal of the Optical Society of America B,* vol. 10, no. 2, pp. 328-332, 1993.

[28] S. McCall, P. Platzman, R. Dalichaouch, D. Smith and S. Schultz, "Microwave propagation in two-dimensional dielectric lattices," *Physical review letters,* vol. 67, no. 15, pp. 2017-2020, 1991.

[29] R. D. Meade, K. D. Brommer, A. M. Rappe and J. D. Joannopoulos, "Existence of a photonic band gap in two dimensions," *Applied Physics Letters,* vol. 61, no. 4, pp. 495-497, 1992.

[30] P. R. Villeneuve, S. Fan and J. Joannopoulos, "Microcavities in photonic crystals: Mode symmetry, tunability, and coupling efficiency," *Physical Review B,* vol. 54, no. 11, pp. 7837-7842, 1996.

[31] J. Joannopoulos, "The almost magical world of photonic crystals," *58 Brazilian Journal of Physics,* vol. 26, no. 1, pp. 58-66, 1996.

[32] S. Fan, J. D. Joannopoulos, J. N. Winn, A. Devenyi, J. C. Chen and R. D. Meade, "Guided and defect modes in periodic dielectric waveguides," *Journal of the Optical Society of America B,* vol. 12, no. 7, pp. 1267-1272, 1995.

[33] P. Petersan and S. M. Anlage, "Measurement of resonant frequency and quality factor of microwave resonators," *Journal Of Applied Physics,,* vol. 84, no. 6, pp. 3392-3402, 1998.

[34] M. Bass, C. DeCusatis, J. Enoch, V. Lakshminarayanan, G. Li, C. MacDonald, V. . Mahajan and .. V. S. E., Handbook of Optics, Volume IV: Optical Properties of Materials, vol. 4, Orlando, Florida: Nonlinear Optics, Quantum Optics, 2009.

[35] A. Mekis, S. Fan and J. Joannopoulos, "Bound states in photonic crystal waveguides and waveguide bends," *Physical Review B - Condensed Matter and Materials Physics,* vol. 58, no. 8, pp. 4809-4817, 1998.

[36] S. G. Johnson, S. Fan, P. R. Villeneuve, J. D. Joannopoulos and L. A. Kolodziejski, "Guided modes in photonic crystal slabs," *Physical Review B,* vol. 60, no. 8, pp. 5751-5758, 1999.

[37] Q. Gong and X. Hu, Photonic Crystals: Principles and Applications, Pan Stanford}, 2014.

[38] T. van Leest, J. Heldens, v. d. G. B. and J. Caro, "Photonic crystal cavities for resonant evanescent field trapping of single bacteria," *Biophotonics: Photonic Solutions for Better Health Care III,* vol. 8427, pp. 84270-84280, 2012.

[39] S. Noda, A. Chutinan and M. Imada, "structure, Trapping and emission of photons by a single defect in a photonic bandgap," *nature,* vol. 407, no. 6804, pp. 608-610, 2000.

[40] M. Scalora, J. P. Dowling, C. M. Bowden and M. J. Bloemer, "Optical limiting and switching of ultrashort pulses in nonlinear photonic band gap materials," *Physical review letters,* vol. 73, no. 10, pp. 1368-1371, 1994.

[41] X. Hu, P. Jiang, C. Ding, H. Yang and Q. Gong, "Picosecond and low-power all-optical switching based on an organic photonic-bandgap microcavity," *Nature Photonics,* vol. 2, no. 3, pp. 185-189, 2008.

[42] M. Koshiba, "Wavelength division multiplexing and demultiplexing with photonic crystal waveguide couplers," *journal of lightwave technology,* vol. 19, no. 12, pp. 1970-1975, 2001.

[43] C. Jin, S. Han, X. Meng, B. Cheng and D. Zhang, "Demultiplexer using directly resonant tunneling between point defects and waveguides in a photonic crystal," *Journal of applied physics,* vol. 91, no. 7, pp. 4771-4773, 2002.

[44] T. Baba and D. Mori, "Slow light engineering in photonic crystals," *Journal of Physics D: Applied Physics,* vol. 40, no. 9, pp. 2659-2665, 2007.

[45] M. Notomi, K. Yamada, A. Shinya, J. Takahashi, C. Takahashi and I. Yokohama, "Extremely large group-velocity dispersion of line-defect waveguides in photonic crystal slabs," *Physical Review Letters,* vol. 87, no. 25, pp. 253902-253905, 2001.

[46] R. Hayakawa, N. Ishikura, H. C. Nguyen and T. Baba, "High-speed delay tuning of slow light in pin-diode-incorporated photonic crystal waveguide," *Optics letters,* vol. 38, no. 15, pp. 2680-2682, 2013.

[47] D. M. Beggs, T. P. White, L. O'Faolain and T. F. Krauss, "Ultracompact and low-power optical switch based on silicon photonic crystals," *Optics letters,* vol. 33, no. 2, pp. 147-149, 2008.

[48] M. Soljačić, S. Johnson, S. Fan, M. Ibanescu, E. Ippen and J. Joannopoulos, "Photonic-crystal slow-light enhancement of nonlinear phase sensitivity," *JOSA B,* vol. 19, no. 9, pp. 2052--2059, 2002.

[49] Y. Vlasov, M. O'boyle, H. Hamann and S. J. McNab, "Active control of slow light on a chip with photonic crystal waveguides," *Nature,* vol. 438, no. 7064, pp. 65-69, 2005.

[50] H. Nguyen, Y. Sakai, M. Shinkawa, N. Ishikura and T. Baba, "10 Gb/s operation of photonic crystal silicon optical modulators," *Optics express,* vol. 19, no. 14, pp. 13000-13007, 2011.

[51] T. Kampfrath, D. Beggs, T. White, A. Melloni, T. Krauss and L. Kuipers, "Ultrafast adiabatic manipulation of slow light in a photonic crystal," *Physical Review A,* vol. 81, no. 4, pp. 043837-043843, 2010.

[52] J. McMillan, X. Yang, N. Panoiu, R. Osgood and C. Wong, "Enhanced stimulated Raman scattering in slow-light photonic crystal waveguides," *Optics letters,* vol. 31, no. 9, pp. 1235-1237, 2006.

[53] M. Soljačić and J. Joannopoulos, "Enhancement of nonlinear effects using photonic crystals," *Nature materials,* vol. 3, no. 4, pp. 211-219, 2004.

[54] B. Corcoran, C. Monat, C. Grillet, D. J. Moss, B. Eggleton, T. White, L. O'Faolain and T. Krauss, "Green light emission in silicon through slow-light enhanced third-harmonic generation in photonic-crystal waveguides," *Nature photonics,* vol. 3, no. 4, pp. 206-210, 2009.

[55] C. Monat, M. Ebnali-Heidari, C. Grillet, B. Corcoran, B. Eggleton, T. White, L. O'Faolain, J. Li and T. Krauss, "Four-wave mixing in slow light engineered silicon photonic crystal waveguides," *Optics express,* vol. 18, no. 22, pp. 22915-22927, 2010.

[56] C. Monat, B. Corcoran, M. Ebnali-Heidari, C. Grillet, B. Eggleton, T. White, L. O'Faolain and T. Krauss, "Slow light enhancement of nonlinear effects in silicon engineered photonic crystal waveguides," *Optics express,* vol. 17, no. 4, pp. 2944-2953, 2009.

[57] T. Krauss, "Slow light in photonic crystal waveguides," *Journal of Physics D: Applied Physics,* vol. 40, no. 9, pp. 2666-2670, 2007.

[58] A. Hocini, M. Maache and D. Khedrouche, "Wideband and low dispersion slow light by altering the geometry of a photonic crystal waveguide," *Optics Communications,* vol. 427, pp. 396-404, 2018.

[59] T. Baba, N. Fukaya and J. Yonekura, "Observation of light propagation in photonic crystal optical waveguides with bends," *Electronics letters,* vol. 35, no. 8, pp. 654-655, 1999.

[60] M. Loncar, D. Nedeljkovic, T. Doll, J. Vuckovic, A. Scherer and T. Pearsall, "Waveguiding in planar photonic crystals," *Silicon-based and Hybrid Optoelectronics III,* vol. 4293, pp. 94-100, 2001.

[61] J. Li, T. White, L. O'Faolain, A. Gomez-Iglesias and T. Krauss, "Systematic design of flat band slow light in photonic crystal waveguides," *Optics express,* vol. 16, no. 9, pp. 6227-6232, 2008.

[62] R. Boyd and D. J. Gauthier, "Controlling the velocity of light pulses," *science,* vol. 326, no. 5956, pp. 1074-1077, 2009.

[63] J. B. Khurgin and R. S. Tucker, Slow light: Science and applications, New York: CRC press, 2008.

[64] R. Engelen, Y. Sugimoto, Y. Watanabe, J. Korterik, N. Ikeda, N. van Hulst, K. Asakawa and L. Kuipers, "The effect of higher-order dispersion on slow light propagation in photonic crystal waveguides," *Optics express,* vol. 14, no. 4, pp. 1658-1672, 2006.

[65] D. Mori and T. Baba, "Wideband and low dispersion slow light by chirped photonic crystal coupled waveguide," *Optics express,* vol. 13, no. 23, pp. 9398-9408, 2005.

[66] Y. Wan, K. Fu, C. Li and M. Yun, "Improving slow light effect in photonic crystal line defect waveguide by using eye-shaped scatterers," *Optics Communications,* vol. 286, pp. 192-196, 2013.

[67] M. Settle, R. Engelen, M. Salib, A. Michaeli, L. Kuipers and T. Krauss, "Flatband slow light in photonic crystals featuring spatial pulse compression and terahertz bandwidth," *Optics Express,* vol. 15, no. 1, pp. 219-226, 2007.

[68] T. Kawasaki, D. Mori and T. Baba, "Experimental observation of slow light in photonic crystal coupled waveguides," *Optics express,* vol. 15, no. 16, pp. 10274-10281, 2007.

[69] A. Y. Petrov and M. Eich, "Zero dispersion at small group velocities in photonic crystal waveguides," *Applied Physics Letters,* vol. 85, no. 21, pp. 4866-4868, 2004.

[70] S. Johnson and J. D. Joannopoulos, "Block-iterative frequency-domain methods for Maxwell's equations in a planewave basis," *Optics express,* vol. 8, no. 3, pp. 173-190, 2001.

[71] Y. Zhao, Y. Zhang, Q. Wang and H. Hu, "Review on the optimization methods of slow light in photonic crystal waveguide," *IEEE Transactions on Nanotechnology,* vol. 14, no. 3, pp. 407-426, 2015.

[72] Y. Zhang, Y. Zhao and J. Li, "Theoretical research on slow light engineering of slotted photonic crystal waveguides with elliptical holes and optofluidic infiltration," *Applied Optics,* vol. 54, no. 7, pp. 1639-1646, 2015.

[73] L. O'Faolain, S. Schulz, D. Beggs, T. White, M. Spasenovic, L. Kuipers, F. Morichetti, A. Melloni, S. Mazoyer and J. Hugonin, "Loss engineered slow light waveguides," *Optics express*, vol. 18, no. 26, pp. 27627-27638, 2010.

[74] B. Wang, S. Mazoyer, J. Hugonin and P. Lalanne, "Backscattering in monomode periodic waveguides," *Physical Review B*, vol. 78, no. 24, pp. 245108-245116, 2008.

[75] S. Hughes, L. Ramunno, J. F. Young and J. E. Sipe, "Extrinsic Optical Scattering Loss in Photonic Crystal Waveguides: Role of Fabrication Disorder and Photon Group Velocity," *Physical review letters*, vol. 94, no. 3, pp. 033903-033907, 2005.

[76] E. Kuramochi, M. Notomi, S. Hughes, A. Shinya, T. Watanabe and L. Ramunno, "Disorder-induced scattering loss of line-defect waveguides in photonic crystal slabs," *Physical Review B*, vol. 72, no. 16, pp. 161318-161322, 2005.

[77] Y. Hamachi, S. Kubo and T. Baba, "Low dispersion slow light and nonlinearity enhancement in lattice-shifted photonic crystal waveguide," in *Quantum Electronics and Laser Science Conference*, Optical Society of America, 2008, p. QTuC1.

[78] S. Schulz, C. Hu, J. Upham, R. Boyd and L. O'Faolain, "Controllable low-loss slow light in photonic crystals," in *Steep Dispersion Engineering and Opto-Atomic Precision Metrology XI*, vol. 10548, International Society for Optics and Photonics, 2018, p. 1054806.

[79] S. Schulz, L. O'Faolain, D. Beggs, T. White, A. Melloni and T. Krauss, "Dispersion engineered slow light in photonic crystals: a comparison," *Journal of Optics*, vol. 12, no. 10, p. 104004, 2010.

[80] S. Kubo, D. Mori and T. Baba, "Low-group-velocity and low-dispersion slow light in photonic crystal waveguides," *Optics letters*, vol. 32, no. 20, pp. 2981-2983, 2007.

[81] R. Hao, E. Cassan, H. Kurt, X. Le Roux, D. Marris-Morini, L. Vivien, H. Wu, Z. Zhou and X. Zhang, "Novel slow light waveguide with controllable delay-bandwidth product and utra-low dispersion," *Optics Express*, vol. 18, no. 6, pp. 5942-5950, 2010.

[82] F. Bagci and B. Akaoglu, "Enhancement of buffer capability in slow light photonic crystal waveguides with extended lattice constants," *Optical and Quantum Electronics*, vol. 47, no. 3, pp. 791-806, 2015.

[83] J. Liang, L. Ren, M. Yun, X. Han and X. Wang, "Wideband ultraflat slow light with large group index in a W1 photonic crystal waveguide," *Journal of Applied Physics*, vol. 110, no. 6, pp. 063103-063109, 2011.

[84] Y. Zhang, Y. Zhao and Q. Wang, "Theoretical Research on Optofluidic Photonic Crystal Waveguide for Broadly Tunable and Ultra-Wideband Slow Light," *International Journal of Optomechatronics,* vol. 8, no. 2, pp. 114-128, 2014.

[85] E. Sayed, K. Karim, Y. Ashish, B. Luigi, Zhengbiao. and Ouyang., "Slow-light transmission with high group index and large normalized delay bandwidth product through successive defect rods on intrinsic photonic crystal waveguide," *Optics Communications,* vol. 418, pp. 73-79, 2018.

[86] Y. Zhai, H. Tian and Y. Ji, "Slow light property improvement and optical buffer capability in ring-shape-hole photonic crystal waveguide," *Journal of Lightwave Technology,* vol. 29, no. 20, pp. 3083-3090, 2011.

[87] Y. Xu, L. Xiang, E. Cassan, D. Gao and X. Zhang, "Slow light in an alternative row of ellipse-hole photonic crystal waveguide," *Applied optics,* vol. 52, no. 6, pp. 1155-1160, 2013.

[88] D. Mori and T. Baba, "Dispersion-controlled optical group delay device by chirped photonic crystal waveguides," *Applied physics letters,* vol. 85, no. 7, pp. 1101-1103, 2004.

[89] D. Mori, S. Kubo, H. Sasaki and T. Baba, "Experimental demonstration of wideband dispersion-compensated slow light by a chirped photonic crystal directional coupler," *Optics express,* vol. 15, no. 9, pp. 5264-5270, 2007.

[90] A. Yariv, Y. Xu, R. K. Lee and A. and Scherer, "Coupled-resonator optical waveguide:? a proposal and analysis," *Optics letters,* vol. 24, no. 11, pp. 711-713, 1999.

[91] M. Notomi, E. Kuramochi and T. Tanabe, "Large-scale arrays of ultrahigh-Q coupled nanocavities," *Nature Photonics,* vol. 2, no. 12, pp. 741-747, 2008.

[92] ,. J. Jágerská, N. Le Thomas, V. Zabelin, R. Houdré, W. Bogaerts, P. Dumon and R. Baets, "Experimental observation of slow mode dispersion in photonic crystal coupled-cavity waveguides," *Optics letters,* vol. 34, no. 3, pp. 359-361, 2009.

[93] A. a. G. A. a. S. P. M. J. Mart{\i}́nez, "Group velocity and dispersion model of coupled-cavity waveguides in photonic crystals," *JOSA A,* vol. 20, no. 1, pp. 147-150, 2003.

[94] K. Üstün and H. Kurt, "Ultra slow light achievement in photonic crystals by merging coupled cavities with waveguides," *Optics express,* vol. 18, no. 20, pp. 21155-21161, 2010.

[95] N. Le Thomas and R. Houdré, "Group velocity and energy transport velocity near the band edge of a disordered coupled cavity waveguide: an analytical approach," *JOSA B,* vol. 27, no. 10, pp. 2095-2101, 2010.

[96] I. H. Rey, Active slow light in silicon photonic crystals: tunable delay and Raman gain, (Doctoral dissertation, University of St Andrews)., 2012.

[97] M. Spurny, L. O'Faolain, D. Bulla, B. Luther-Davies and T. Krauss, "Fabrication of low loss dispersion engineered chalcogenide photonic crystals," *Optics express,* vol. 19, no. 3, pp. 1991-1996, 2011.

[98] B. Corcoran, C. Monat, M. Pelusi, C. Grillet, T. White, L. Faolain, T. Krauss, B. Eggleton and D. Moss, "Optical performance monitoring at 640Gb/s via slow-light in a silicon nanowire," *arXiv preprint arXiv:1505.03224,* 2015.

[99] T. Baba, H. Nguyen, N. Ishikura, K. Suzuki, M. Shinkawa, R. Hayakawa and K. Kondo, "Photonic crystal slow light devices fabricated by CMOS-compatible process," *IEICE Electronics Express,* vol. 10, no. 10, pp. 20132002-20132002, 2013.

[100] Z. Hayran, M. Turduev, M. Botey, R. Herrero, K. Staliunas and H. Kurt, "Slow light enabled wavelength demultiplexing," *Transparent Optical Networks (ICTON), 2016 18th International Conference on,* pp. 1-4, 2016.

[101] A. Petrov, Slow light photonic crystal line-defect waveguides, (Doctoral dissertation, University of Technical University Hamburg-Harburg), 2008.

[102] Y. Zhang, Y. Zhao, J. . Li and R. . Lv, "High-sensitive refractive index sensor based on slow light engineered photonic crystal cavity," in *SENSORS, 2014 IEEE,* Shenyang, IEEE, 2014, pp. 358-361.

[103] H. Nguyen, S. Hashimoto, M. Shinkawa and T. Baba, "Compact and fast photonic crystal silicon optical modulators," *Optics express,* vol. 20, no. 20, pp. 22465-22474, 2012.

[104] G. Reed, G. Mashanovich, F. Gardes and D. Thomson, "Silicon optical modulators," *Nature photonics,* vol. 4, no. 8, pp. 518-526, 2010.

[105] C. Hu, S. Schulz, A. Liles and L. O'Faolain, "Tunable Optical Buffer through an Analogue to Electromagnetically Induced Transparency in Coupled Photonic Crystal Cavities," *ACS Photonics,* vol. 5, no. 5, pp. 1827-1832, 2018.

[106] R. Boyd, D. Gauthier and A. Gaeta, "Applications of slow light in telecommunications," *Optics and Photonics News,* vol. 17, no. 4, pp. 18-23, 2006.

[107] S. Virally, A Review of Slow Light Physics and Its Applications, Ecole Polytechnique de Montreal, 2008.

[108] Y. a. Z. Y.-n. a. W. Q. Zhao, "High sensitivity gas sensing method based on slow light in photonic crystal waveguide," *Sensors and Actuators B: Chemical*, vol. 173, pp. 28-31, 2012.

[109] H. Awad, I. Hasan, K. Mnaymneh, T. Hall and I. Andonovic, "Gas sensing using slow light in photonic crystal waveguides," *Fibre and Optical Passive Components (WFOPC), 2011 7th Workshop on*, pp. 1-3, 2011.

[110] J. Garcia-Ruperez, V. Toccafondo, M. Bauls, J. Castello, A. Griol, S. Peransi-Llopis and A. Maquieira, "Label-free antibody detection using band edge fringes in SOI planar photonic crystal waveguides in the slow-light regime," *Optics Express*, vol. 18, no. 23, pp. 24276-24286, 2010.

[111] F. Hosseinibalam, S. Hassanzadeh, A. Ebnali-Heidari and C. Karnutsch, "Design of an optofluidic biosensor using the slow-light effect in photonic crystal structures," *Applied optics*, vol. 51, no. 5, pp. 568-576, 2012.

[112] Y. Zhang, Y. Zhao, J. Li and R. Lv, "High-sensitive refractive index sensor based on slow light engineered photonic crystal cavity}," *SENSORS, 2014 IEEE*, pp. 358-361, 2014.

[113] A. Lavrinenko, J. Laegsgaard, N. Gregersen, F. Schmidt and T. Sondergaard, Numerical methods in photonics, New York: Numerical Methods in Photonics, 2015.

[114] L. Tsang, J. Kong, K. Ding and C. Ao, Scattering of electromagnetic waves: numerical simulations, John Wiley \& Sons, 2004.

[115] L. K. M. and Y. Liu, "Photon band structures: The plane-wave method," *PHYSICAL REVIEW B*, vol. 41, no. 14, pp. 10188-10190, 1990.

[116] K. Karls and J. Raymond, The Finite Difference Time Domain Method for, Boca Raton: CRC Press, 1993.

[117] C. Yu and H. Chang, "Compact finite-difference frequency-domain method for the analysis of two-dimensional photonic crystals," *Optics Express*, vol. 12, no. 7, pp. 1397-1408, 2004.

[118] J. D. Joannopoulos, R. Meade and J. Winn, Photonic Crystals: Molding the Flow of Light, Princeton University Press, 1995.

[119] S. Johnson, Photonic crystals: from theory to practice, (Doctoral dissertation, Massachusetts Institute of Technology), 2001.

[120] S. Guo and S. Albin, "Simple plane wave implementation for photonic crystal calculations," *Optics Express*, vol. 11, no. 2, pp. 167-175, 2003.

[121] A. Taflove and S. C. Hagness, Computational electrodynamics: the finite-difference time-domain method, Artech house, 2005.

[122] G. R. Sergio, Optical Properties of Nanostructured Metallic, spain: Doctoral dissertation, The University of Zaragoza), 2012.

[123] K. Yee, "Numerical solution of inital boundary value problems involving maxwell's equations in isotropic media," *IEEE Transactions on Antennas and Propagation*, vol. 14, no. 3, pp. 302-307, 1966.

[124] A. Taflove and M. Brodwin, "Numerical solution of steady-state electromagnetic scattering problems using the time-dependent Maxwell's equations," *IEEE transactions on microwave theory and techniques*, vol. 23, no. 8, pp. 623-630, 1975.

[125] J. Berenger, "A perfectly matched layer for the absorption of electromagnetic waves," *Journal of computational physics*, vol. 114, no. 2, pp. 185-200, 1994.

[126] S. Wolfram, "Computer software in science and mathematics," *Scientific American*, vol. 251, no. 3, pp. 188-203, 1984.

[127] I. RSoft Design Group, RSoft CAD 4.1 user guide, license 16847214, 1999-2008.

[128] I. RSoft Design Group, FullWAVE 6.1 User Guide, license 16847214,, 1999-2008.

[129] J. Foresi, P. Villeneuve, J. Ferrera, E. Thoen, G. Steinmeyer, S. Fan, J. Joannopoulos, L. Kimerling, H. Smith and E. Ippen, "Photonic-bandgap microcavities in optical waveguides," *nature*, vol. 390, no. 6656, pp. 143-145, 1997.

[130] L. Yang, "Suggested procedure for the use of the effective-index method for high-index-contrast photonic crystal slabs," *Optical Engineering*, vol. 44, no. 7, pp. 078002-078009, 2005.

[131] C. Chen, Foundations for guided-wave optics, West Lafayette, Indiana: John Wiley \& Sons, 2006.

[132] M. Qiu, "Effective index method for heterostructure-slab-waveguide-based two-dimensional photonic crystals," *Applied physics letters*, vol. 81, no. 7, pp. 1163-1165, 2002.

[133] B. Jaskorzynska, "Properties and applications of 1D and 2D photonic-crystals," *Transparent Optical Networks, 2004. Proceedings of 2004 6th International Conference on*, vol. 1, pp. 259-259, 2004.

[134] Z.-Y. Li, J. Wang and B.-Y. Gu, "Creation of partial band gaps in anisotropic photonic-band-gap structures," *Physical Review B*, vol. 58, no. 7, pp. 3721-3729, 1998.

[135] M. Banihashemi and V. Ahmadi, "Nonlinear response of high efficient in-plane channel drop filter in Si heterostructure photonic crystal slab," *Journal of Modern Optics,* vol. 58, no. 7, pp. 587-592, 2011.

[136] Y. He, T. Wang, W. Yan and e. al., "All-optical switching based on the electromagnetically induced transparency effect of an active photonic crystal microcavity," *Journal of Modern Optics,* vol. 61, no. 5, pp. 403-408, 2014.

[137] M. Maache, A. Hocini and D. Khedrouche, "Geometrically tunable slow light based on a modified photonic crystal waveguide," *Chinese Journal of Physics,* vol. 55, no. 6, pp. 2318-2324, 2017.

[138] A. Kahlouche, A. Hocini and D. Khedrouche, "Band-gap properties of 2D photonic crystal made by silica matrix doped with magnetic nanoparticles," *Journal of Computational Electronics,* vol. 13, no. 2, pp. 490-495, 2014.

[139] L. Frandsen, A. Lavrinenko, J. Fage-Pedersen and P. Borel, "Photonic crystal waveguides with semi-slow light and tailored dispersion properties," *Optics Express,* vol. 14, no. 20, p. 9444–9450, 2006.

[140] A. Säynätjoki, M. Mulot, J. Ahopelto and H. Lipsanen, "Dispersion engineering of photonic crystal waveguides with ring-shaped holes," *Optics Express,* vol. 15, no. 13, p. 8323–8328, 2007.

[141] R. Hao, E. Cassan, H. Kurt, J. Hou, X. Le Roux, D. Marris-Morini, L. Vivien, D. Gao, Z. Zhou and X. Zhang, "Novel kind of semislow light photonic crystal waveguides with large delay-bandwidth product," *IEEE Photonics Technology Letters,* vol. 22, no. 11, pp. 844-846, 2010.

[142] Y. Zhao, Y. Zhang and Q. Wang, "Optimization of slow light in slotted photonic crystal waveguide with liquid infiltration," *Journal of Lightwave Technology,* vol. 31, no. 14, pp. 2448-2454, 2013.

[143] L. Nuttall, F. Brossard, S. A. Lennon, B. Reid, J. Wu, J. Griffiths and R. Taylor, "Optical fabrication and characterisation of SU-8 disk photonic waveguide heterostructure cavities," *Optics Express,* vol. 25, no. 20, pp. 24615-24622, 2017.

[144] M. Notomi, A. Shinya, S. Mitsugi, E. Kuramochi and H. and Ryu, "Waveguides, resonators and their coupled elements in photonic crystal slabs," *Optics express,* vol. 12, no. 8, pp. 1551-1561, 2004.

[145] K. Yamada, M. Notomi, A. Shinya, I. Yokohama, T. Shoji, T. Tsuchizawa, T. Watanabe and J.-I. a. T. E. a. M. H. Takahashi, "SOI-based photonic crystal line-defect waveguides," *Active and Passive Optical Components for WDM Communications II,* vol. 4870, pp. 324--339, 2002.

[146] M. Kumar and A. Sharma, "Flat band slow light in silicon photonic crystal waveguide with large delay bandwidth product and low group velocity dispersion," *IET Optoelectronics,* vol. 9, no. 1, pp. 24-28, 2015.

[147] A. Khodamohammadi, H. Khoshsima and V. Fallahi, "Slow light engineering in a photonic crystal slab waveguide through optofluidic infiltration and geometric modulation," *Pleiades Publishing,* vol. 124, no. 5, pp. 712-717, 2017.

[148] J. Tang, W. Li, J. Wu and Z. Xu, "Slow light with large group index – bandwidth product in lattice-shifted photonic crystal waveguides," *Journal of Modern Optics,* vol. 63, no. 19, pp. 1-6, 2016.

[149] F. Long, H. Tian and Y. Ji, "A study of dynamic modulation and buffer capability in low dispersion photonic crystal waveguides," *Journal of lightwave technology,* vol. 28, no. 8, pp. 1139-1143, 2010.

[150] D. Mori and T. Baba, "Wideband and low dispersion slow light by chirped photonic crystal coupled waveguide," *Optics Express,* vol. 13, no. 23, p. 9398, 2005.

[151] T. Niemi, L. Frandsen, K. Hede, A. Harpoth, P. Borel and M. Kristensen, "Wavelength-division demultiplexing using photonic crystal waveguides," *IEEE Photonics Technology Letters,* vol. 18, no. 1, pp. 226-228, 2006.

Publications

- ✓ **M. Maache**, A. Hocini and D. Khedrouche, "Geometrically tunable slow light based on a modified photonic crystal waveguide," *Chinese Journal of Physics*, vol. 55, no. 6, pp. 2318-2324, 2017.
- ✓ A. Hocini, **M. Maache** and D. Khedrouche, "Wideband and low dispersion slow light by altering the geometry of a photonic crystal waveguide," *Optics Communications*, vol. 427, pp. 396-404, 2018.

International Communications with proceeding

- ✓ **M. Maache,** A. Hocini and D. Khedrouche: "SLOW LIGHT IN PHOTONIC CRYSTAL WAVEGUIDE". International Conference on Advanced Technology & Sciences (ICAT'17), Istanbul, Turkey; 05/2017
- ✓ **M. Maache**, A. Hocini and D. Khedrouche: "SLOW LIGHT IN A MODIFIED PHOTONIC CRYSTAL WAVEGUIDE". International Conference on Electronics and New Technologies (ICENT'2017). M'sila, Algeria, 14-15 November, 2017.

Doctoral thesis: *Design and optical studies of photonic components using slow light properties*

By: *Mouhssin MAACHE*

Supervisor: *Abdesselam HOCINI*

Co-supervisor : *Djamel KHEDROUCHE*

الملخص

البلورات الفوتونية هي ترتيب دوري مصطنع لمواد عازلة . اكتشاف البلورات الفوتونية التي تتميز بفجوة فوتونية فتح طرق جديدة للتحكم في الضوء. مما ادى إلى اقتراحات لعدد كبير من الأجهزة. عنصر مهم في الدوائر الضوئية هو دليل الموجي الخطي لنقل الضوء من وإلى المكونات، بالاضافة الى ذلك توفر البلورات الفوتونية مزايا فريدة لدلائل الموجة. دلائل الموجات الضوئية البلورية, موجهة بواسطة الفجوة الضوئية للبلورات الفوتونية وهي واحدة من أحسن الهياكل الجذابة والملائمة لتحقيق تأثير الضوء البطيء، لأن مثل بنية العيب الخطي هاته تعمل في درجة حرارة الغرفة لديها قدرة عالية على الإدماج على شريحة عن طريق تعديل بنية البلورات الفوتونية الاولية. يعمل الضوء البطيء على تعزيز تفاعل الضوء مع المادة ؛ فهو يوفر تحكمًا إضافيًا في عرض النطاق الترددي الطيفي للتفاعل، ويسمح لنا بتأخير وتخزين الضوء مؤقتًا في جميع الذاكرات البصرية. وفي هذا السياق، فإن الهدف من هذا البحث هو دراسة وتصميم اثنين من الدليل الموجي الكريستال الضوئية PCW1 و PCW2 لتحقيق ضوء بطيء في المنطقة المسطحة للأنماط الموجهة مع NDBP كبير مع الحفاظ عل قيم أصغر لتشتت سرعة المجموعة. لإختبار التطبيق لخاصية دليل الموجة الثاني PCW2 ,حسبنا سعة التخزين المؤقت , ووجدنا أنها تصل إلى أكثر من 148 بيت على افتراض أن طول الجهاز هو 1 مم . النتائج المتحصل عليها يمكن الاستفادة منها في إنشاء مخازن مؤقتة ضوئية على رقاقة و خطوط تأخير.

الكلمات المفتاحية: البلورات الضوئية, دليل الموجة , الضوء البطيء, PWE , تخزين مؤقت.

Résumé

Les cristaux photoniques (CP) sont des arrangements périodiques artificiels de matériaux diélectriques. La découverte de cristaux photoniques avec une bande interdite, a ouvert de nouvelles méthodes pour le contrôle de la lumière, conduisant à des propositions de nombreux nouveaux dispositifs. Le guide d'onde pour le transport de la lumière vers et à partir des composants est un élément important des circuits optiques. De plus, les cristaux photoniques offrent des avantages uniques pour les guides d'ondes. Les guides d'ondes à cristaux photonique, sont guidés par la bande du CP et c'est l'une des structures les plus appropriées et les plus attrayantes pour réaliser l'effet de la lumière lente car, la structure de défaut linéique fonctionne à température ambiante et a un fort potentiel pour l'intégration sur puce à travers la modification de la structure initiale de CP. La lumière lente améliore l'interaction de la lumière avec le matériau ; elle offre un contrôle supplémentaire sur la largeur de la bande spectrale de l'interaction, et nous permet de retarder et de stocker temporairement la lumière dans les mémoires optiques. Dans ce contexte, le but de cette thèse est d'étudier et de concevoir deux guides d'ondes à cristaux photoniques PCW1 et PCW2 afin d'obtenir une lumière lente dans la région de bande plate des modes guidés avec un grand NDBP tout en maintenant des valeurs plus faibles de dispersion de la vitesse du groupe. Afin de tester l'applicabilité de notre guide d'ondes PCW2, on a calculé la capacité du tampon et montré qu'elle peut atteindre 148 bits, en supposant que la longueur du dispositif est L= 1mm. Les résultats obtenus peuvent être utiles pour fabriquer des tampons optiques sur puce et lignes de retard.

Mots clés : cristaux photonique, guides d'ondes, lumière lente, PWE. Tampon.

Summary

Photonic crystals (PhCs) are artificially constructed periodic arrangements of dielectric materials. The discovery of photonic crystals with a photonic band gap, has opened up new methods for controlling light, leading to proposals for many novel devices. An important element of optical circuits is a linear waveguide to carry light to and from components, in addition, photonic crystals provide unique advantages for waveguides. Photonic-crystal waveguides, guided by the band gap of the PhC and it is one of the most suitable and attractive structures for realizing the slow light effect, because such a line defect structure operates at room temperature and has a high potential for on-chip integration by modifying the initial PhC structure. Slow light promotes a stronger light–matter interaction; it offers additional control over the spectral bandwidth of the interaction, and it allows us to delay and temporarily store light in all-optical memories. In this context, the aim of this thesis is to study and design two photonic crystal waveguides PCW1 and PCW2 designed to achieve slow light in the flat band region of guided modes with large normalized delay bandwidth product (NDBP) while maintaining smaller values of group velocity dispersion. To further test the applicability of our waveguide PCW2, the buffering capacity is calculated, which is found to be as high as 148 bits on the assumption that the device length is L=1mm. The reported results can be useful in making on-chip optical buffers and delay lines.

Keywords: Photonic crystal, waveguides, slow light, PWE. Buffer.